Surface Topography/Chemistry Modification through the Creation of Pseudo-Periodic Surface Micro-structures using Pulsed Nanosecond Fiber Laser Irradiation

by

Negar Rasti

presented to the University of Waterloo

in fulfillment of the

thesis requirement for the degree of

Doctor of Philosophy

in

Mechanical Engineering

Waterloo, Ontario, Canada, 2014

Author's Declaration

I hereby declare that I am the sole author of this thesis. This is a true copy of the thesis, including any required final revisions, as accepted by my examiners.

I understand that my thesis may be made electronically available to the public.

Abstract

The focus of this thesis is on the development of a methodology for modifying the surface of titanium implant devices to improve biocompatibility and osseointegration properties utilizing three approaches: 1) developing Pseudo-Periodic (PP) micro-structures on the surface of the implant to increase nano and micro roughness, 2) engraving parallel microgrooves on the surface of the implant, 3) modifying the chemistry of the substrate by increasing the oxide layer to augment the biocompatibility. A single-mode, inexpensive, pulsed nanosecond ytterbium fiber laser is used to modify pure titanium surfaces to improve surface topographical, chemical and mechanical properties, thereby improving surface biocompatibility properties.

The laser processing setup was designed to control different process parameters, including laser power, laser frequency, and scanning speed. The effect of each of these process parameters on the modified surface properties is then evaluated. The laser processing results in the formation of PP micro-structures, which protrude from the surface of the substrate and form nano and micro roughness on the laser path. Offsetting the laser beam in a desired space develops microgrooves.

The PP micro-structures are generated in two stages: 1) the initiation of structures, which occurs when the laser intensity is close to the threshold Intensity of the material (*i.e., 1.27 MW/cm*^{2} for titanium); and 2) the growth of the structures. The main factor in the growth of PP-based micro-structures is effective energy. The growth of the PP based micro-structures is observed through surface characterization techniques using scanning electron microscope (SEM) and profilometry analysis. The roughness of the micro-structures on titanium can increase to an average roughness of *1.7 μm*. The size of the micro-structures can also increase to 30-50 *μm*, which is compatible with osteoblast (bone) cells and is, therefore, suitable for improving the biocompatibility properties of the implant's surface.

The introduced laser processing technique simultaneously results in both surface chemical improvement and topographical improvement. The chemical properties of the modified surfaces are characterized using Energy-dispersive X-ray spectroscopy (EDAX) and X-ray Diffraction (XRD) analysis. The chemical characterization of the modified surfaces demonstrates the presence of the metastable anatase form of titania on surfaces developed at temperatures above 1650^0C. Anatase usually transforms to a rutile structure at temperatures higher than 700-1000^0C; therefore, this finding indicates that the introduced laser processing results in a solidification mechanism that does not take place in an equilibrium manner; as such, the resulting structures may not follow a conventional phase transformation diagram. The XRD characterization also demonstrates the transformation of αTi to βTi on the surface that forms above the Ti transus temperature, induced by laser processing using the introduced parameters. The increase in the hardness of the titanium is quantified through the nano-hardness characterization, which demonstrates a hardness increase from 5 to 35 MPa on the surfaces of the modified structures. The XRD results also show the presence of the rare structure of the titanium oxide, hongquiite, which has the same structure as TiC with high surface hardness.

To investigate the effect of the modified surfaces on the surface biocompatibility behaviour, MG-63 cells are cultured on the six selected surface categories for time durations of: 10 hours, 1 day, and 3 days. These time periods permit the observation of the first stages of bone integration, including cell attachment, cell adhesion and cell viability, which are the essential cell characteristics for a successful cell proliferation. Cell behaviour on each substrate is analyzed using three different characterization techniques; (i) Statistical analysis based on SEM images using ImageJ software to characterize and quantify cell morphology, area, density, and orientation; (ii) Trypsinization analysis for quantifying cell adhesion strength; and (iii) Cell

metabolic activity characterization on different substrates, which is quantified by analyzing cell viability using alamar blue.

The results demonstrate an increase of cell orientation on the modified surfaces up to four times,, compared to the unmodified surfaces. The trypsinization analysis of the surfaces shows an increase in cell adhesion strength of the PP based rough and grooved surfaces for 4 to 4.9 times compare to the unmodified surfaces. The results from the alamar blue test demonstrated an increase in cell viability up to eleven times greater than cell viability on polished surfaces.

Acknowledgements

I am extremely grateful to my supervisor, Dr. Ehsan Toyserkani for his support and guidance throughout the completion of my PhD program. I also express my deep gratitude to my committee members: Dr. Fathy Ismail; Dr. Mohammad Kohandel; Dr. Michael Mayer; and also my external committee member, Dr. Gene Zak from Queen's University, for their helpful comments and constructive feedbacks. I am extremely grateful to Dr. Maud Gorbet for granting me permission to access her lab for conducting the cell culturing tests, and also for her great support and guidance. I am also thoroughly thankful to Dr. Gorbet's group members: William Francis, Saman Mohammadi and Sara Molladavoodi for their support in conducting these tests.

I would also like to acknowledge the financial support from NSERC, OGS and Academic Institutional presidential Award. I am also grateful to work with my colleagues at University of Waterloo; Dr. Hamidreza Alemohammad, Dr. Yaser Shanjai, Hanieh Aghighi, Dr Neda Darivandi, Atefeh Shadpour, Dr Hamid Bolandhemmat, Dr Nasim Paryab, Dr Homeyra Pourmohammadali, Dr. Mihaela Vlasea, Xixi Zhang, and Ahmad Basalah. My sincere thanks go to my dear friends, Dr Panthea Sepehrband and Nasim Bakhshizadeh who not only have been extremely helpful in my academic path, but also been the great emotional support and made my experience at the University of Waterloo wonderful and unforgettable.

Last but not least my greatest appreciation to my husband Sasan, for his unlimited love, support and encouragement, and also to my parents, Hoorieh and Kiumars, for their constant and unconditional love and motivation. I would also extremely thankful for all the support and inspiration I got from my sisters, Nahal and Negin and my brother, Navid and extremely thankful for the younger members of our family the lovely Parsa, Sepehr and Ryan for making my life extremely happy and meaningful.

Dedication

To Sasan, my Mom and Dad

For their unconditional love and support

List of Contents

List of Figures

List of Tables

1 Chapter One –

Introduction

1.1 Introduction

Due to an aging population, there has been a significant growth in the percentage of elderly people, and a corresponding increase in the demand for orthopaedic implants and dental devices. The design of durable implants and devices is, therefore, of vital importance for the health and well-being of a significant portion of the population.

The performance of an implanted device depends on both the bulk properties and surface properties at the implant/tissue interface. The failure of implant devices is most often due to fracture or loosening over the years. Therefore, in addition to the proper material selection for dental and orthopaedic applications (i.e., materials that are capable of tolerating load bearing conditions), the surface properties of the material (i.e., topography and chemistry) should be modified to improve the biocompatibility and osteoconductivity of the bone and dental implants.

Due to their superior mechanical properties and their excellent biocompatibility, pure titanium and titanium alloys have been widely used in both orthopaedic and dentistry applications. The superior biocompatibility of titanium and titanium alloys is due to their inertness, which is caused by the formation of an adherent oxide layer that rapidly turns into titanium dioxide (titania: TiO_2) on exposure to the air. The oxide creates a stable layer on the device and provides good bedding to bond with hydroxyapatite, which is the primary organic component of bone. However, despite the promising properties of bulk titanium, there is a need to improve the surface properties of the implant to avoid the loosening of the device as a result of

wear debris, stress shielding or movement of the implant in the body. For example, most of the problems with the dental implants (endosseous) occur at the interface of the implant and tissue, which can lead to loosening of the device. Therefore, the success of implant aging is dependent on many physio-biological factors of the surface of implant.

Understanding of the entire process of implant adaption to the body is essential to the design of a proper implant surface with certain properties (i.e., surface topography, surface chemistry, and surface energy) to avoid the events that lead to the failure of implants. Some of the problems that result in the failure of implanted devices include:

1) Mechanical factors, such as high stress at the interface, and the migration of implant devices that are dependent on the mechanical properties of the material and the implant geometry. The presence of high stress in the bone can trigger biological signals and the activation of bone cell formation (i.e., osteoblast cells), resulting in an increased bone mass and size in order to cope with the added stress. Higher bone mass enables the bone to tolerate larger loads; however, the increased mass also causes the migration and loosening of the implant. To avoid these problems, a material with mechanical properties similar to and compatible with the bone properties should be chosen.

2) Wear debris, which is caused during mechanical motion, friction or corrosion of the implant from various biological activities. The presence of the wear particles around the bone can also lead to the dissolution and degradation of the surrounding bone.

3) The encapsulation of the implanted device, which usually manifests itself in the first days of the implantation. After a foreign material is implanted in the body, various processes occur around the new device, including acute or chronic inflammation, the formation of tissue, foreign body reaction and eventually fibrosis. The results of these processes determine either the

adaptation of the implant into the body (i.e., regeneration of tissue around the material), or the encapsulation of the implant to isolate it from the body. Surface properties, such as chemistry, energy, and topography, can also be responsible for this failure.

1.2 Objective

In this study, the objective is to modify the surface properties of commercially pure titanium (CpTi), through the creation of multi-scale surface topography and by altering surface chemistry (i.e., variations in the oxide structure, and titanium phase transformation) to improve the osseointegration process. To achieve this objective, a single-mode, pulsed, Ytterbium nanosecond fiber laser with a randomly polarized Gaussian beam is used. The laser material interaction results in the formation of a thick oxide layer with proper structure for biocompatibility improvement. Furthermore, utilizing a single laser path results in self-assembled pseudo periodic (PP) structures on the material surface. Controlling the laser parameters controls the size, shape and roughness of the developed micro-structures. This laser processing method is capable of altering the surface roughness and forming parallel grooves, simultaneously.

Therefore, the primary objective of this thesis is to:

Develop a controlled method for improving biocompatibility of titanium implants by altering surface properties, using a single mode pulsed Ytterbium nanosecond fiber laser irradiation under different laser parameters and by exposure to different effective energies and different oxidized media for creating optimum surface topography and chemistry.

To this end, the following tasks were pursued:

- Develop a controlled laser processing protocol to achieve an optimized surface;
- In vitro testing and investigation of cell adhesion on the candidate surfaces.

1.3 Organization

The first chapter of this thesis provides a brief introduction. A comprehensive literature review of the osseointegration process, particularly the effect of the chemistry and topography on the process, and different modification methods is presented in Chapter 2. In Chapter 3, the experimental design for the development of the modified surfaces is explained. The effects of the laser parameters, effective energy, and media on the micro-structure, topography, hardness and chemistry are studied. Surface characterization is performed using Scanning Electron Microscope (SEM) Energy-dispersive X-ray spectroscopy (EDAX), X-ray Diffraction (XRD), optical profilometry and nanoindentation analysis. In Chapter 4, laser processing in liquid media and its effects on different types of oxidation is studied. In Chapter 5, the effects of laser modifications on different stages of osseointegration are studied through SEM analysis, enzymatic detachment analysis of alamar blue and through trypsinization testing. Finally, the conclusion and future work are presented in Chapter 6.

2 Chapter Two – Literature Review

2.1 Introduction

Surface modification of implants for the purpose of increasing biocompatibility is dependent on many factors, such as the material used for the implant, cell type and size, and the extracellular matrix required for cell culturing. In this chapter, the biological studies that have been conducted to understand the integration of osteoblast cells (i.e., bone forming cells) into the surface of titanium and titanium alloys are reviewed. Different types of surface modifications to improve biocompatibility of endosseous and bone implants are discussed. The studies are categorized into four different types of modification; i) generation of nano roughness, ii) generation of micro roughness, iii) engraving microgrooves, and iv) modification of the surface chemistry of the substrate. Different surface modification techniques, including laser-processing techniques, are introduced. The scarcity of literature on the utilization of a fiber nanosecond pulsed laser processing for surface modification of titanium substrates to be used as bone/dental implants is also discussed.

2.2 Bone Structure and Bone Cells

Bone structure is divided into two categories: Cortical bone and Trabecular bone, which are composed of collagen (organic) and hydroxyapatite (inorganic) components. Cortical bones are stiffer than trabecular ones (with the Young's modulus of 17 GPa vs. 1 GPa) and have less porosity (with 30% porosity vs. 50-90% porosity of trabecular bones). Therefore, the implant material that is chosen to replace bone in the body should exhibit at least this stiffness [1].

There are different types of bone cells; among them, osteoblast, osteoclasts, and osteocytes are responsible for osseointegration. Osteoblast cells are composed of collagen I and hydroxyapatite. The osteoblast and osteoclast cell sizes are approximately 30-50 μm and 20-100 μm, respectively. The turnover of osteoblast and osteoclast reaction leads to bone remodelling. Osteoclasts resorb the bone and osteoblasts immediately fill the created cavities in the bone and form new bone, consisting of bone collagen and other protein [2, 3].

Different proteins are involved in osteoblast adhesion. According to their roles in the adhesion, these proteins are categorized as: extracellular matrix (ECM) proteins, cytoskeleton proteins and adhesion molecules. ECM proteins are composed of 90% collagenic and 10% non collagenic proteins. They are responsible for the first stage of cell-surface interaction, which is the protein absorption. Cytoskeleton is a network of fibers composed of proteins contained within a cell. Adhesion molecules are proteins on the cell surface, involved in binding with other cells or ECM.

Adhesion molecules are categorized according to the type of the ligands that they are attached toThe four categories are (i) selectins, (ii) the immunoglobulin super family, (iii) cadherin, and (iv) integrin. Cadherins and integrins are the two primary important types and are inherent in the adhesion process between ECMs and the bone cell. The adhesive property of bone proteins is due to the Arg–Gly–Asp (RGD) sequence, which is specific to the fixation of the cell membrane receptors, such as integrin. The adhesion of the cell-substrate through integrin forms the focal adhesion sites. The external face of the sites interacts with the cytoskeleton structure through various proteins including: talin, paxillin, vinculin, tensin and catenin, as shown in Figure 2-1. These proteins send a signal from the integrins to the actin filaments. The cytoskeletal response to the signals sent from the substrate has a significant biological response

to cell adhesion and cell topography. The characteristics of the surface affect the signalling process and, therefore, influence cell behaviour. The distance between the cell and substrate for the formation of focal adhesion (FA) for osteoblast cells is in the range of 10-15 nm [4].

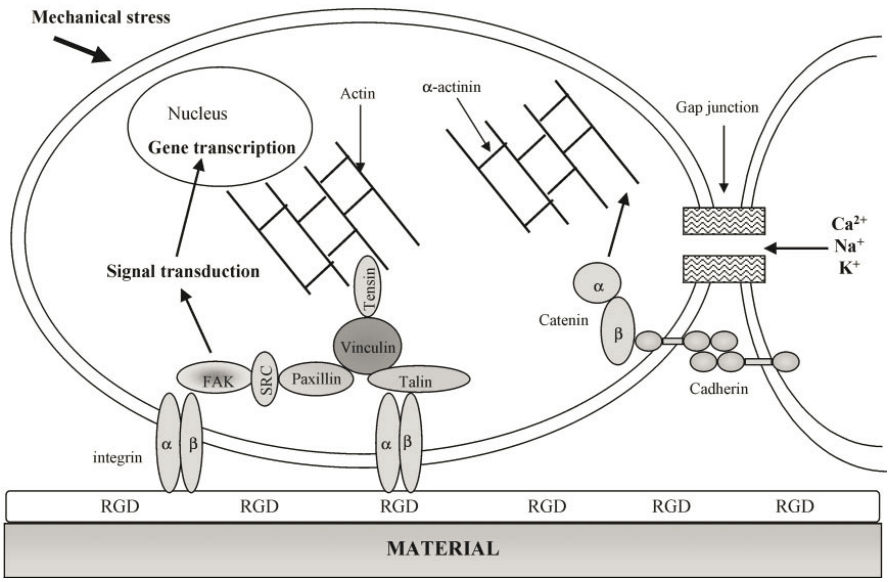

Figure 2-1 Cell proteins that are involved in the cell adhesion process. adopted from [5]

The adhesion of an osteoblast cell to the biomaterials is achieved through the bonding of the integrins with the surface of the biomaterials (i.e., FA points). Therefore, to improve the adhesion of osteoblast cells, the surface of implants must be modified to facilitate bonding with the integrins. The effect of the surface topography and surface chemistry modifications on the osseointegration process is discussed in the following sections.

2.3 Materials Exhibiting Bone Bonding

When an artificial material is designed to be implanted into the body, the surface property of the material is critical in the improvement of the cell integration. Surface properties must be modified in such a way that the osteoblast cells can easily bond to the surface without bonding to the fibrous cells. It has been reported by previous researchers that most of the materials that have been shown to form bone bonding contain crystal apatite or its constituents (i.e., CaO, P_2O_5) in their components [6]. However, it was later proven that the essential requirement of biomaterials used as bone in the body to form bone bonding is the capability to form bone-like apatite on their surface. Therefore, the surface must have some functionality that is effective for the nucleation and super saturation of apatite in respect to the surrounding apatite in the body and the material does not necessarily need apatite in its structure [6,7]. Therefore, metals with a high strength can be modified to improve their surface properties and increase the chance of bonding to the apatite structure. Titanium and titanium alloys have shown superior properties for fulfilling the above-mentioned criteria.

2.4 Titanium and Titanium Alloys

The selection of the materials for implant into the body is dependent on their applications. A number of different materials have been used as orthopaedic and dental implants, all of which required tolerating high load bearing conditions. Typically, titanium and its alloys are chosen for use in biomedical devices, mostly for hard tissue replacements in orthopaedics and dentistry [1] as their high strength to weight ratio, and low density make them ideal for orthopaedic implants, which require a high load bearing with low weight parts.

The relatively low Young's modulus of titanium and its alloys results in reduced stress shielding, corrosion resistance, formability, and proper fatigue strength. Titanium and its alloys are also shown to have superior biocompatible properties due to the presence of an oxide layer of titania, which is formed by exposure to the air. The presence of the 2-5 nm oxide layer provides the stability and appropriate chemical inertness, corrosion resistance and biocompatibility of the titanium and titanium alloys [8,9]. The increased biocompatibility results from the negatively charged oxygen TiO, which has ion exchange properties and can bind to the calcium ion in the presence of body fluid. TiO_2 has the ability to bind calcium, serum proteins, and acid macromolecules, such as albumin and glycosaminoglycans.

Among all the titanium alloys, commercial pure titanium with an α structure, Ti-6Al-4V with an $\alpha+\beta$ structure, and nickel-titanium alloys with special shape memory effects with a metastable β structure (NITINOL) are the most commonly used in biomedical applications.

Despite the proper bulk properties and favourable characteristics of titanium for biomaterial applications, sometimes it cannot be integrated into the body without loosening between the implant and surrounding bone [10]. To prevent this problem there is a need to conduct surface modifications. In the following sections, a review of various modification techniques for titanium and titanium alloys and the influence of the material properties (i.e. mechanical, chemical and physical) on the biological behaviours is presented.

2.5 Mechanical and Tribological Properties of Ti and Ti Alloys

The mechanical properties of an implant affect the accumulated stress on the surface. The stress on the implant sends a signal to the bone-modeling unit (osteon) to activate the bone remodelling process. This happens as the result of differentiating of the osteoclast cells and

activation of osteoblast cells. The signals sent from the accumulated stress identify whether the density and mass of bone needs to be increased, decreased or remain in balance. An increase or decrease in the mass of the implanted bone leads to loosening or breaking of the implant, respectively. Therefore, it is critical to select a material with a high strength and properties close to the bone properties to keep the stress distribution in balance [10].

Titanium and its alloys demonstrate very promising properties for dental and orthopaedic implants due to their high strength (i.e., yield strength 692-1060 MPa, ultimate strength 785-1100 MPa), and low Young's modulus (i.e., 74-110 MPa). However, metals exhibit poor tribological properties, including low wear and abrasion due to the inferior hardness (i.e., 70 HRB, 24 HRC). Various methods are suggested in the literature [11-13] to improve these mechanical and tribological properties of titanium.

2.6 Chemical Properties of Ti and Ti Alloys

The surface chemistry of an implant determines the osseointegration process. The chemical composition of a surface affects the surface reactions. The surface layer contains reaction bonds and the exchange of water and different ions influences the binding of the proteins to the surface. The peptide sequence molecules (i.e., RGD sequence), which are derived from bioactive sequences, result in the increase of the integrin-mediated bonds and improve the adhesion of osteoblast cells. These sequences can be inactivated by macro molecular interactions; therefore, in order to avoid inactivation surfaces of the implanted materials are usually coated by other molecules (i.e., Hydroxyapatite, Oxide layer). Hydroxyapatite (HA) is one of the key components of bone. Synthesized HA has good bioactivity properties that form a coating on the surface of the material to modify the chemical property of the surface and it has been

demonstrated that an osteoblast can spread well on the HA coated material due to its bioactivity. However, in spite of the good properties of HA (i.e., inertness, and bioactivity), it has been shown that osteoblast cells can be better differentiated on a non-coated titanium substrate [14].

The oxide layer on titanium and its alloys improves the corrosion resistance, adherence, and bioactivity of the metal [11], thereby promoting cell adhesion and infiltration [6]. The tribological properties and wear rate of the natural oxide surface is a function of the oxide layer's thickness [63,64]. XRD analysis shows a variety of titanium oxide on the surface of the titanium, such as Ti_3O, Ti_6O, Ti_2O, Ti_3O_2, TiO(II), Ti_2O_3(III), Ti_3O_5, and TiO_2(IV), with a gradual change of the Ti/O ratio and corresponding physical properties. This change is due to the high solubility of oxygen in titanium and the fact that titanium exists in different oxidation states. Titania (TiO_2) is the most stable oxide composition of titanium (in addition to the TiO composition) that has a significant effect on the biocompatibility of the materials. There are three polymorphic forms of titania structures: a) stable black rutile; b) metastable colorless anatase, which converts to rutile at high temperatures; and c) unstable white brookite [65]. Despite the higher stability of rutile, anatase shows the best properties for biomedical applications as it exhibits a stronger interaction with metals and a strong ability to absorb OH^- and PO_4^{3-}. In addition, the high tendency of anatase to bond with free ions aids the deposition of hydroxyapatite on bone [64,66,67].

The surface charge of the substrate is another property that affects the osseointegration process. It has been shown that cells spread better on positively charged surfaces than on negatively charge surfaces [16]. The hydroxide ions (OH^-) of titanium can lead to the formation of negative and positive surface charges according to the following chemical reaction:

$$Ti - OH + H_2O \Leftrightarrow \left[Ti - O\right]^- + H_3O^+$$
$$Ti - OH + H_2O \Leftrightarrow \left[Ti - OH_2\right]^+ + OH^-$$

This shows that the oxide layer on titanium surface has acidic properties. The normal PH of blood and interstitial fluids in the body is 7.35-7.45. In the first two weeks of implanting a device in the body, the PH decreases to 5.2 due to presence of amino acid and chloride ions in the blood plasma, but returns to 7.4 within two weeks. However, titanium and titanium alloys corrode either too quickly or too slowly in this environment. The presence of TiO_2 can cause the surface to switch to the slow corrosion mode [1].

2.7 Physical Properties of Ti and Ti Alloys

Physical properties refer to the different surface characteristics, including the surface energy and surface topography. Surface energy is influenced by the unsatisfied bond on the surface. Surfaces with high energy have a high tendency to absorb and form new bonds with the surrounding proteins, which results in a better osseointegration quality [17-19]. The presence of the physio-chemical bond makes the surface bioactive. An increase in the surface energy leads to a corresponding increase in the hydrophilicity and wettability of the surface, thereby increasing the osteoblast cells adhesion [20]. The effect of hydrophilicity to increase the adhesion is due to the mediating monocyte and differentiating macrophage, which helps proteins form an advantageous coating on the surface and improve adhesion [21]. However, it has been shown that osteoclast adhesion sometimes decreases with a high surface energy, which can also increase the adhesion of undesirable cells, such as fibroblasts or osteoclasts, on the implants [22 23]. Therefore, an optimized surface energy that leads to the balance between osteoblast and other cells should be identified.

Unlike some theories, which are derived from the belief that the surface chemistry plays the most important role in the bioactivity property of materials [24], surface topography has been

shown to demonstrate a significant influence on cellular behaviour and bone formation. Surface topography can affect cellular behaviour on different scales [25,26, 27].

In the literature, the effect of each topography scale on cell behaviour is categorized as follows:

- Nano-topography (structures smaller than 1 micron)
- Micro-topography (structures larger than 1 micron)
- Micro-grooves

A surface with all three topographies may include the benefit of each.

2.7.1 Effect of Surface Nano-Topography on the Osseointegration Process

Previous studies have demonstrated an increase in osteoblast adhesion to different materials due to nano-topography. This reveals that cells have the ability to sense the nano-structures and somehow can respond better to surfaces with nano-structures [28,29]. The nano-features of a substrate affect cell adhesion and cell mobility. The presence of nanostructures within the range of 11-38 nm enhances osteoblast cell spreading, adhesion and proliferation. Andersson et al. have suggested that having nano-structures in the range of 70-100 nm on the surface of implants function directly with the focal adhesion of the cell [30]. It has been shown that the closest distance of a cell and substrate is approximately 10 nm. This distance is due to the length of focal contact points, which are recorded at 10-15 nm. Therefore, the nano-structures should be larger than this distance for bonding [31,32]. The exact mechanism of how cells respond to the nano-structures is still unknown; however, a number of theories have been suggested to explain the effect of nano-structures on cellular behaviour:

- Matching of the nano-structures with natural extra-cellular matrix proteins and binding of vitronectin and other adhesive proteins [33,34].

- Increase of osteoblast cell adhesion to nano-structures as the result of an increase in the particle boundaries with higher percentages of possible adhesion sites [28]. These nano-structures will result in an increase in the organization of the cytoskeleton elements, especially actin [35]. They will also lead to the alternation of the cytoskeletal structure of cells on different surface characteristics [36].

- Influence of the mechanical, topographical and physiochemical properties at the nano scale due to the different surface properties present at the atomic that are influenced by quantum phenomena [37,38]. Therefore, the interaction of a cell with a substrate is different at the nano scale as could be seen in Figure 2-2. The effect of cell-surface interactions at the nano scale could be explained by the actin organization behaviour, affecting the cell behaviour and cell modulus, and the response to its environment. Actin stress fibres contribute to the viscoelastic properties of cells, by the distribution of actin on the surface, which results in a decrease in the elastic modulus of the cells. This decrease of the elastic modulus enhances cell spreading, adhesion and cell proliferation [36].

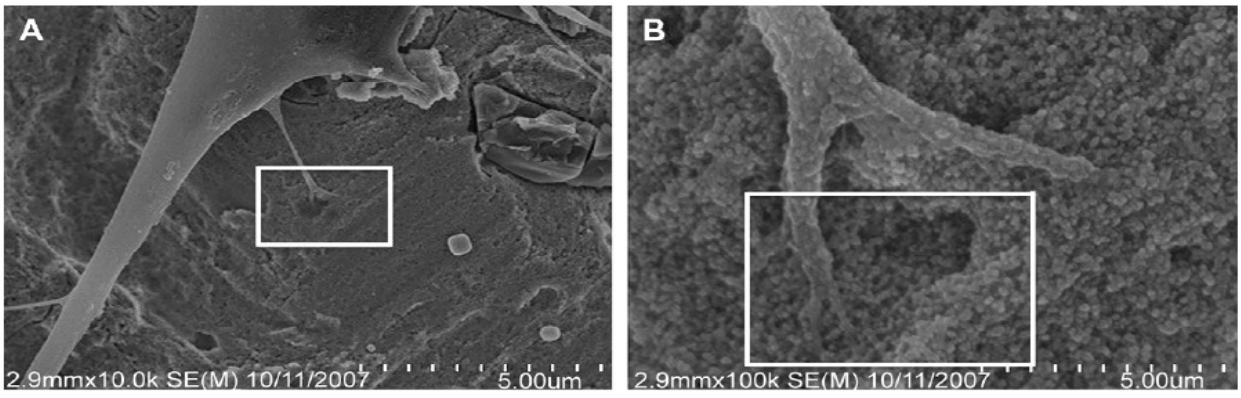

Figure 2-2 Nano-structure, in the range of 20-40 nm, interactions with integrin proteins on the cell, adopted from [37]

2.7.2 Effect of Surface Micro-Topography on the Osseointegration Process

The significance of micro scale topography on cell behaviour and on the different phases of the osseointegration process has been studied for decades. Some researches have reported improved cell adhesion or proliferation on rough surfaces [28], while others have found the opposite [5]. Cooper states that surface topography has different effects on different stages of osseointegration; therefore, the effect of micro-topography on cell behaviour must be considered separately at each stage of cell attachment, adhesion, proliferation, and differentiation [39].

The influence of surface micro-topography on proliferation has conclusively demonstrated a decrease of cell proliferation due to the increasing roughness. An inverse relationship between cell proliferation and differentiation has also been reported [40]. From these findings, it can be concluded that differentiation increases on rougher surfaces where the proliferation is low.. Increased cell differentiation on rougher surfaces has been observed in several other studies [41,42].

The different cell behaviours observed due to surface roughness in different analyses may be a result of the presence of different conditions, such as different materials and cell types. Kunzler et al. have studied the influence of surface roughness on both osteoblast and fibroblast cells on a surface with a wide range of roughness gradients. As a result, the proliferation rate of osteoblast cells was shown to significantly increase as a function of the roughness increase, whereas fibroblast cells demonstrated the opposite proliferation behaviour; however, both osteoblast and fibroblast morphology were found to be similar [22].

Several studies that investigated the behaviour of osteoblast cells on the titanium substrates reported an increase in cell adhesion and ECM mineralization on rough surfaces [43-46].

There are several different, well-accepted theories (described below) that explain the influence of micro roughness on improving cell behaviour, despite the type of cell or the experimental condition.

- Ricci et al. explained the effect of micro-topography through the contact osteogenesis concept, which is developed according to the differences in the distance and contact osteogenesis. According to their theory, any condition that forms the contact osteogenesis improves the bone growing and healing processes. Increasing the surface roughness within the range of the platelet activates the platelet and also increases the surface capacity to retain the fibrin clot. The resultant undistributed progression of osteoconductive growth, such as osteoconductive and de novo bone formation, is the key to contact osteogenesis. Increased roughness and topographical enhancement facilitates the stabilization of a fragile ECM scaffold for the conduction of cells to the implant surface. Based on this theory, the best topography is a roughness in the range of 1-5 μm [47-49]. Figure 2-3 shows the effect of micro-topography on the contact osteogenesis.

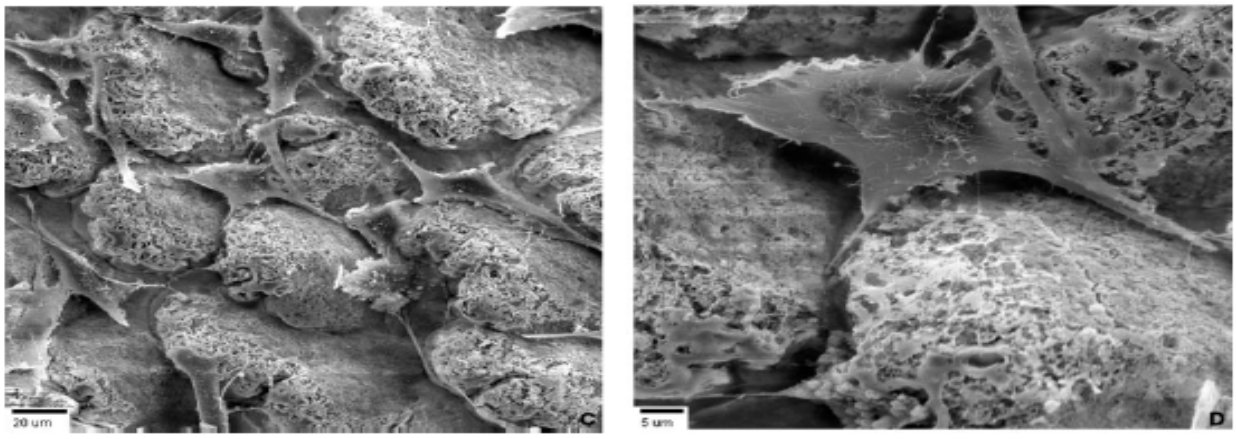

Figure 2-3 Effect of micro roughness on the integration of osteoblast cells, adopted from [47]

- Davies et al. pioneered a popular theory to explain the effect of surface roughness on osteointegration [2]. Their theory is based on the bone-bonding concept. This theory involves the structure of the resorbed bone surface and the cement line interface between the implant and bone. In this model, the cement line acts as an anchor between the new and old bone in the body. This concept can help to simulate the phenomenon to modify the implant surface by forming an interfacial cement line on the surface for anchoring to the surrounding bone. Therefore, a surface that has the properties to allow a cement line to form can simulate the characteristics of the resorbed surface, thereby providing a proper bedding structure for the osteoblast to initiate the bone remodelling process.

- Another theory that is proposed by several authors describes the advantage of micro roughness for improving mechanical interlocking at the micro stage due to an increase in the bone implant interfacial shear strength with rougher surfaces [50-53]. In support of this theory, the biomechanical theory of Hansson and Norton established a mathematical relationship between the roughness and interfacial shear strength [51]; this theory has been further supported by several other studies [30, 52].

- Another theory proposed by Schwartz et al. explains the improvement of osseointegration on surfaces with micro-topography as a result of the cell signalling process [46]. The proliferation rate of adherent cells is measured as an index of cytocompatibility. Surface-to-cell signalling results in an increased rate of proliferation [45].

2.7.3 Effect of Micro-grooves on the Osseointegration Process

Other than providing a uniform roughness on the surface, the presence of the parallel microgrooved topography on surfaces is significantly effective in improving cellular behaviour and bone formability.

Microgrooves align the cells and guide them to line up in the grooves. This phenomenon is called contact guidance. The biological effect of the grooves on cells has attracted many scientists [54-60]. It has been proven that the grooves create a pattern for the mechanical stress that influences cell spreading in an aligned direction, as shown in Figure 2-4. The alignment of the cell spreading can be explained by the fact that the cell sends signals through the actin filaments to its surroundings to form focal adhesion points that start spreading and moving. Cell signalling propagates in different directions; however, when it encounters the edges of the microgrooves, the signalling cannot propagate through the blocked faces. Therefore, the cell signalling in a non-blocked direction directs cell spreading. Aligning cells in one direction improves cell proliferation and cell differentiation and offers a better cell growth environment [55]. The orientation of the cells in the same direction provides the bone with the uniform mechanical properties. Moreover, the microgrooves reduce scar tissue (fibroblast) formation and promote osseointegration [61].

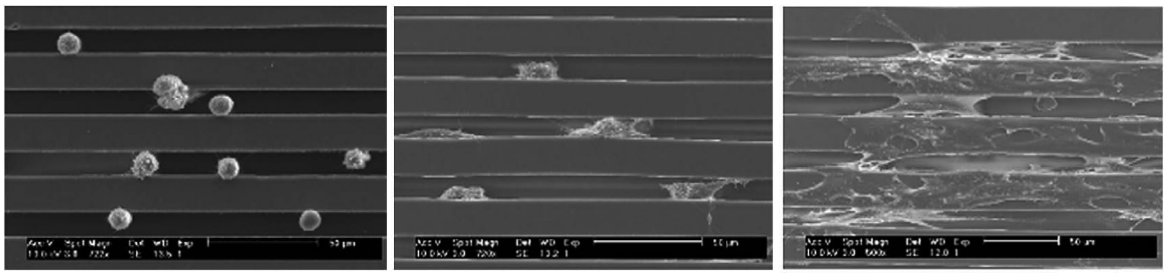

Figure 2-4 Effect of parallel microgrooves on HOS cell orientation after (a) 2h, (b) 4h, (c) 5 days; adopted from [60]

The effective range of the microgrooves is between 3 and 30 μm. Chesmel et al. reported that osteoblast cells begin orienting on a microgroove with a depth of 5 μm and ignore the surface topography on a 0.5 μm groove [56]. Chehroudi et al. found that epithelial cells are oriented along the long axis with 10 μm deep grooves on a titanium-coated implant [57]. The width of grooves is also important for the orientation of the osteoblast. No cell alignment is found on surfaces with the grooves wider than 120 μm; [58].

The shapes of the grooves have also been shown to influence cell behaviour. In contrast with previous studies, where grooves with continuous edges (sharp edge) were superior to those with discontinuous edges [59], discontinuous edges have more recently been shown to behave well for improving contact guidance and cell alignment [61].

2.8 Modification of Titanium for Improving Osseointegration Properties using Non Laser Techniques

Various methods have been utilized to modify the surface of titanium-based implants to improve bone formability and the cell adhesion process. There are different techniques of altering the surface properties of titanium to improve cell behaviour at each stage of the osseointegration. These techniques include mechanical (i.e., machining grinding, blasting), physical (i.e., thermal spraying, physical vapour deposition, ion implantation), and chemical techniques (i.e., chemical treatment, so-gel coating, chemical vapour deposition) [11,74]. A comprehensive study of the advantages and disadvantages of different methods of modifying titanium for improving osteoconductivity was completed by Liu et al. [11].

One of the main chemical modifications for improving osseointegration is to increase the anatase structure on the surface of the implant. The effect of different techniques on the anatase-rutile transition has been investigated in different studies [68-71]. The anatase-rutile transition can be controlled by controlling the solidification process [68] and also by inducing chemical reactions [69]. Thermal oxidation is the most favourable method for application on implants because it results in the formation of a thick, highly crystalline titania film on the surface [68]. Laser processing is shown to be an effective thermal treatment method for the formation of a thick anatase structure due to the fast annealing process [71,72]. Hydrogen peroxide alone or with a mixture of an acid or metal chloride (i.e., without a laser) has also been used for surface treatment of titanium to induce chemical reactions to form oxide layer [64,73].

2.9 Modification of Titanium for Improving Osseointegration Properties using Laser Based Techniques

In this section, the focus is on the studies that have utilized laser processing techniques for modifying the surface of titanium. Laser processing is an advanced technique used to modify the surface of metals to improve their biocompatibility [75,76,77]. Laser processing has certain advantages over other surface treatment methods due to its ability to simultaneously control the topography and chemistry of the modified surface. Conventional techniques can only modify either randomized topography or the chemistry of the surface. In the following sub-sections, the effect of laser processing techniques on different surface alternations is explained and the advantages of the proposed method over conventional laser processing methods are described.

2.9.1 Laser Processing Techniques for Surface Composition Modification

One of the advantages of laser processing is the presence of heat, which facilitates the generation of a thick oxide layer on the substrate. There are different techniques for modifying and increasing the oxide layer of titanium surfaces, including anodization, oxygen diffusion, ion implantation, sol-gel direct oxidation, electro-deposition, DC magnetron sputtering, RF sputtering, chemical vapour deposition, and thermal oxidation [11]. Among all of these methods, thermal oxidation is the most favourable method for modifying implants as it results in the formation of a thick, highly crystalline, oxide film, which includes titania, on the surface [15]. Laser processing techniques, including pulsed laser deposition [78-81] and pulsed laser irradiation [82-85], have been shown to be very good thermal treatment methods for modifying the surface of titanium and its alloys. The advantage of the laser treatment method over other thermal treatment methods is in its annealing conditions (i.e., temperature and rate). The formation of different types of titania structures is highly dependent on the annealing process. Laser irradiation is the best choice to form a thick layer of anatase structure on the surface, which is the best titania structure for biocompatibility. Pulsed laser irradiation can also be used to modify the surface topography by creating micro-structures on the surface while forming the oxide layer using the perfect annealing process; this method does not alter the lattice of the material nor does it cause any dramatic phase change of the material.

Laser processing in an oxide medium has been conducted to increase the thickness of the titania [86]; however, it has been shown that laser processing in the oxide medium also affects the topography of the structure, unlike laser processing conducted in air [86-89]. There have been some studies on the effect of oxide liquid mediums on the chemistry of titanium [88]; however, there is no reported study on laser processing using hydrogen peroxide (HP) as the

medium. In this study, we conduct the laser processing using the pulsed nanosecond fiber laser on the samples that are immersed in HP to investigate its effect as an oxidized medium.

2.9.2 Laser Processing Techniques for Creation of Micro-Grooves on the Titanium Surfaces

A laser micro ablation method has been used to modify the topography of the titanium surface through the creation of microgrooves. The advantage of this method is the formation of localized, multi-scaled (i.e., from a nano to micro roughness) roughened structures on the edges of the grooves under laser irradiation. . The micro scale roughness activates the platelets and retains the fibrin clot. The roughness also provides good sites for focal adhesion during cell locomotion and spreading and increases the interfacial strength of the adhesive cells [90-96].

Different laser techniques have previously been used to create the microgrooves. Ricci et al. used an Excimer ultra-violet (UV) laser with large area masking techniques and a top-hat intensity profile for creating the microgrooves, as shown in Figure 2-5(a). However, due to the high photon energy in the UV wavelength range, micro-cracks and a heat-affected zone (HAZ) appear on the surface [61,97]. To avoid such cracks Diode Pumped Solid State (DPSS) lasers are substituted for the UV lasers. Figure 2-5(b) shows one of the structures developed by DPSS laser. Nd:YAG and Nd:YVO_4 IR lasers were also used to form microgrooves due to their good laser beam quality with Gaussian beam intensity distribution [94,98,99]. Both DPSS and IR lasers provide a focused high fluence laser beam for the creation of microgrooves on metal surfaces. The depth of the grooves is affected by the laser energy per pulse and the frequency of pulses [98].

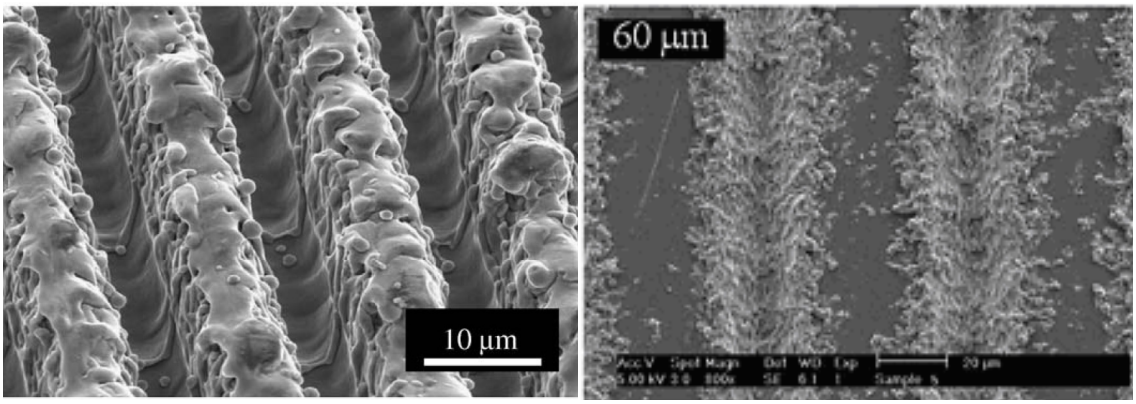

Figure 2-5 Microgrooves produced in laser processing using (a) Eximer Laser [61] and (b) IR laser [adopted from 103].

The structures that are generated using these laser processing techniques display micro-roughness in the width and depth of microgrooves that act as the sites at which bone cells adhere. However, to increase the cell adhesion and, more importantly, cell orientation, there must be more roughness on the spacing of the grooves, which have greater contact with the surrounding cells [103]. Therefore, in this study, a new surface modification is conducted using inexpensive nanosecond pulsed IR fiber lasers to generate microgrooves that have more nano roughness on the spacing of the grooves.

2.9.3 Laser Processing Techniques for Creation of Micro/Nano roughness on the Titanium Surfaces

For decades, laser processing has been a common method for creating micro features on different types of materials (i.e., semiconductors, metals, and ceramics) [100-122]. These features were developed using pulsed lasers at a variety of wavelengths from UV to IR, with short durations (i.e., ranging from nano to picosecond duration) and different intensities. Micro-structures can be created at the bottom of craters or can grow from the substrate by protruding

from the surface. Different theories are proposed to explain generation of micro-structures that protrude from the surface of materials including: the interference effect theory, which does not involve the photon wavelength explicitly [101], and capillarity theory that is governed by the instabilities resulting from the Marangoni effect [102,114]. The later theory explains the development of structures with periodic spaces that are equal to the laser's wavelength.

The formation of micro-structures with a spacing period equal to the laser wavelength has been explored be previous researchers [103, 115-121]. However, the theory behind the micro-structures with a higher period generated under pulsed laser irradiation is still vague and is under investigation [104,122]. When a laser irradiates the surface of a material, the electromagnetic waves interact with the materials. Usually, free or conductive electrons (i.e., seed electrons) are available on the surface. The absorbed laser irradiation energizes the free electrons and causes further collisions of the electrons, resulting in ionization. By irradiating more energy, the material is broken down until critical plasma density is reached and the dielectric material becomes absorbable. When a high intensity beam is used, the optical breakdown of the surface becomes a new issue to be considered in addition to the other thermal effects of the laser. Laser irradiation is one of the intense techniques that lead to the extreme thermodynamic non-equilibrium condition in a short time. Different phenomena may occur as a result of laser irradiation to the material, such as: optical breakdown, plasma formation, photomechanical effects, and thermal processes. The main process affecting the material as a result of laser irradiation may differ based on the laser properties, particularly the pulse duration of laser beam. The thermal and structural effects explain the theory, which results in the ablation of material using a laser with 1-100 ns pulse width. The effect of laser material interaction and the physics of

ablation in the 1-100 ns range for metals and the type of thermal analysis at a specific process parameters have previously been investigated [106,107].

The main theory behind the formation of micro-structures under irradiation of pulsed nanosecond laser is explained through melt displacement and the solidification process. The design of the experiment is discussed in the next chapter and the theory of the developed micro-structures using the study's laser system is identified.

2.10 Summary

The focus of this chapter was the study of the effect of material properties (bulk and surface properties) on the osseointegration process. The advantages of using titanium in bone and dental implants were presented. Different types of proposed surface modifications for improving the surface properties of titanium were introduced. Different techniques that are used for surface modification of implants were introduced with their associated physical theories. Laser processing is used as one of the main effective techniques for surface modification of titanium due to the unique solidification properties that permit simultaneous modification of both surface topography and chemistry. A comprehensive review on different types of lasers that are utilized for surface modification of titanium was presented, and a gap was identified with respect to the usage of the inexpensive nanosecond fiber IR laser for surface modification of titanium-based implants. In the next chapter, a laser processing methodology designed to overcome the gaps in the literature will be introduced.

3 Chapter Three –

Design of Experiments and Theoretical Analysis of the Pseudo-Periodic Micro-structure Formation

3.1 Introduction

In this chapter, a study of the formation of Pseudo-Periodic (PP) micro-structures resulting from irradiation by a single-mode, pulsed, nanosecond Ytterbium fiber laser on two materials (i.e., titanium and stainless steel) is presented. The effects of 100 ns pulsed laser beam properties, including laser power, laser frequency, beam polarization, laser spot size, angle of incidence, and scanning speed, on the formation of the PP micro-structures are also studied. The associated process parameters are grouped into two representing quantities: laser intensity and effective energy. The effects of these two quantities on the surface topography (i.e., shape, periodicity and roughness), surface chemistry (i.e., oxidation and titanium phase transformation), micro-structure on the heat affected zone (HAZ), and surface mechanical properties (hardness) are presented.

3.2 Material Preparation

To prepare the samples for the experiments, 0.6 cm thick titanium plates (Alfa Aesar, USA) were cut into pieces of approximately 0.5 cm x 1 cm. Each piece was mounted in hard bakelite under pressure and heat. The deposition surfaces were ground down on a circular grinding wheel by hand at 150 rpm with silicon-carbide paper and water for the coolant. The grinding of titanium was accomplished using an MD Piano machine with silicone carbide 25 paper and a paper grit progression up to 4000 was used. Each grit was used until the previous step's lines

were removed consistently across the ground surface. Mechanical polishing was conducted using 9 μm diamond suspension. The maximum physical pressure allowed by the operator was used to press the surface to the polishing pad. Each stage was performed until a consistent surface was formed. The final stage was a chemical-mechanical polishing with a mixture of colloidal silica (OP-S), and hydrogen peroxide (30%) on MD Chem plate. After each stage, the surface was cleaned with water, ethanol, and then compressed air. The sample preparation was determined to be complete when the material had a mirror-like surface.

3.3 Laser Setup

An opto-mechanical set-up is designed for this study. The set-up is used to deliver a single mode IR nanosecond Ytterbium fiber laser (IPG Photonics, YLR-1/100/20/20, MA, USA) with a Gaussian laser beam with maximum power of 20 W. The pulse repetition rate of the laser machine can be controlled between 20 and 80 kHz with a fixed pulse duration of 100 ns. The laser beam is randomly polarized and its output beam diameter is 7 mm. The laser system is controlled using a program written in MATLAB to control laser power and laser frequency. The schematic and physical images of the laser setup are shown in Figure 3-1.

As shown in Figure 3-1, the laser collimator is held vertically towards the sample, which is fastened to a micro-stage to control the working distance of the beam. The beam is then passed through the beam splitter, which is set in the laser path to control the power and polarity of the transmitted laser beam.

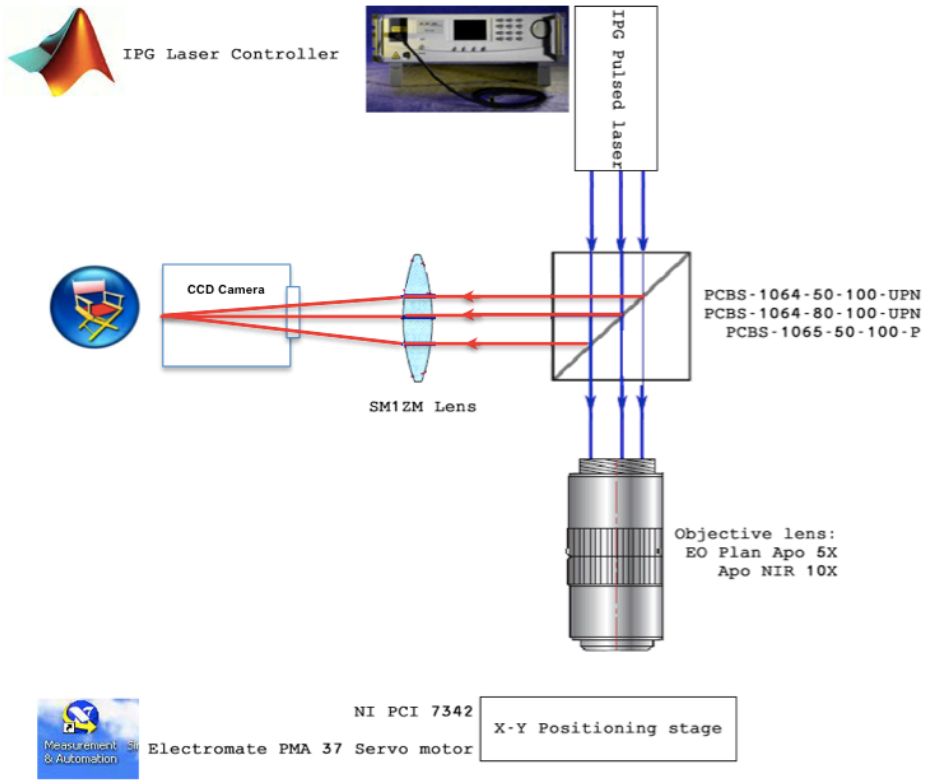

(a)

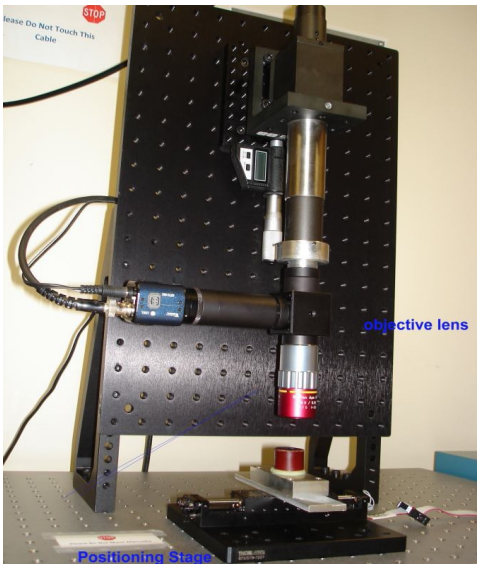

(b)

Figure 3-1 Schematic and physical image of the experimental set up

To see the effect of the beam polarization on the developed micro-structures, three different beam splitters were replaced in the associated mount for different tests. Two of the beam splitters transmit a fixed ratio of 50% (PCBS-1064-50-100-UNP) and 80% (PCBS-1064-20-100-UNP) of the beam and the third beam splitter is a polarizer (PCBS-1064-20-100-P), which transmits about 50% of the polarized laser beam (CVI Melles Griot).

Part of the beam is directed into the camera to capture an image of the substrate (1/3" CCD, Edmund optics-WAT 902H3 Supreme Monochrome Camera using a Cyberlink power director. The image is adjusted by passing through a non-rotating adjustable lens (Thorlabs SM1ZM) with a 4mm linear travel at a resolution of 0.5 mm per revolution. This high-precision zoom housing provides the ability to accurately control the exact working distance of an optical element within a system. The focal point is adjusted through several adaptors with different lengths.

The rest of the laser power is transmitted to the sample through the objective lens. Two different objective lenses are selected to focus the laser beam; EO Plan Apo 5X and M plan Apo NIR 10X. The specifications of the lenses are presented in Table 3-1. The diameter of the beam spot on the surface (d) at the associated working distance (WD) is found to be 13.85 μm and 6.9 μm for the above-mentioned objects. This is calculated using Equation 3.1 for the plane front circular beam, where λ is beam wavelength, f is the focal length, and D is the initial beam diameter (beam diameter out of collimator) [123].

$$d = 2.44\frac{f\lambda}{D} \qquad \textbf{(3.1)}$$

Table 3-1 Objective lens specifications

Lens	WD (mm)	Spot Dia. (μm)	Focal length (μm)
EO Plan 5X	34	13.85	14
NIR 10X	30.5	6.9	4.1

The scanning speed is controlled by locating the samples on the x-y stages (Edmundoptics #55-788). The stages are controlled using a PCI controller card (NI PCI-7342 2-Axis Stepper/Servo) that is programmed in LabVIEW.

The optical setup is capable of controlling different parameters, including laser power, laser frequency, laser beam spot, working distance (i.e., beam spot size diameter on the substrate), as well as scanning velocity, and media (i.e., shield gas, oxidized liquid medium). Variations in these parameters will lead to the formation of different structures with different geometries, chemical composition, contamination, and various HAZ and hardnesses, as shown in Figure 3-2

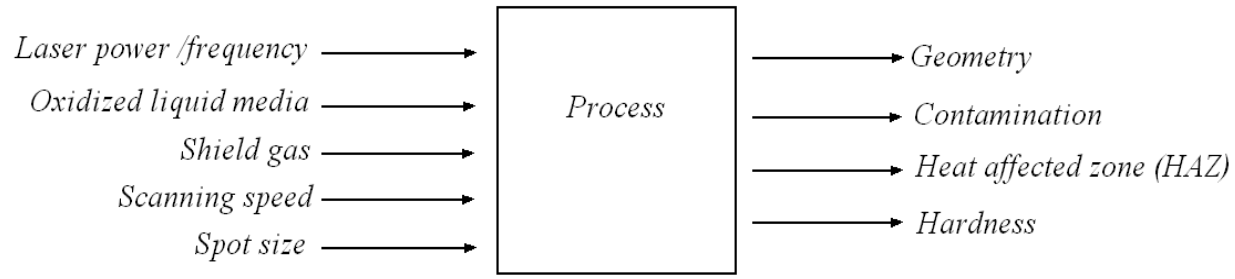

Figure 3-2 Overall input and output parameters of the introduced laser processing

The input laser power can be controlled with an IPG program as a percentage of the maximum laser power, which is 20 W. The output laser power on the workstation will exhibit a huge loss after passing through different lenses and other optical components. The output power on the workstation was measured by using a power meter (L30A thermal head, OPHIR). The power was changed from 30% to 100% of the maximum laser power, at increments of 10%. Different screening laser parameters are listed in Table 3-2. These sets of the parameters were changed during the "screening phase"; however, the variations of some of these parameters were observed to create no PP microstructures or have no meaningful effects on PP micro-structures. Thus, some of these parameters were kept constant, as will be noted in the following sections.

Table 3-2 Screening laser process prameters

Screening process parameters	Range	Increment
Laser power measured at the process zone	1-12 W (30%-100%)	10%
Laser frequency	20-80 KHz	10 KHz
Laser scanning speed	0.05-0.5 mm/s	0.005 mm/s
Laser beam diameter (with offset from WD)	20-160 μm	10 μm
Beam polarization	S-ray, P-ray, Circular	---
Angle of incidence	45-90 degree	5 degree
Media	Water/HP/Air	---

3.4 Experimental Methodology

3.4.1 Surface Topography Characterization

The effect of laser processing parameters on how micro-structures are being formed and their topography is observed via optical microscopy (BH2-UMA model Olympus microscope) and Scanning Electron Microscopy (SEM) (WYKO NT 1100 Veeco) analysis. The micro and nano roughness are quantified using an optical profilometry (JEOL: JSM-6460) analysis.

The average roughness (R_a) and root mean square (R_q) roughness are two amplitude roughness parameters that are measured over the specific length of (L) such that:

$$R_a = \frac{1}{L}\int_0^l |Z(x)|\,dx \qquad \textbf{(3.2)}$$

and

$$R_q = \sqrt{\frac{1}{L}\int_0^L Z^2(x)\,dx} \qquad \textbf{(3.3)}$$

where the definition of these parameters is conveyed in Figure 3-3.

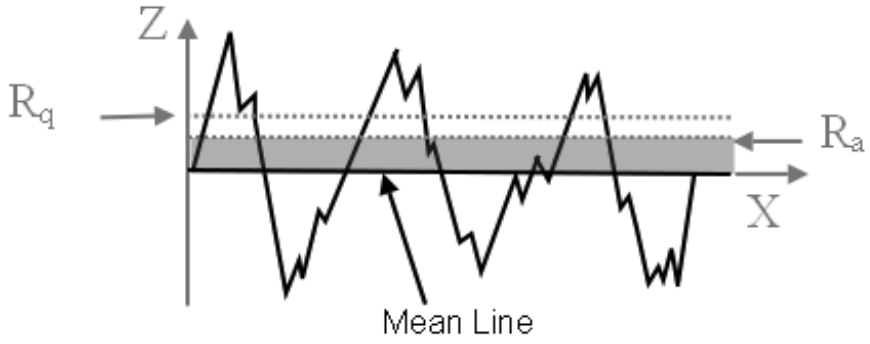

Figure 3-3 Two main amplitude roughness parameters; R_a and R_q (adopted from [www.finetubes.co.uk])

3.4.2 Micro-structural Characterization

Titanium alloys are in the form of alpha (α) and beta (β) classifications. Alpha titanium has a hexagonal close-packed, crystal structure, and beta titanium has a body-centered, cubic crystal structure, which is harder than the alpha structure. The Titanium alloy transus temperature is 883^0C. Below this temperature, the micro-structure consists of a mixed black alpha and white beta phase [89]. Deformation of micro-structures as a result of HAZ is also investigated through optical microscopy analysis. To do so, samples were polished and etched by Kroll's reagent solution (90–92% distilled water, 5% nitric acid and 3–5% hydrofluoric acid) for 30 seconds. Laser processing of the titanium samples results in changes in the micro-structure of the irradiated region.

3.4.3 Surface Composition Characterization

The chemical composition and structure of the modified surfaces were determined by both Energy-Dispersive X-ray spectroscopy (EDAX) (LEO FESEM 1530, Genesis, USA) and X-ray Diffraction (XRD) (Max AFC8, Rigaku, USA). The apparatus of the XRD machine has a total radiation voltage of 50 kV, with total current of 40 mA and power of 2 kW. Two collimators were selected to scan the surface: one with a 0.8 mm diameter and a total measurement time of 25 s and one with 0.3 mm diameter and a total measurement time of 60 s.

3.4.4 Surface Mechanical Properties Characterization

An increase in surface hardness is expected as a result of laser processing due to its effects on different properties, including an increase in the oxide layer on the surface [9]. The effects of

laser processing on mechanical properties of the developed surface are investigated through nanoindentation analysis, which is performed using a Hysitron Tribo Indenter machine and analyzed using Triboscan software. The effects of laser processing and the oxidized media are investigated in reference to the polished pure titanium. Six indentation locations are selected for the measurement. The surface hardness (H) is calculated using the Oliver-Pharr method (equation 3.4) where P_m is the maximum applied force and A is the indentation contact area [80]:

$$H = \frac{P_m}{A} \quad \textbf{(3.4)}$$

The Young modulus is averaged from the initial slope (equation 3.5) of load displacement curve.

$$S = \frac{2\alpha E_r A^{1/2}}{\sqrt{\pi}} \quad \textbf{(3.5)}$$

where α is the correction factor of the indenter shape, and E_r is the reduced modulus of elasticity, which is calculated based on the modulus of elasticity of the specimen and the indenter and the Poisson's ration (ν) defined by equation 3.6.

$$\frac{1}{E_r} = \left(\frac{1-\nu^2}{E}\right)_{specimen} + \left(\frac{1-\nu^2}{E}\right)_{indenter} \quad \textbf{(3.6)}$$

The main challenge in measuring surface hardness is the presence of developed roughness on the surface. To avoid polishing the roughness and destroying the developed path, the nanoindentation test is conducted on a cross section of the laser path. To complete the nanoindentation testing, the samples were cut through the developed laser path and remounted in the transparent mounts. The sample cross sections were then ground and polished prior to

testing. The nano-indenter detects the surface of a sample at five different points along a path of approximately 30 µm starting at the edge of the laser path cross section.

Two different comparisons have been made for this study: 1) Comparison of the results of the nanoindentation test at different laser conditions with a pure (i.e., unprocessed) sample; and 2) Comparison of the variations in surface hardness on the samples at five different points along the cross section of the laser path for the two laser intensities used, as illustrated in Figure 3-4.

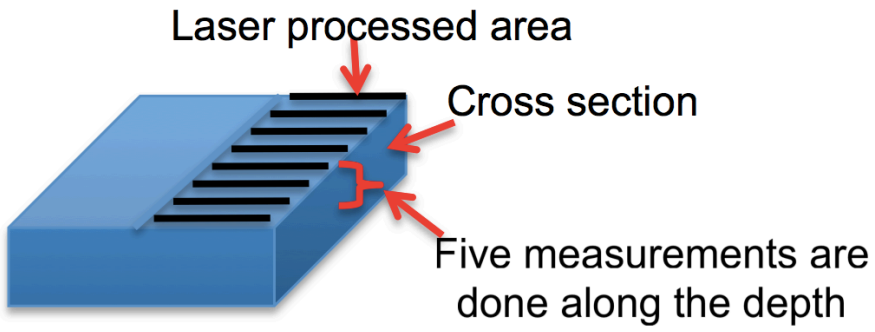

Figure 3-4 Different points at the cross section of laser path, where nanoindentation analysis is conducted

3.5 Results and Observations

3.5.1 Identifying the Main Process Parameters Effective in the Formation of the PP-Based Micro-structures

PP micro-structures are generated on the surface of the laser irradiated specimen. The micro-structures will then continue to grow, when additional pulses irradiate the substrate. In order to understand the theory of the process, the Design of Experiment (DOE) analysis is conducted in this section to study the effect of the several process parameters on the generation of the micro-

structures. In order to narrow down the significant parameters affecting the process, a screening procedure was conducted to determine the relevant screening parameters, as listed in Table 3-2.

Beam polarization has been reported as one of the main factors in the creation of periodic structures on titanium using ultra-fast laser systems [25, 47, 105]. In order to study if the beam polarization has any effect on the generation of the micro-structures, a polarized beam splitter (PCBS-1065-50-100-P, CVI Melles Griot, USA) was placed in the beam path. The results exhibited no significant changes to the micro-structures developed by the original beam, which was randomly polarized. As a result of this observation, beam polarization was set at the system default for the rest of the experiments.

The next parameter to be examined was the angle of incidence between the laser beam and the sample. In order to stimulate the angle of incidence, an angle was induced at the sample located on the workstation. The optical microscopy images of the generated micro-structures developed with the angle of incidence were less periodic than those generated by irradiation with the perpendicular beam. As a result of this observation, the angle of incidence was kept at 90° for the rest of the experiments.

Laser power was shown to be a significant parameter for the creation of micro-structures. Below a certain value of laser power, there is no considerable footprint by the laser on the surface. A significant increase in laser power will, result in melting the surface to a relatively deep depth, with no periodic structures formed on the surface. Therefore, it was concluded that PP structures develop on the surface of specimen only within a specific range of laser power at the process zone, between 8 to 12 W. Laser frequency, laser spot size and scanning speed have also been shown to be significant in the formation of the micro-structures.

To correlate the effects of all the parameters, two effective parameters representing the effects of the initiation and growth of the generated micro-structures were selected: 1) laser intensity and 2) effective energy.

Parameters that govern the initiation of self-assembled structures are represented by the laser intensity (I), introduced in equation 3.7, where P is the laser power and A is the beam spot size area.

$$I(W/cm^2) = \frac{P(W)}{A(cm^2)} \qquad \textbf{(3.7)}$$

The micro-structures will continue to grow by increasing the frequency and decreasing the scanning speed. The laser frequency is kept fixed at the optimum designed frequency of 20 kHz. This is done in order to achieve the maximum power. Therefore, the laser scanning speed determined to have the most significant effect on the growth of structures. To evaluate the amount of energy per surface area, the second effective parameter is defined in equation 3.8.

$$\tau_{eff}(J/m^2) = \frac{P(W)}{v(m/s)D(m)} = \frac{E(J/pulse)F(1/s)}{v(m/s)D(m)} \qquad \textbf{(3.8)}$$

where τ_{eff} is the effective energy, v is the process scanning speed, and D is the spot size diameter on the substrate.

All the significant parameters could therefore be included in the two main parameters of laser intensity and effective energy. Some of the representative parameters and the associated laser intensity and effective energies utilized for the generation of PP-based micro-structures are listed in Table 3-3 to be used for discussion related to the growth mechanism of PP structures. Laser

intensities and effective energies in this table are calculated at beam spot size of 50 μm. This spot size is measured based on the offset from the beam focal point at the working distance. At this spot size, the PP micro-structures have uniform roughness along the laser path width. Further increase in the spot size resulted in ununiformed roughness on laser path width. Thus the spot size value was kept constant.

Table 3-3 Process parameters effective in altering surface structure and their associated laser intensity and effective energy (F=20 kHz, D=50 μm)

#	P (W)	*v* (mm/s)	I (MW/cm^2)	τ_{eff} (x10^4 J/cm^2)
1	8	0.05	1	32
2	8	0.1	1	16
3	8	0.25	1	6.4
4	8	0.5	1	3.2
5	10	0.05	1.27	40
6	10	0.1	1.27	20
7	10	0.25	1.27	8
8	10	0.5	1.27	4
9	12	0.05	1.5	56
10	12	0.1	1.5	28
11	12	0.25	1.5	11.2
12	12	0.5	1.5	5.6

The trend of initiation and growth of self-assembled structures and their dependency on laser intensity and velocities is depicted in Figure 3-5 for titanium.

According to Figure 3-5 the formation of self-assembled micro-structures is initiated on the surface of titanium at an intensity of 1.27 MW/cm^2. Increasing the effective energy by decreasing the process speed (i.e., irritating more laser energy to the substrate) will result in the growth of these structures. The SEM and optical microscopy analyses demonstrate that self-assembled PP-based micro-structures do not develop at low intensities below 8 MW/cm^2.

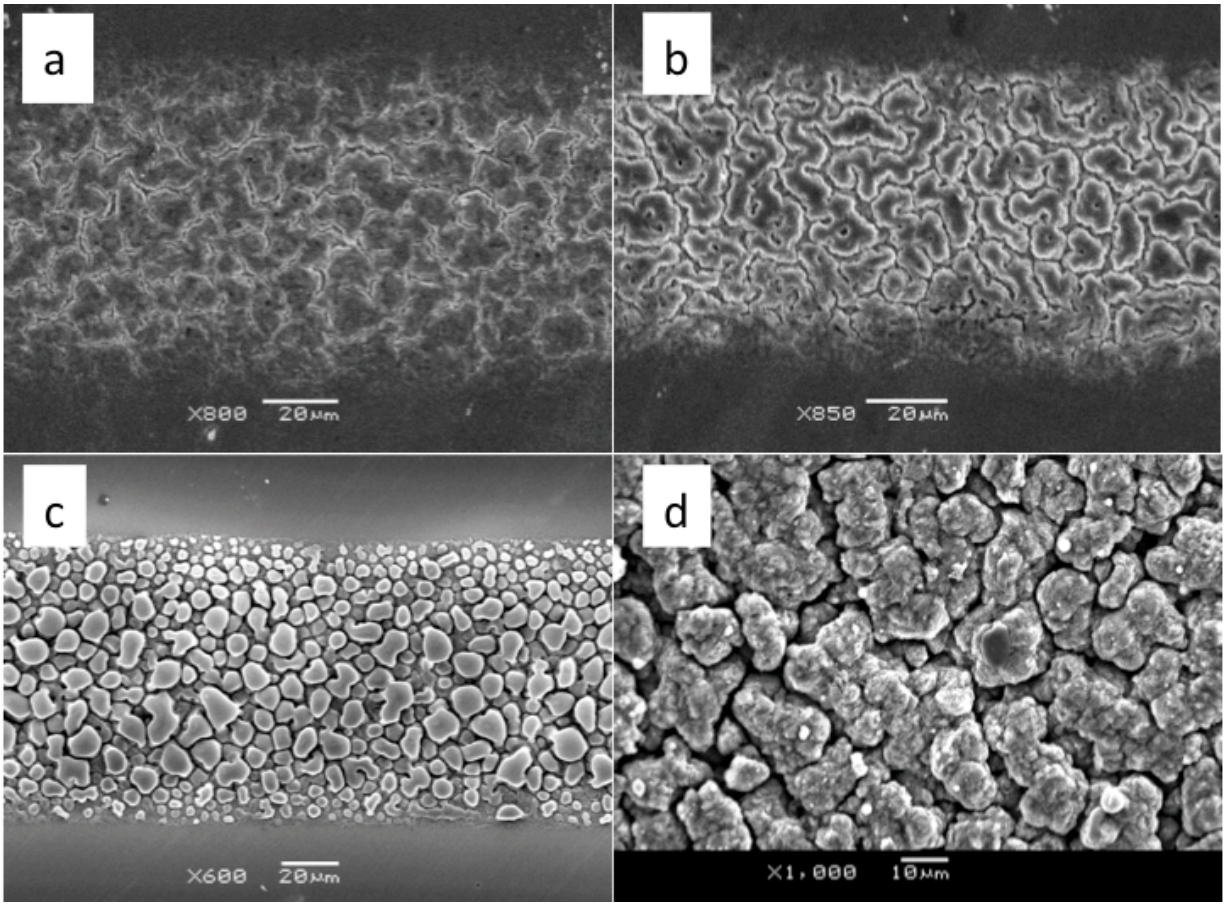

Figure 3-5 Pseudo-periodic micro-structures on titanium surfaces initiated at 1.27 MW/cm2 Intensity and continue to grow at (a) 0.5, (b) 0.25, (c) 0.1, (d) 0.05 mm/s velocities (P=10 W, F=20 kHz, D=50 µm)

As a parallel study on stainless steel (SS), a set of experiments at a laser power of 10 W, beam diameter of 110 µm, frequency of 20 kHz and different velocities of 0.05, 1, 1.5 and 2 mm/s were chosen. The PP micro-structures have the highest uniformity at 110 µm spot size on the SS structures and 20 kHz frequency. Figure 3-6 depicts the trend on the surface of stainless steel, which is the same as titanium. The structures start to form at intensity of 0.26 MW/cm^2 and will continue to grow by increasing the effective energy through decreasing the process speed. From SEM results and analysis of the effect of different laser parameters, one could understand the theory behind the formation of these structures. Due to relatively large pulse duration (in the range of a nanosecond) the process is explained by thermal variation of the surface.

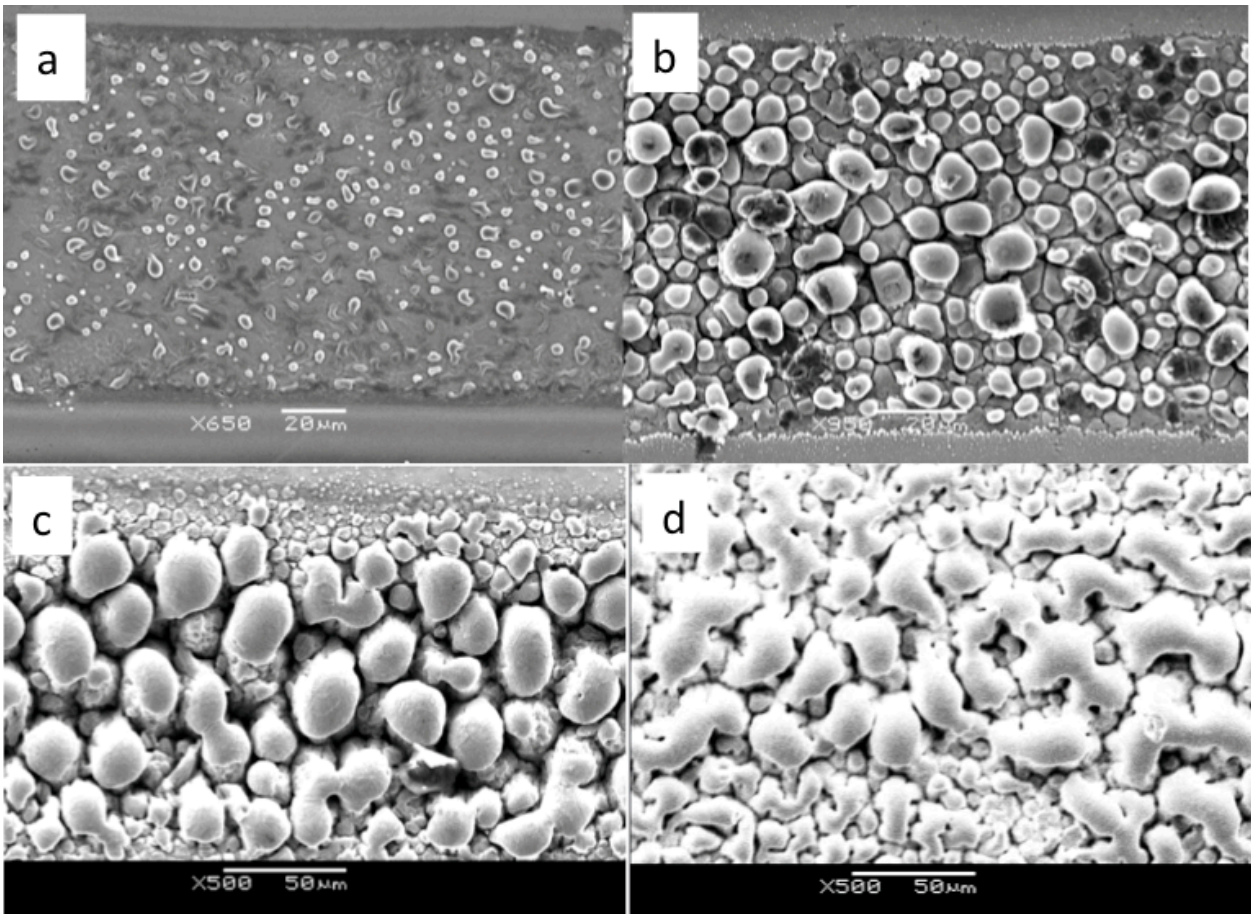

Figure 3-6 Pseudo-periodic micro-structures on SS surfaces initiated at 0.26 MW/cm2 intensity and continue to grow at a) 2, b) 1.5, c) 1, d) 0.5 mm/s velocities (P=10 W, F= 20 kHz, D=110 µm)

This could explain why polarization did not have an effect on the formation of micro-structures. Thermal processes occur on the surface of the material during laser processing due to capillary wave formation, which leads to melt displacement and creation of waves on the surface; this process is illustrated in Figure 3-7. When a laser is irradiated on the flat surface, the laser-irradiated zone reaches its melting point while the surrounding zone remains cold. The temperature gradients will cause the melt flow to travel from the hot zone to the cold zone due to differences in the surface energy. After irradiating more pulses, the structures will start to grow due to the presence of the capillary waves on the surface. After a much longer irradiation and an increased number of pulses, these initially formed structures will grow. This curvature of the structures will cause different absorption on the surface and will lead to increased temperature gradients. Both the capillary waves and thermo capillary force help the growth of the structures.

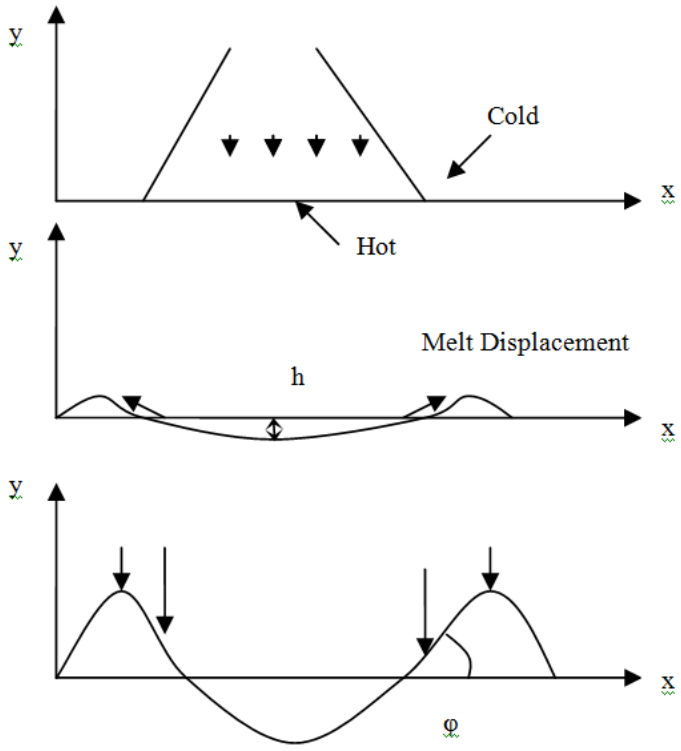

Figure 3-7 Schematic image of the process of the formation of self-assembled PP based micro-structures

3.5.2 Effect of Laser Process Parameters on Topographical Properties of PP Micro-structures

In order to investigate the effects of effective energy on the topography of the structures, image processing analysis has been conducted on the developed surfaces.

The surface topographical properties are studied using different parameters, including: the roughness of the structures (Ra and Rq), the area of the structures (A), the distance between each structure (S), and the ratio of the largest to the smallest length of the structures (b/a), which represents how much each structure deviates from its equiaxed shape. Figure 3-8 shows how the three parameters, A, S and b/a, are defined.

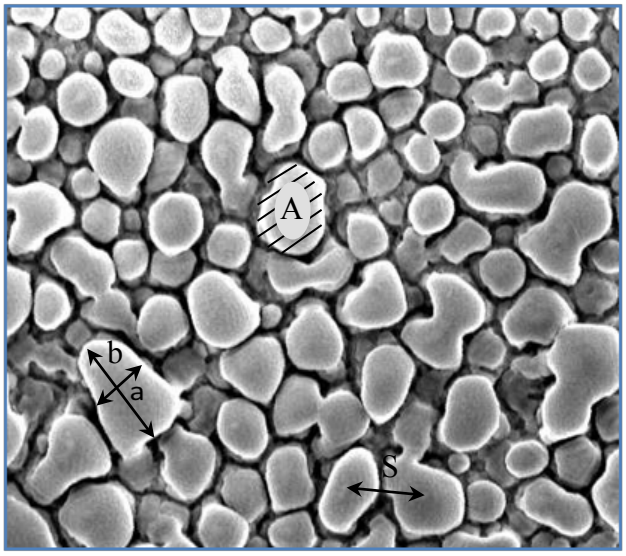

Figure 3-8 Schematic definition for geometrical properties of surface, A: area, b/a: equiax quality, S: periodic space

SEM images of the micro-structures show the variation in the shape of micro-structures formed on the surface of stainless steel and titanium. After irradiating the surface of different materials and their re-solidification, the actual shape of the structures freezes. The shape of the

micro-structures is different for different conditions and different materials. They are either ridged or conical. More conical structures are formed on the surface of stainless steel, while the micro-structures that are formed on the surface of titanium consist of wave-like ridges. This variation in the structures can be explained by the variations in different material properties of stainless steel and titanium.

Irradiating the surface with a relatively fast laser scanning speed at the proper laser intensity will result in the initiation of PP-based micro-structures. By decreasing the velocity, these small structures will continue to grow until the surface reaches the critical temperature, which would lead the structures to melt leaving no specific pattern visible on the surface. The trend of the increasing of the micro-structures as the result of effective energy increase (i.e., decreasing scanning speed) is depicted in Figure 3-5 and Figure 3-6.

As discussed in the literature review, the spacing between the micro-structures that are developed by irradiating the pico- and femto-second lasers are in the range of the laser wavelength [71]; however, as demonstrated here, the spacing between the PP-based micro-structures can be controlled by changing the laser processing parameter of effective energy. This is one of the advantages of using nanosecond pulse laser irradiation techniques. Figure 3-5 and Figure 3-6 show how the structures appear at a specific intensity and then, with an increase in effective power, increase due to the merging of the micro-structures, which will lead to an increase in the spacing between the self-assembled structures. Figure 3-9 shows how the spacing increases by decreasing the effective power for both titanium and stainless steel. This is a result of the merging of the micro-structures, which leads to the increasing of spacing between the self-assembled structures. Growth of the self-assembled structures continues until they reach a critical value, after which point, the level of melting will increase on the substrate and the shape

of the structure will be destroyed due to an increase in the number of irradiating pulses as the result of decreasing scanning speed. The maximum periodic spacing is approximately 38-µm for titanium and 52-µm for stainless steel.

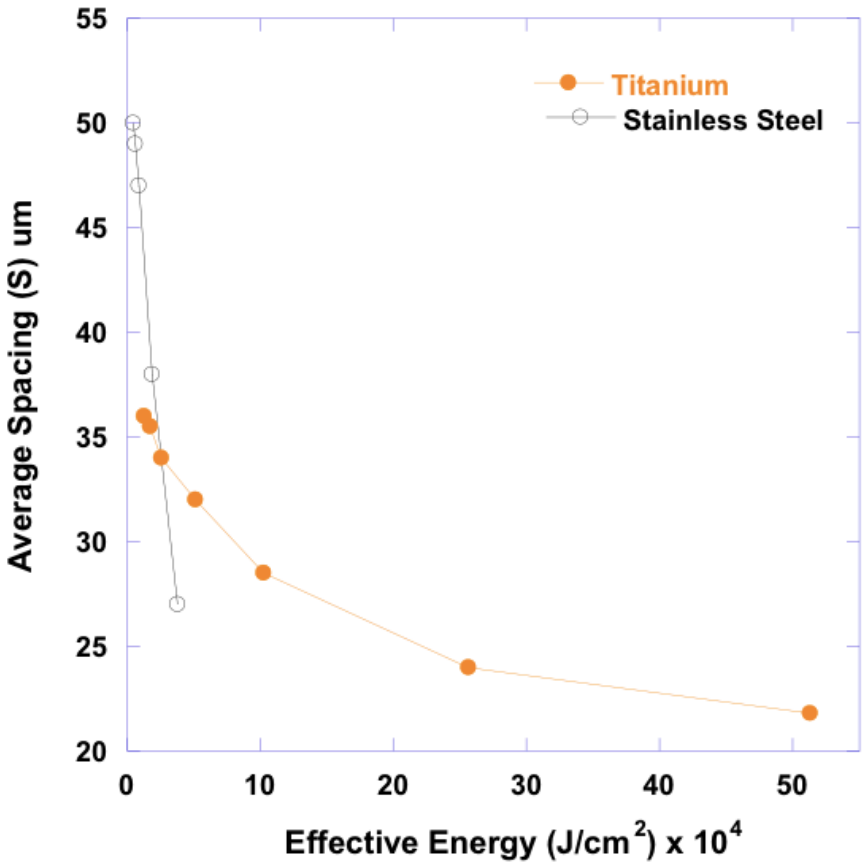

Figure 3-9 Effect of laser parameters on the periodic space between the micro-structures (I_{Ti}=1.27 MW/cm^2, v_{Ti} =0.05 mm/s, $I_{Stainless\ Steel}$=0.26 MW/cm^2, $v_{Stainless\ Steel}$=0.5 mm/s)

The profilometry analysis results of two developed PP-based micro-structures are shown in Figure 3-10 and Figure 3-11. These figures represent the profilometry results of the titanium surface processed at the intensity of 1.27 MW/cm^2 and processing speed of 0.05 mm/s and stainless steel processed at the intensity of 0.26 MW/cm^2 and processing speed of 0.5 mm/s, respectively. The SEM image and 2D color spectrum of the surface and the height distribution of lines passing in

two directions of X (passing through the middle of the laser pass) and Y (perpendicular to laser pass) are shown in Figure 3-10 and Figure 3-11. Both X and Y profiles show essentially uniform patterns, which reflect the periodicity of these micro-structures. In these profiles the base surface is located at zero elevation. The results illustrate two different sets; micro roughness and nano roughness. A high pass filter is used on the profilometry results to assess nano-roughness.

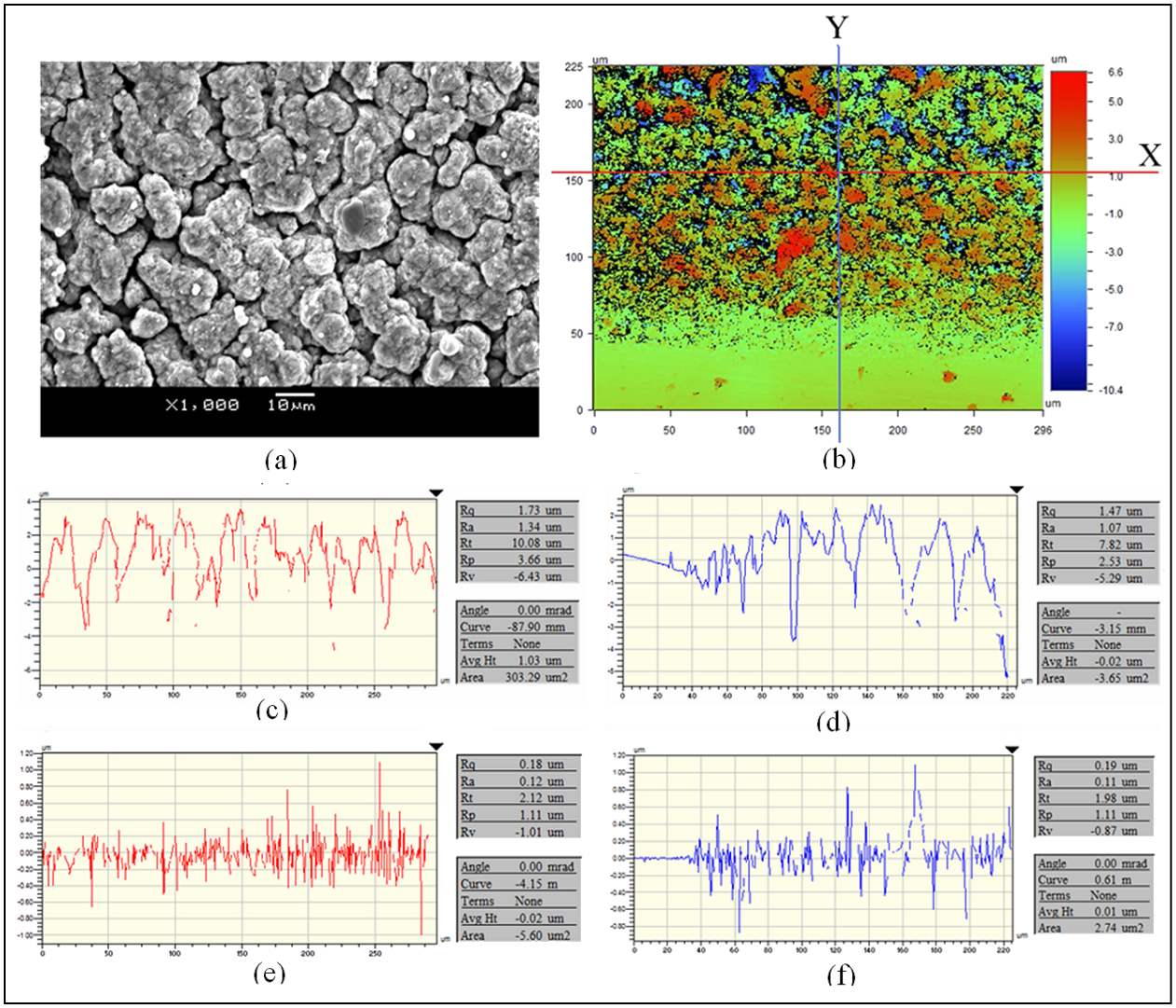

Figure 3-10 Profilometery analysis result of titaium, (a) SEM images, (b) 2D profile, (c,d) micro roughness, (e,f) nano roughness

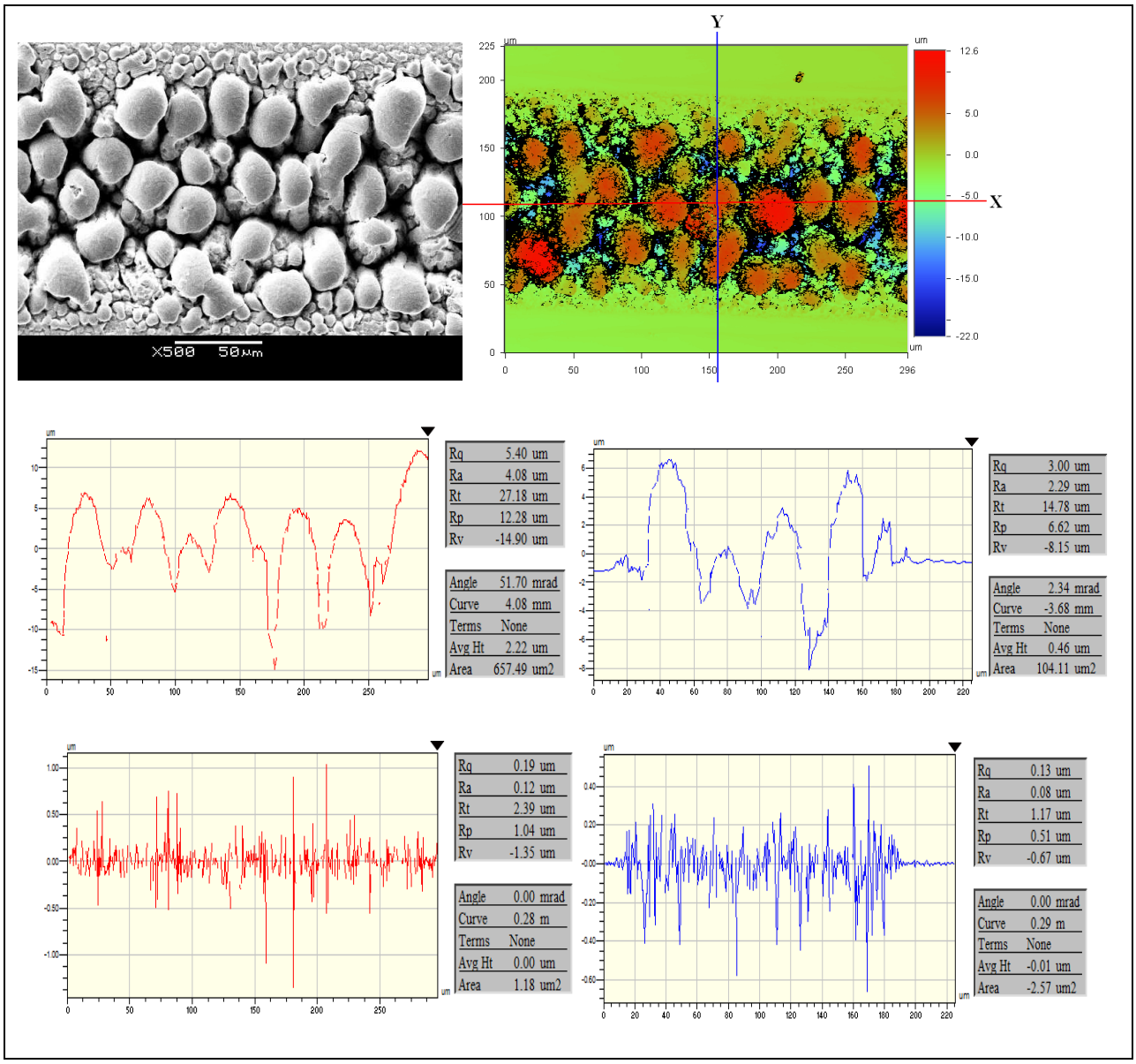

Figure 3-11 Profilometery analysis result of stainless steel, (a) SEM images, (b) 2D profile, (c,d) micro roughness, (e,f) nano roughness

Figure 3-12 and Figure 3-13 present the arithmetic average (R_a) and root mean square (R_q) of the roughness, which vary according to the effective energy. The figures suggest that by increasing

velocity the size of micro-structures decreases and lower surface roughness is achieved. This trend will continue until, no visible micro-structures are created on the surface.

Laser intensity does not significantly increase the roughness of these self-assembled micro-structures. Figure 3-12 and Figure 3-13 demonstrate the variation of R_a and R_q, respectively, with the effective energy for stainless steel and titanium representing the increase in both R_a and R_q as the result of increasing τ_{eff} via decreasing the velocity The increase of the roughness parameters is higher in stainless steel than titanium due to the differences in the properties of the two materials.

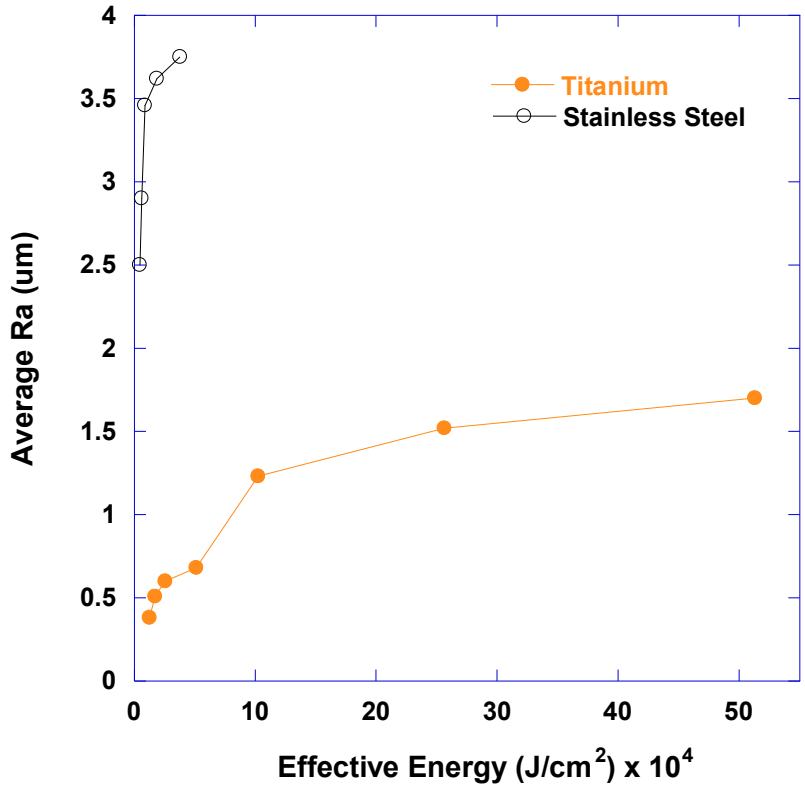

Figure 3-12 Variation of R_a with increasing the effective energy (I_{Ti}=1.27 MW/cm^2, v_{Ti} =0.05 mm/s, $I_{Stainless\ Steel}$=0.26 MW/cm^2, $v_{Stainless\ Steel}$=0.5 mm/s)

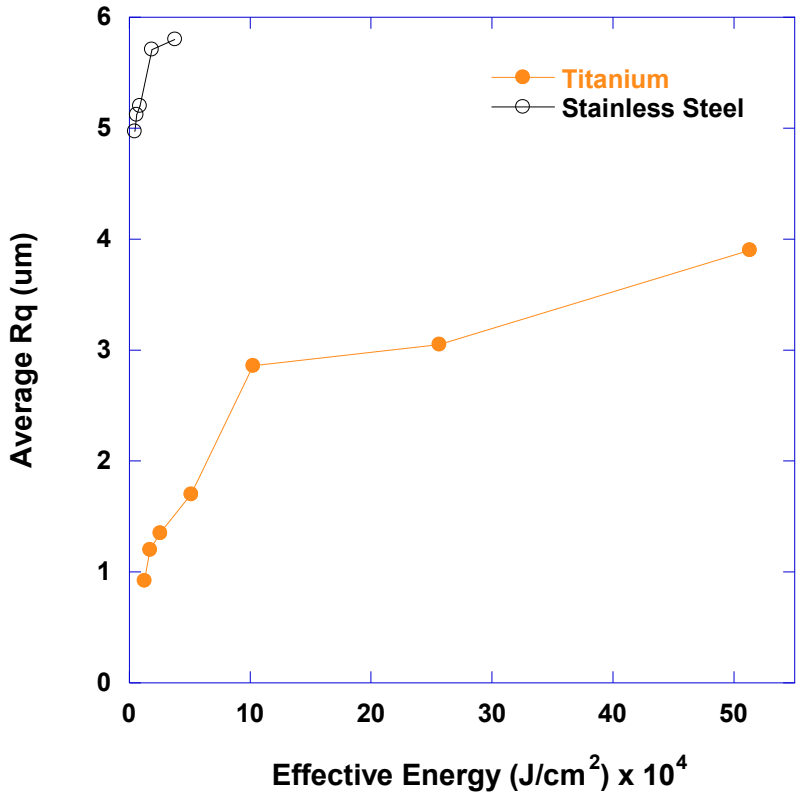

Figure 3-13 Variation of Rq with increasing the effective energy (I_{Ti}=1.27 MW/cm^2, v_{Ti} =0.05 mm/s, $I_{Stainless-Steel}$=0.26 MW/cm^2, $v_{Stainless\ Steel}$=0.5 mm/s)

3.5.3 Effect of Laser Processing on the Micro-structures

Optical microscopy analyses of micro-structures of HAZ are presented in Figure 3-14, which shows the micro-structure of an unprocessed sample covered with an undeformed α grain micro-structure. The average grain size diameter of the micro-structure is approximately 25 µm. Figure 3-14b presents the HAZ region created by the laser processing. The surface is covered with both dark elongated hexagonal close-packed α grains in a matrix of white continuous body-centered cubic β phase. The size of the elongated micro-structures is approximately 25-40 µm. The α phase platelets are aligned in the HAZ under the laser path, compared to the random distribution

of α platelets in the unaffected zones. This alignment is attributed to the nucleation and growth of α platelets as a result of thermal effects due to directional heat flux generated by the moving laser beam. No micro-cracking was observed on the surface. The HAZ region extends approximately 150-200 µm away from the laser path and is more than three times the laser path kerf.

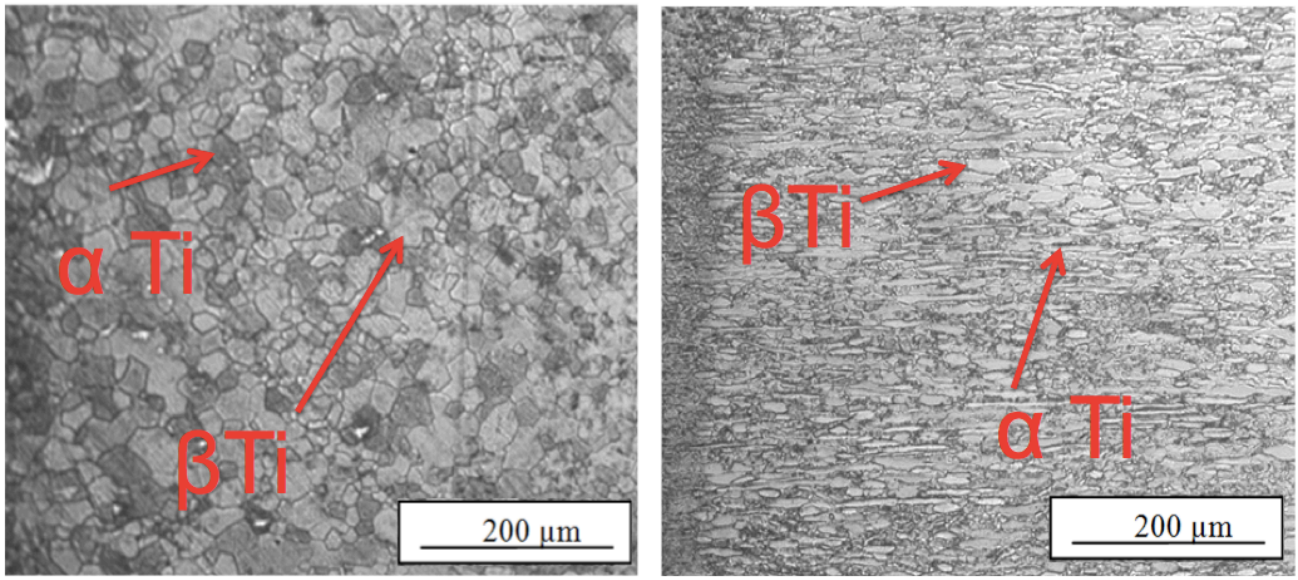

Unprocessed surface

Processed Surface

(a) (b)

Figure 3-14 Optical Microscopy photomicrograph depicting the α/β micro-structure of sample (a) on unprocessed surface (b) close to laser path of the processed surface

Figure 3-15 also shows the micro-structure of surface on the cross section of the laser-processed area, which represents no change in micro-structure after laser processing of the surface.

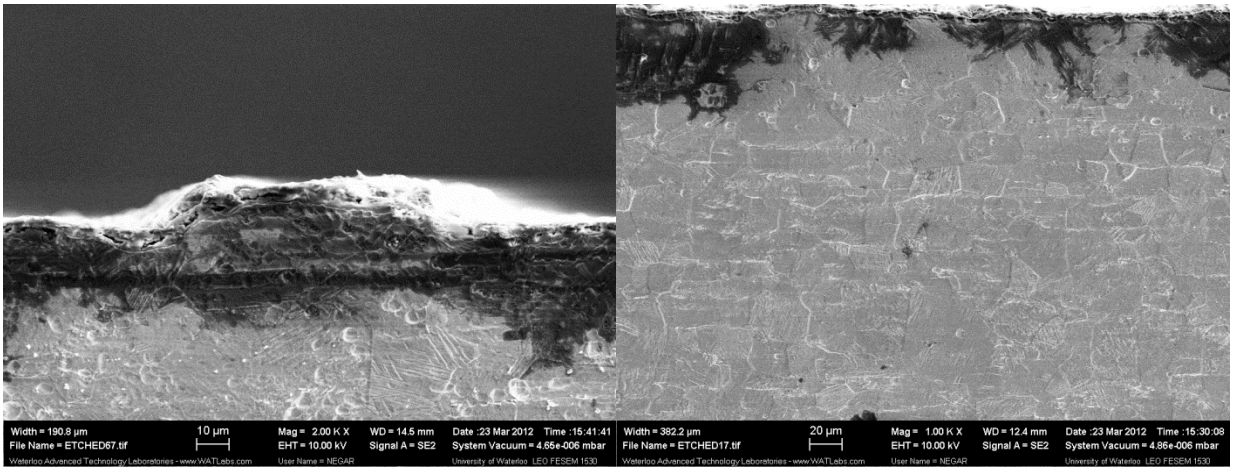

Figure 3-15 Surface micro-structure at the cross section of laser processed titanium surface, right image represents the higher magnification of the same cross section (at different location) shown in the left image

3.5.4 Effect of Laser Parameters on Chemical Composition

The effects of laser process parameters on variations of the two main compositions, titanium and titanium dioxide (i.e., titania) was investigated. The effects of the laser parameters on different mineral forms of titania (i.e., rutile, anatase, and brookite) are demonstrated in the XRD results. Variations in the chemical composition are compared for the six test conditions listed in Table 3-4. The first experiment is related to the composition of the oxide layer on the pure unprocessed titanium, which is exposed to air at room temperature. The XRD result of test 1 will be used as the reference point for other analyses. The next three tests (i.e., tests 2, 3 and 4) demonstrate the composition of the surface of the laser path at three different laser intensities: 1, 1.27 and 1.5 MW/cm^2 at constant velocity of 0.05 mm/s Comparison of the XRD results for tests 2, 3, and 4 are used to study the effect of laser intensity on surface composition. Tests 3, 5 and 6 represent the surface composition at a constant intensity of 1.27 MW/cm^2, but at different effective energies of 40 x10^4, 20x10^4 and 8x10^4 J/cm^2, respectively.

Table 3-4 Test condition of XRD case analyses

Test Number	Laser Power (W)	Intensity (MW/cm^2)	Scanning speed (mm/s)	Effective Energy ($x10^4$ J/cm^2)
1	---	---	---	---
2	8	1	0.05	32
3	10	1.27	0.05	40
4	12	1.5	0.05	48
5	10	1.27	0.1	20
6	10	1.27	0.25	8

The XRD results of all the six tests listed in Table 3-4 are shown in Figure 3-16. Chemical components of the surface are present at specific peaks. The common difference in composition between the laser processed surfaces and the unprocessed pure titanium at room temperature is the presence of new peak at 82^o. This peak belongs to anatase (224) and βTi (220). The presence of the oxide layer could be easily explained by increasing the oxidation process during the laser processing. It was expected to see more rutile structures on the surface due to their stability at temperatures above 700-1000^{o}C, if an equilibrium process is performed. The reason for the presence of a new peak of anatase on the surface is the method of solidification of the pulsed laser processing, which entails very high cooling rates [10]. Due to this fact, the solidification mechanism would not take place in an equilibrium manner; therefore, the structures may not follow a conventional phase transformation diagram.

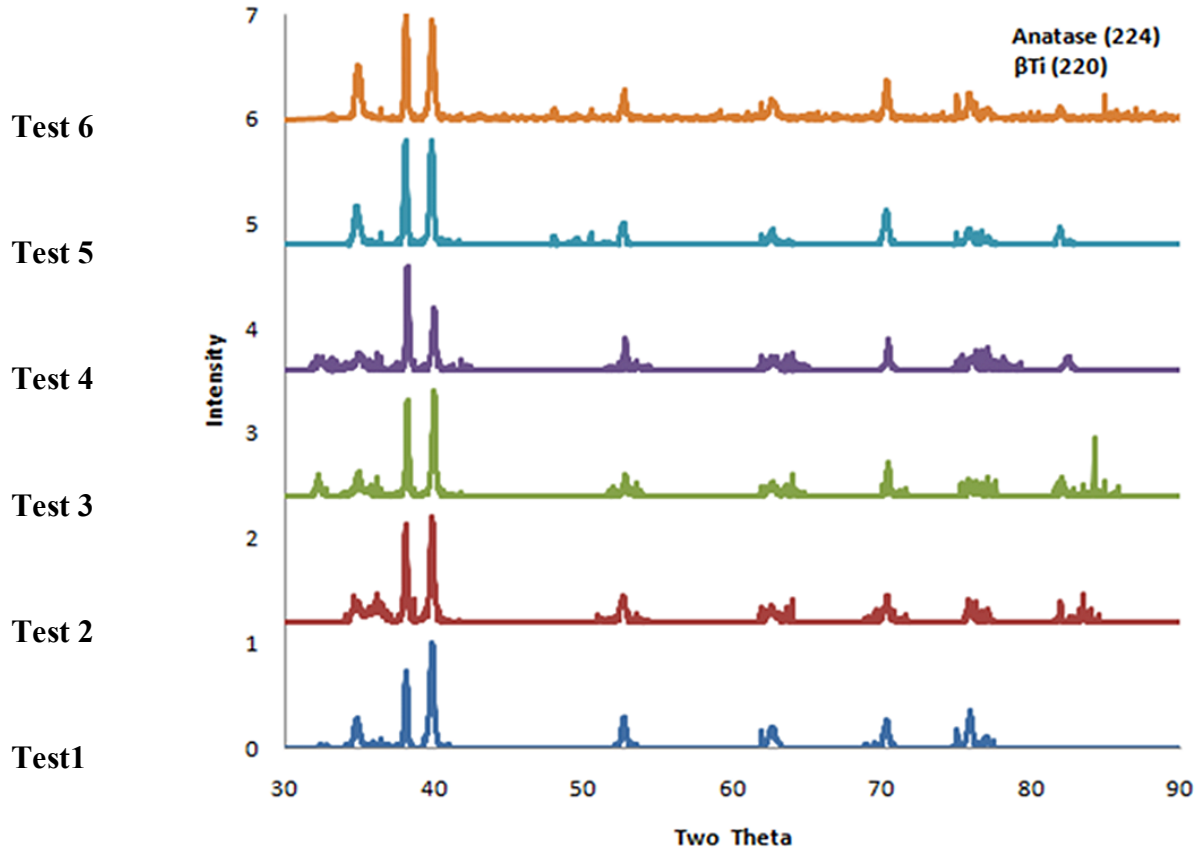

Figure 3-16. Comparison of five laser processed experiments with the reference-unprocessed surface

Laser processing also increases the surface temperature. By going above the transus temperature of titanium, αTi will transform to βTi, which is a harder structure of titanium. This observation is supported by the elevated hardness measurement explained in the next section.

There are other variations in the surface chemical composition under different conditions. In order to focus the discussion, a selection of XRD results (angles 30 to 42^{o}) for tests 2, 3, and 4 is shown in Figure 3-17 to help investigate the effect of laser intensity on the chemical composition. Figure 3-18 shows the XRD results (angles 30 to 50^{o}) for tests 3, 5, and 6 compared to the reference surface. The results show the effect of the effective energy on the chemical composition while keeping the laser intensity constant at 1.27 MW/cm^{2}.

Considering Figure 3-16 and Figure 3-17, at a relatively low intensity of 1 MW/cm^2 , the height of the peak at two theta of 38.4^0, which belongs to the highest peak of a type of Ti (110), starts to increase. By increasing the laser intensity, both peaks at the alpha to beta transformation will be increased. Another difference in the XRD results for test 2 compared to the other tests is the presence of new peak at 36.9^o due to presence of anatase (103) structure. By increasing the laser intensity to 1.27 MW/cm^2, the anatase structure at 36.9^o vanishes, but a new peak of brookite (200) at 32.7^o is developed. The new peak of brookite appears on the XRD result for a laser intensity of 1.5 MW/cm^2. The variation of XRD peaks at different velocities is also studied between the 30 and 50^o range, which represent the highest variations in peaks, as shown in Figure 3-18. This occurs due to a shorter laser/material interaction, which results in less oxidation on the surface. In the XRD analysis of lower effective energies of 20 and $8x10^4$ J/cm^2, a new peak of anatase (200) is developed at 48^o. The XRD results are, however, very similar at both conditions.

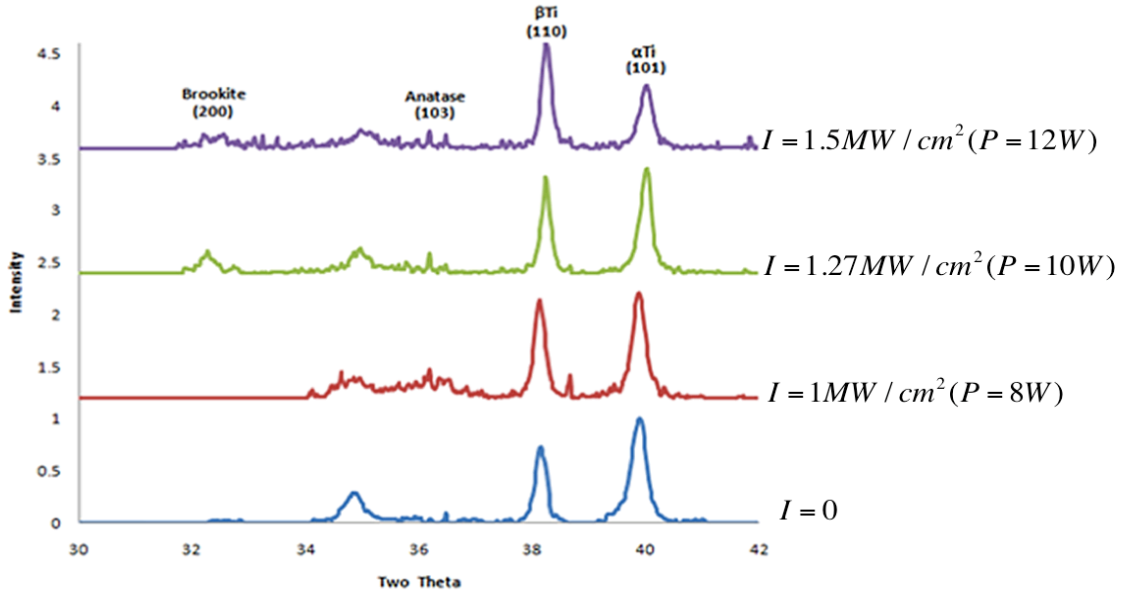

Figure 3-17. Effect of laser intensity on surface composition at the constant velocity of 0.05 mm/s

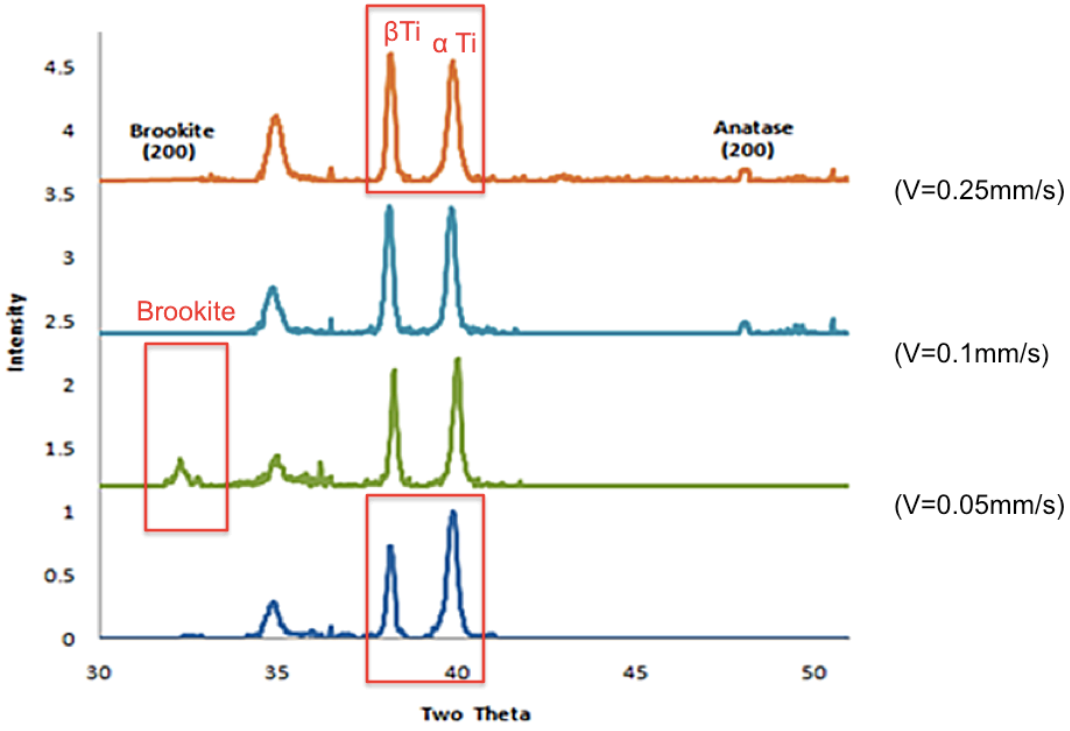

Figure 3-18. Effect of effective energy (scanning speed) on surface composition at the constant intensity of 1.27 MW/cm^2

3.5.5 Effect of Laser Processing on the Surface Hardness

Surface hardness is measured for three different conditions: unprocessed titanium and laser processed titanium samples processed at two different laser intensities. Three samples from each condition are used for the measurements and the average value is reported in Table 3-5. The surface hardness for two laser-processed conditions was measured along the surface edge at five different points, as was illustrated in Figure 3-4.

The loading-depth curves for the three conditions are depicted in Figure 3-19. The loading curves of the laser processed samples demonstrate steeper slope and an obvious higher hardness than the unprocessed titanium. The hardness results in Figure 3-20 suggests that the hardness is significantly high in the HAZ; however, at distances greater than 10 μm away from the surface of the track, the hardness sharply drops to the level of the unprocessed sample (~5 GP).

There are two factors that could cause the increase in the hardness of the developed surface: the presence of oxide layer and the increase in βTi, which appeared on the surface due to high temperatures. Increasing the laser intensity, which leads to the increase in βTi, will in turn result in a higher surface hardness.

Table 3-5 Nanoindentation results of two different processed samples with reference to unprocessed titanium (v=0.05 mm/s)

Test Condition	Points	hc (nm)	Maximum force Pmax (μN)	Reduced Er (GPa)	Hardness H (GPa)	Contact Area (um^2)	Hf (nm)
Unprocessed Ti	Ti Surface	116.86	1983.45	116.29	3.1	4.62	98.23
I1=1.27 MW/cm^2	Point1	21.91	1992.039	154.41	24.24	14.82	1.60E-06
	Point2	81.92	1986.042	81.39	5.08	20.98	65.78
	Point3	89.91	1984.713	81.67	4.48	22.46	74.71
	Point4	81.69	1987.07	99.71	5.10	11.91	63.49
	Point5	95.54	1984.606	98.64	4.13	18.33	80.71
I2=1.5 MW/cm^2	Point1	15.06	1993.457	155.39	34.32	32.31	0.376
	Point2	80.18	1985.941	90.24	5.23	19.79	64.29
	Point3	89.58	19.85.101	90.24	5.23	19.79	64.29
	Point4	94.91	1984.713	100.057	4.17	11.89	77.72
	Point5	98.58	1984.663	98.83	3.95	13.57	82.24

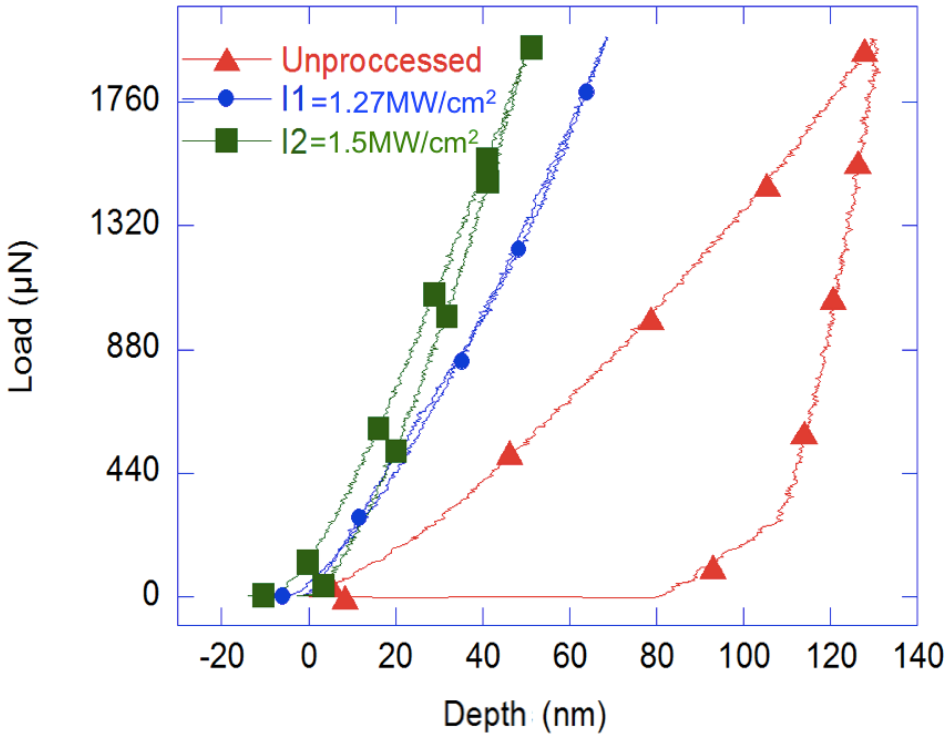

Figure 3-19 Nanoindentation results for three conditions; unprocessed titanium, and laser processed samples at I_1 and I_2

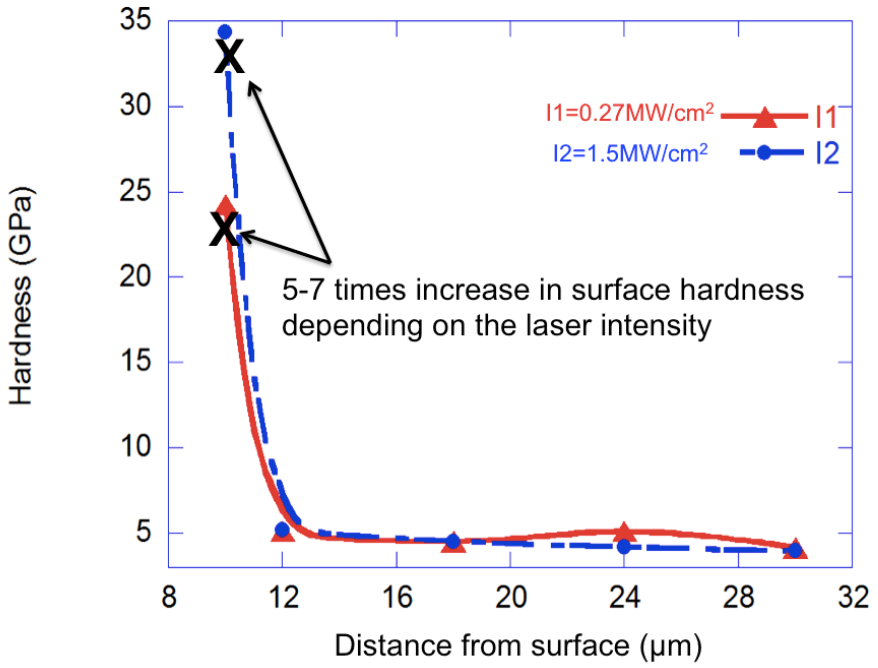

Figure 3-20 Variation of hardness value measuring from the edge of laser path from 10µm, to about 30 µm distance

3.6 Summary

The effect of laser processing parameters on the development of micro-structures was investigated in this chapter. Based on the results, laser intensity and laser effective energy (via the change in the process speed) have significant roles in the formation of such micro-structures. It was shown that the micro-structures initiation is not possible until laser intensity reaches a certain value close to the damage threshold of the material. After the micro-structures are initiated, the laser intensity may remain constant and the growth of structures is mainly controlled by the effective energy through the velocity change. Increasing the effective energy resulted in higher roughness and larger area and periodic spacing. The results showed that the micro-structures of the surrounding area of the laser processed track is mainly the β structure, whereas the micro-structure of the unprocessed surface is the α structure. The experiments also revealed that the heat-affected zone (HAZ) with Tiβ structure, with elongated micro-structures, covers the area up to three times of the laser path width. X-ray diffraction (XRD) results of the laser processed experiments at different conditions all showed an increase in the oxide layer, and also α to β transformation of titanium. Nanoindentation analysis also supported the XRD and microstructural results.

4 Chapter Four –

Chemical Modification of Titanium using Nanosecond IR Laser Irradiation in Oxide Media

4.1 Introduction

In this chapter, the results of the nanosecond laser processing of the titanium surface in liquid oxidized media will be studied. Hydrogen Peroxide (HP) and water are used as the media to study their effects on increasing the anatase composition on the titanium substrates irradiated by the laser. The variations of anatase-rutile transformation generated in HP are compared with those generated in air. X-Ray diffraction (XRD) analysis suggests that three titanium dioxide structures, brookite, anatase, and rutile, are present on the substrates irradiated by the laser beam. Additional peaks appeared in XRD results of HP immersed samples, indicating the presence of new anatase peaks and a rare titanium oxide structure, Hongquiite. Energy-dispersive X-ray (EDAX) spectroscopy analysis also reveals an increase in the oxide layer on the surface of HP-treated samples.

Laser irradiation affects the chemical properties and changes the surface topography simultaneously. The phase transformation of the material can be controlled through the laser processing parameters. The thermal treatment of the surface also results in the formation of a thick oxide layer on the surface of the titanium, which will improve the surface properties for biomedical applications. To control the level of oxidation on the surface, the laser parameters can be changed to affect the temperature and annealing process of the surface. Conducting the laser

processing in the oxide media also results in an increase in the ability of the surface to bond with the oxygen. Water, O_2 gas and H_2O_2 are known to be good mediums for oxygen bonding.

The Anatase-rutile transition in this study is achieved through the combined effects of thermal control and chemical reaction. XRD, SEM and EDAX are employed to investigate the effect of nanosecond pulsed fiber laser processing of titanium immersed in HP on the anatase-rutile transition.

4.2 Sample Preparation

The experiments were conducted in a 30% hydrogen peroxide medium and in water using the arrangement shown in Figure 4-1.An epoxy mould was produced in which a cylindrical space was created to hold the medium. The results of the experiment are presented in the following sections.

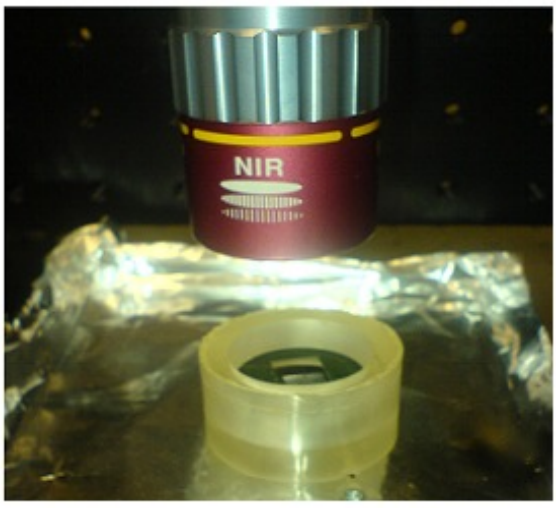

Figure 4-1 Sample held in liquid media with 4mm liquid on the surface

4.3 Micro-structures Developed in Liquid Media

To investigate the effects of the medium on the surface topography and the PP-based micro-structures, the titanium samples were immersed in two liquid-based media: HP (H_20_2) and water (H_2O). The liquid-based media affect not only the micro features, developed by the irradiation of the laser beam, but also influence the chemical structure of the surface. In this section, the effect of the liquid media on the topography of the micro-structures is investigated and in the following sections, its effect on the chemical behaviour of the surface is demonstrated.

Laser processing in liquid media presents different results than in atmosphere due to various physical processes, including the presence of bubbles, plasma, shock waves, and light diffraction. During laser processing, the liquid medium reaches its boiling temperature. The boiling liquid creates bobbles on the sample, resulting in the reflection of the laser beam in various directions, which in turn changes the structures on the sample.

Other differences between the structures formed through laser processing in liquid media versus air arise from the fact that the surface of the material cools down faster in liquid-based media than in the atmosphere. Another factor affecting the process is that HP has a higher heat capacity than air. HP absorbs more energy during laser processing. In addition, by using liquid-based media, some of the laser beam might be scattered by the surface of the liquids and suspensions and the focal spot size of the beam changes due to the diffraction of the light passing through the liquid surface.

Figure 4-2 and Figure 4-3 show the SEM images of the developed self-assembled structures produced by immersing titanium samples in hydrogen peroxide and water at identical process parameters, respectively. Both the secondary and backscattered images are presented to show both the topography and the variations of different phases on the surface. The trends of the

structures are very similar in both media. The periodic structures could be still observed on the surface of samples; however, the heights of the self-assembled PP-based micro-structures produced in liquid-based media are much lower than those produced in air. There are some cracks and holes present on the surface of both samples. Additional studies should be undertaken to explore the reasons for the presence of these cracks and holes.

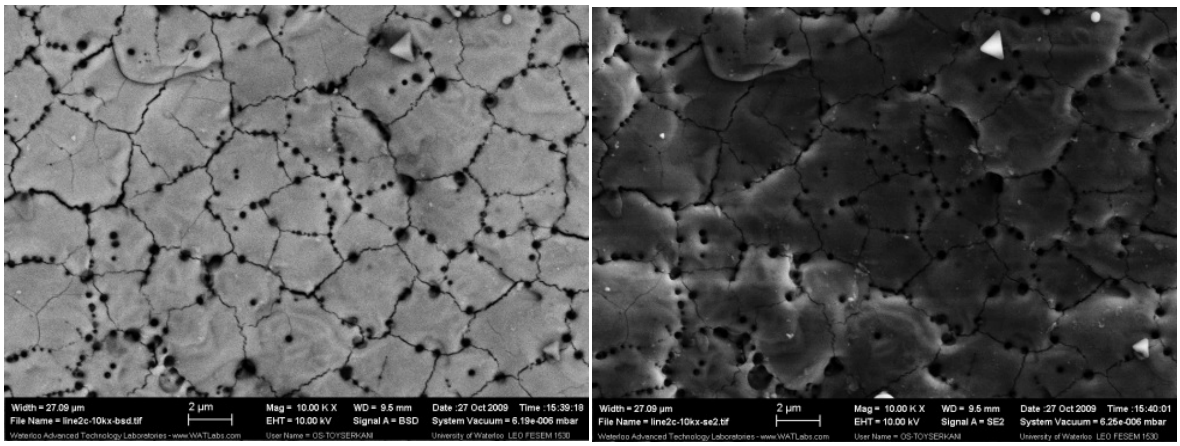

Figure 4-2 Micro features developed under laser processing in HP (left) backscattered image (right) secondary image, (P=10 W, F=20 kHz, D=60 µm, V=0.1 mm/s)

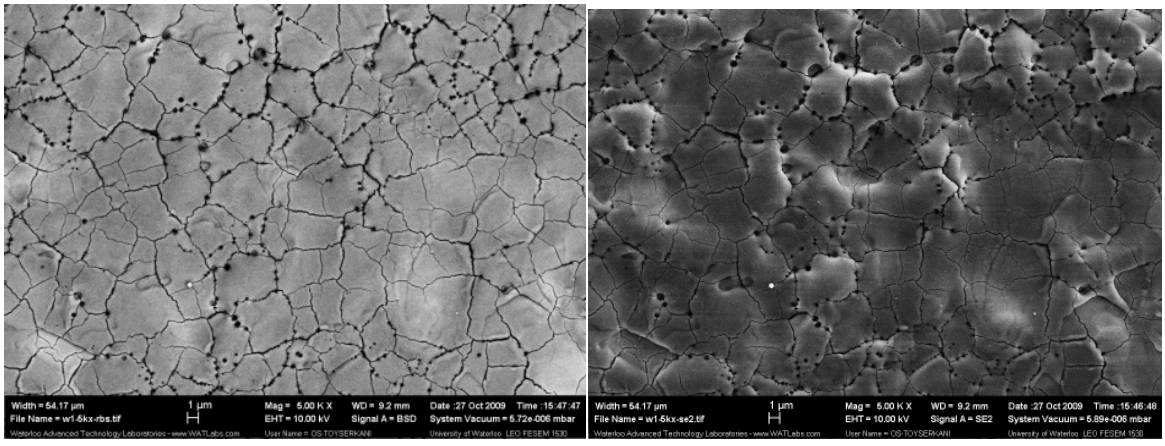

Figure 4-3 Micro features developed under laser processing in water (left) backscattered image (right) secondary image (P=10 W, F=20 kHz, D=60 µm, V=0.1 mm/s)

The backscattered images represent the phase variations on the surface of samples; these can be explained by the presence of an oxide layer on the structures. To study these phase variations, XRD and EDAX analyses were conducted on the samples and that the results are presented in the following sections.

4.4 Chemical Modification of Titanium Immersed in the Liquid Oxide Media

In order to compare the percentage of oxygen and titanium in two different mediums of HP and oxygen, the different components of the processed surfaces are observed at fifty points along a line passing through the laser-processing path. The EDAX results are shown in Figure 4-4 and Figure 4-5. The number of counts representing the oxide composition is higher on the experiments that are conducted in hydrogen peroxide compared to those conducted in water. Figure 4-4 and Figure 4-5 also demonstrate sudden drops in the composition of both oxygen and titanium due to the cracks and the holes that are generated through the laser processing. The levels of oxidization on the samples immersed in HP encourage the use of HP as a candidate for the laser processing to improve biocompatibility of titanium. The effect of HP on the structure of titania is studied through XRD analysis, and will be discussed in the next section.

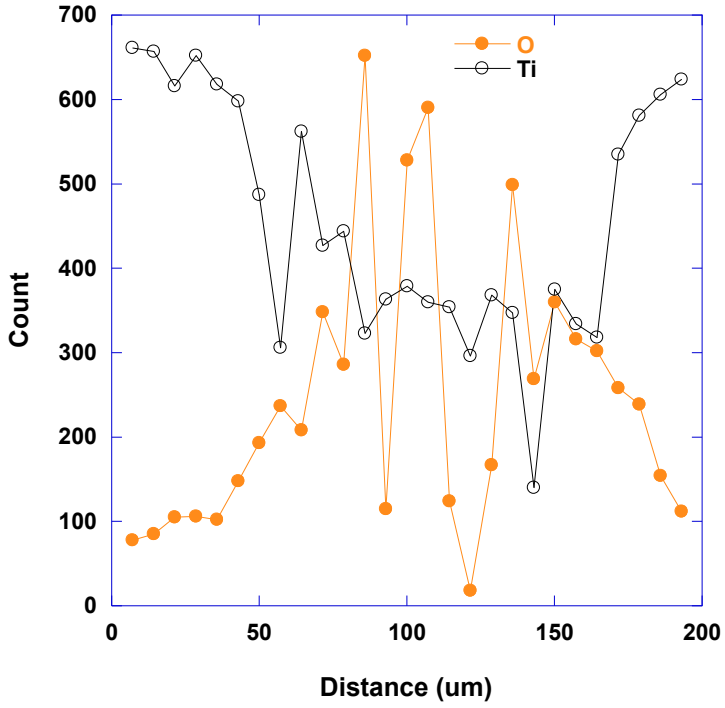

Figure 4-4 EDAX analysis of the sample immersed in H_2O_2 (P=10, F=20 kHz, D=60μm, V=0.1mm/s)

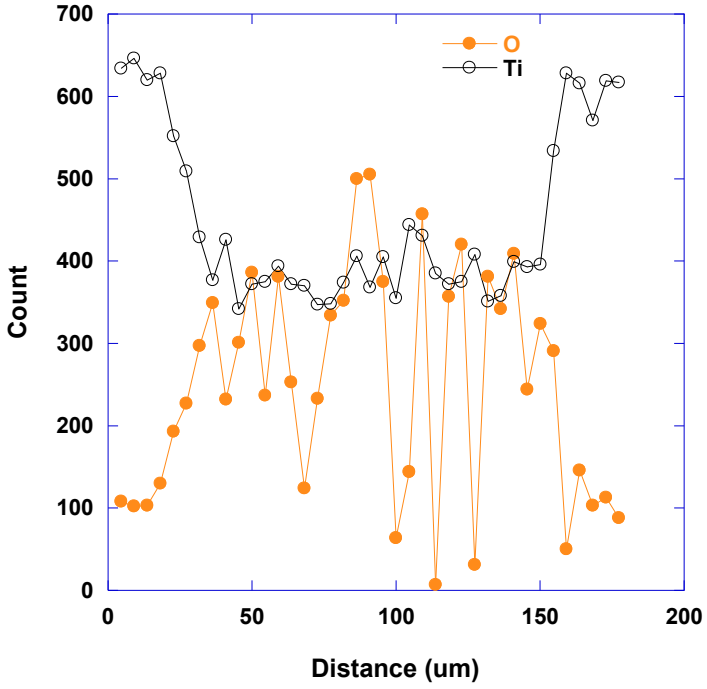

Figure 4-5 EDAX analysis of the sample immersed in water (P=10, F=20 kHz, D=60μm, V=0.1mm/s)

Table 4-1 lists five selected process conditions of treated samples. The laser scanning speed was kept constant at 0.05 mm/s in all the experiments, with a laser frequency of 20 kHz and spot size diameter in the range of 60 μm.

Table 4-1Different processed conditions selected for XRD analysis

Test #	Medium	Measurement location used for XRD	Process conditions/parameters
1	Air	On the surface of sample	No laser processing
2		50 μm from the laser track (HAZ)	P1 =10 W
3		On the center of laser path	P1 =10 W
4	HP	On the center of laser path	P1=10 W
5		On the center of laser path	P2=12 W

Figure 4-6 shows the XRD results for tests 1-5. Comparison of the XRD results of tests 1 and 2 demonstrates the presence of new peaks at 59^{o} and 83^{o}, which belong to the (211) and (312) anatase structures of titania, respectively. The same peaks are also observed in XRD graphs associated with the HAZ area irradiated in HP, which are not presented. Both the XRD and EDAX results revealed higher amounts of oxide elements in HP-processed samples.

The XRD results of tests 3 and 4 are presented in Figure 4-6 c and d, respectively. These results show that despite the high temperature generated by laser irradiation, a new peak is generated at 48^{o} associated with (200) anatase structure for the samples treated in both air and HP. This peak remained even on melted areas. The melting temperature of titanium is above 1650^{o}C, which is much higher than the range of anatase-rutile transition, which occurs at 700-

1000^{o}C. The presence of titania structure on the surfaces that were processed at a higher temperature that the melting temperature may be explained by: a) the laser irradiation could lead to point defects in the target structure due to its high temperature, b) the rapid annealing process, and c) the electron bombardment of the target. Any process that increases oxygen vacancies could accelerate surface oxidation and crystallization by increasing titanium's interstitial content [3]. Having negative free energy, titanium is highly reactive in variety of oxidation media, including HP. The effects of HP on the surface composition of titanium in the absence of a heat source was observed by comparing the EDAX results for two titanium specimens, one kept in air and the other immersed in HP for two weeks. The EDAX analysis shown in Figure 4-7 represents the increase in the intensity of the oxide layer on the latter sample, where the ratio of oxygen per titanium element was approximately 4:2. These experiments demonstrated the oxidized reaction in the HP medium without any thermal modification.

XRD results of heat-treated specimens in HP show the influence of hydrogen peroxide on the titanium dioxide and titanium oxide (hongquiite) compositions. hongquiite is a very rare structure of titanium oxide with a cubic structure that is close to the structure of TiC. hongquiite is observed by new peaks at 37^{o} and 43^{o} in tests number 4 and 5, as shown in Figure 4-6 d and e, respectively. The SEM analysis of the sample used in test 4 is shown in Figure 4-8a, which represents the formation of white nanoparticles on the surface. According to the EDAX analysis of these nanoparticles, shown in Figure 4-8b, the concentrations of different elements on the surface of the specimen are oxygen 19.57%, Au 69.47%, Ti 10.96%. This shows that the oxygen to titanium element ratio is almost 2:1, indicating the presence of TiO_2 particles.

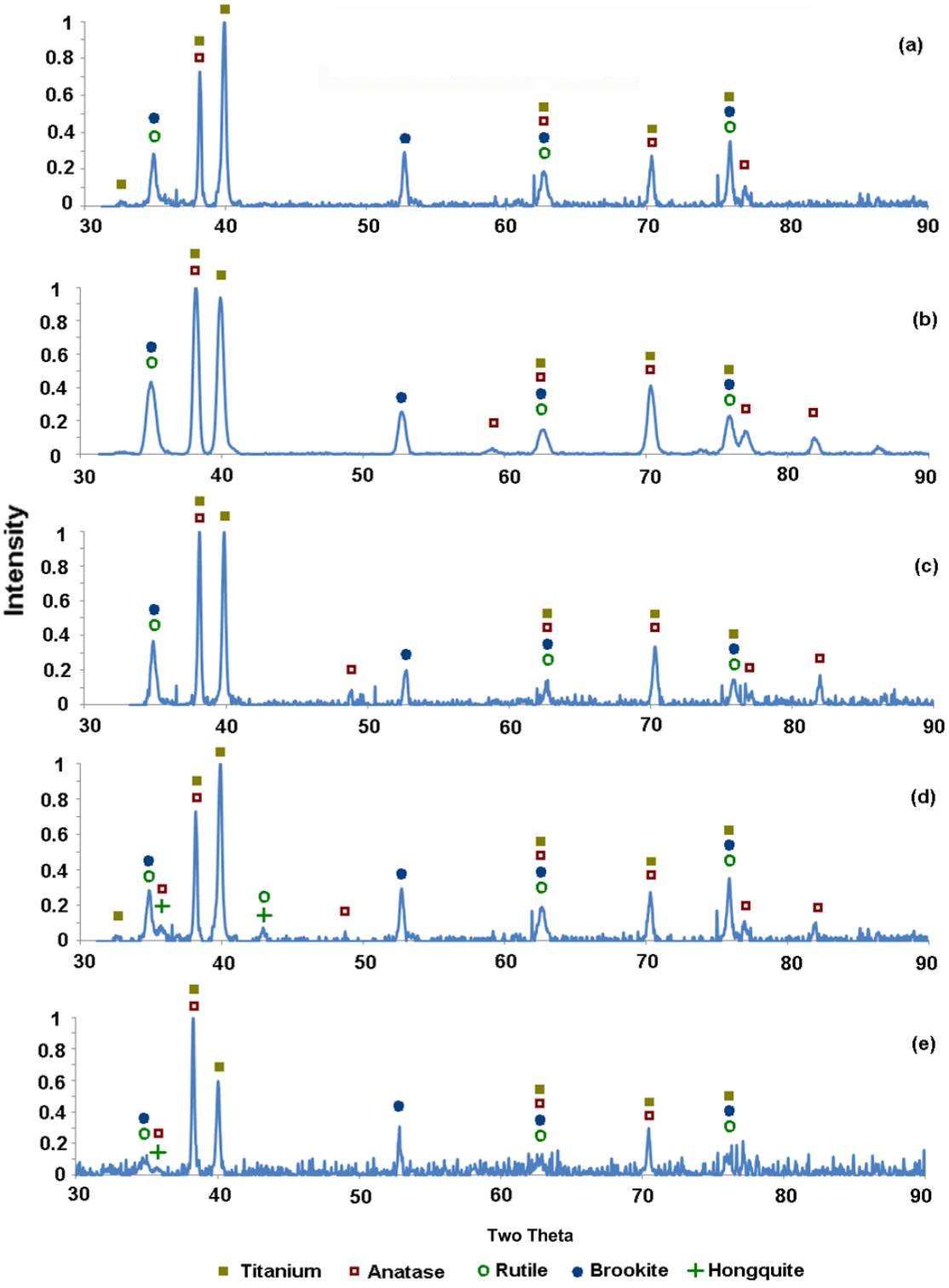

Figure 4-6 XRD results (a) to (e) representing the composition of test conditions 1 to 5, respectively.

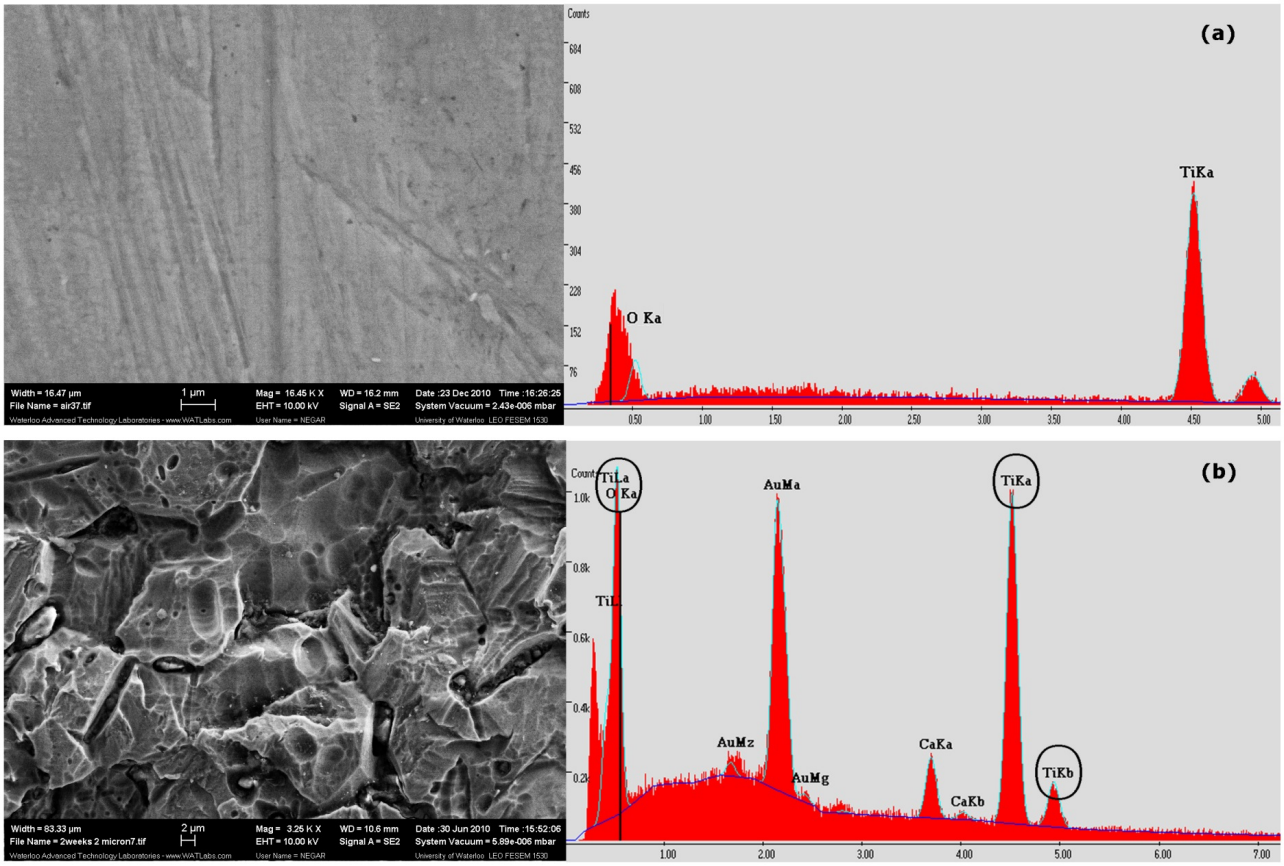

Figure 4-7 SEM and EDAX results of samples kept (a) in air (b) in HP for two weeks

This ratio, of course, is lower than the oxidation level of titanium that has been immersed in HP for two weeks without heat treatment. In heat-treated processes, the oxidation develops selectively and in a much shorter period of time. The presence of a high percentage of Au in the sample is attributed to the gold sputtering process required for SEM/EDAX analysis. The presence of these nanoparticles, TiO_2, for the samples treated in different liquid media has also been reported by other researchers [6-7]. However, there is no reported research on the creation of these nanoparticles in HP. The white color of these particles could be related to the white brookite form of titania.

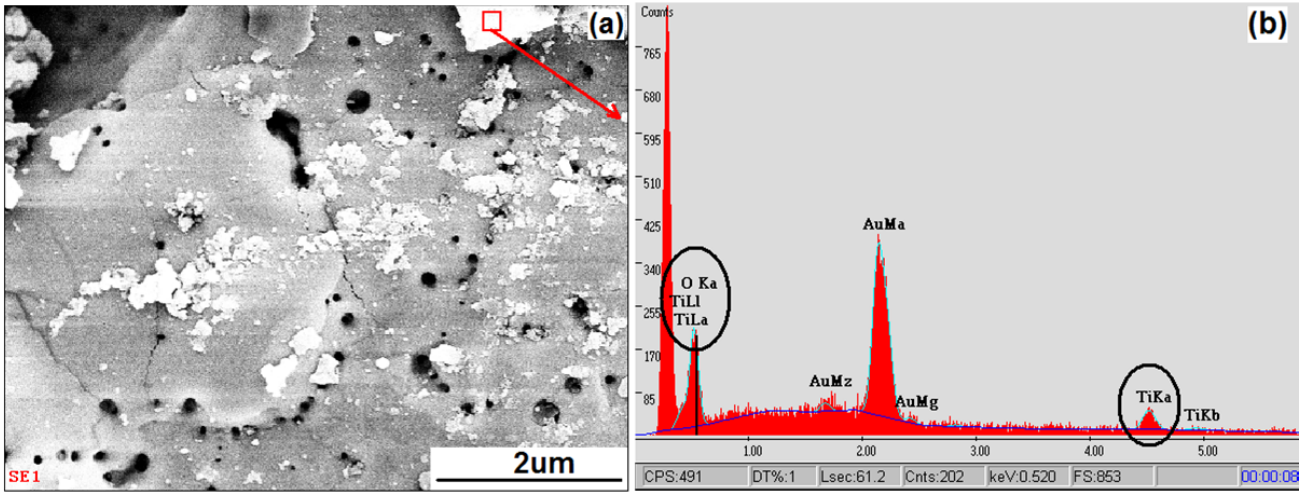

Figure 4-8 Nanoparticles of titania on the titanium surface (a) SEM image (b) EDAX result

Increasing the laser power tends to decrease the anatase phase and increase the rutile phase, as heat treatment leads to grain growth and anatase-rutile transformation. Such grain growth is indicative of the transition between anatase and rutile [9]. However, comparison of tests 4 and 5 reveals a noticeable reversal in level between the two large-intensity peaks at 38^{o} and 40^{o}. Based on the XRD database [10], the peak at 38^{o} belongs to αTi with a hexagonal close-packed structure and anatase (112) titania, and the peak at 40^{o} includes both cubic ßTi and αTi. The swap of intensity levels between these two angles can only be explained by an increase in the anatase titania at this high temperature because, based on the Ti-O phase diagram, a temperature rise can transform αTi to ßTi, and that would result in the increased intensity at 40^{o}. This, however, is not the case in test 5. As observed, the intensity at 40^{0} is lower than 38^{0}, which may be attributed to the formation of an anatase structure and might be explained by the fact that the anatase-rutile transformation is also affected by the method of synthesis and the atmosphere. The presence of a high-density oxygen atmosphere provided by a HP medium will decelerate the

process of anatase-rutile transformation. Therefore, at the same laser intensity and exposure time, the samples processed in HP have more anatase than those processed in air.

In addition to all of the observations from the XRD results above, another peak at 25^0 associated with anatase (101) titania was expected as it has been reported in other studies conducted on titanium immersed in oxide liquid [2,6]. Yet, there was no evidence in the current study of such a peak in either the laser-treated or room-temperature treated samples, including test 1.

4.5 Summary

Titanium surface treatment was conducted through nanosecond fiber laser irradiation in two liquid media: water and HP. This study showed that a nanosecond pulsed fiber laser irradiation technique can be used to form a relatively thick layer of oxidation on the surface of titanium, while increasing the anatase structure on the surface. The rapid annealing process of the pulsed fiber nanosecond laser may also control titania-rutile transformation, either by changing the lattice of material or by phase changes. In pulsed laser processing, the laser intensity and its effects on surface temperature may result in anatase rutile transformation at much higher temperatures than at a uniform substrate temperature.

The nanosecond pulsed fiber laser irradiation process conducted in HP leads to formation of titania nanoparticles on the surface. An HP medium can increase the level of oxidation and also leads to formation of new peaks for anatase-titania and a rare structure (Hongquiite), unlike specimens generated in air. An HP medium may also delay anatase-rutile transformation.

5 Chapter Five –

Effect of Formation of Roughness and Microgrooves on Osseointegration Properties of Titanium Substrates

5.1 Introduction

In this chapter, biocompatibility properties of the surfaces treated by the proposed laser processing are studied through in-vitro analyses. For these analyses, the effects of the following specifications on improving surface osseointegration properties, including cell morphology, orientation, migration, adhesion, growth and viability, will be studied:

- Topography modification with controlled surface roughness of PP-structures;
- Creating microgrooves with structures that sputtered from the substrates;
- Chemistry modifications, including an increase in the amount of TiO_2, particularly the anatase structure developed as a result of the rapid solidification process.

The overall conclusion from this chapter will provide a comprehensive understanding of the effects of the introduced laser-modified surfaces on bone integration processes. This will be effective for aiding in the selection of laser process parameters for the introduced controllable technique for a successful osseointegration process. The main cell-surface interactions occur in the initial stages of cell culturing. Failure at the initial stages will result in cell death (apoptosis). The initial stages involve the following processes:

(i) Medium and protein absorbance, which provide a viable environment for cells;

(ii) Cell attachment and spreading process, which affects cell orientation, area, shape and density;

(iii) Cell adhesion process as a result of integrin bond and focal adhesion formation; and

(iv) Cell metabolic activity and growth, which prepare cells for successful post-integration stages of proliferation and differentiation.

This section provides a comprehensive discussion of the results of cell culturing and the cell integration process of investigated surfaces at the initial stages of cell culturing (i.e., up to 3 days). Moreover the effect of surface properties (i.e., topography and chemistry) on the osseointegration process will be investigated in the following sections, with the goal of quantifying the schematic process diagram shown in Figure 5-1.

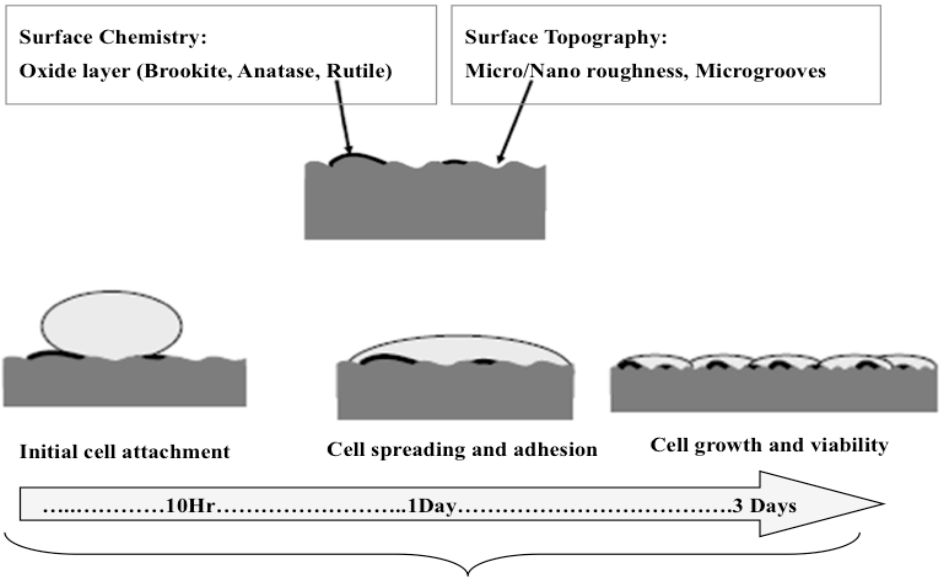

Figure 5-1 Schematic diagram demonstrating the important factors and stages of the osseointegration process

5.2 Sample Selection Criteria

Six surface categories were used for cell culturing analysis. Five samples from each category were used and the average result is presented. Properties of each surface category are listed in .

Table 5-1.

Table 5-1 Different Surface Conditions used for in vitro analysis

	Surface	Surface Quality	Surface Description	
1	1	Polished CP-Ti (P)	Polished, Ra<100nm	
2	2	Grinded based surface (G), grinded with paper grit of 600	Ra	Rq
			500 nm	600 nm
3	3	HP soaked sample (HP), Remained in 3% HP for two weeks,	Ra	Rq
			600 nm	850 nm
4		Pseudo-Periodic based Rough Surface (R), Processed at P= 10 W, F= 20 kHz, D=50 μm, with processing speed of 0.5, 0.25 and 0.1 mm/s for test 4, 5 and 6 respectively	R_a (μm)	R_q (μm)
	4		0.8 (R_a1)	1 (R_q1)
	5		1 (R_a2)	2.5 (R_q2)
	6		1.6 (R_a3)	3.05 (R_q3)
5		Pseudo-Periodic based microgrooves (MG), Processed at P= 10 W, F= 20 kHz, D= 50 μm, and ν= 0.25mm/s	Spacing (S), (μm)	R_a (μm)
	7		10	1
	8		60	1
	9		120	1
6	10	Ablated based Microgrooves (A), Processed at P= 15 W, F= 20 kHz, D= 50 μm, ν= 0.4 mm/s	Depth	5 μm

A polished CP-Ti (P) substrate is used as a reference to represent a surface with little (i.e., in the range of nanometer) or no roughness, with a stable titanium oxide layer formed at room temperature. As discussed in chapter three, polished surfaces were finished following surface grinding, followed by diamond and OPS polishing, which resulted in a surface roughness of less than 100 nm.

Hydrogen Peroxide (HP) soaked samples are surfaces kept in HP for two weeks. The interaction between HP and titanium results in the corrosion of titanium and the formation of roughness with an R_a of approximately 600 nm and R_q of approximately 850 nm. Immersing titanium in an HP oxidizing environment also results in the formation of a thick layer of titanium dioxide with three different structures (brookite, anatase and rutile), which are expected to affect on the biocompatibility of surface. Optical microscopy and optical profilometry images of HP soaked substrates are shown in Figure 5-2. The 2D and 3D images of optical profilometry analysis reveal the random roughness on the substrate. The x and y profile of the roughness on a random path exhibit an R_a and an R_q of 500 and 800 nm, respectively.

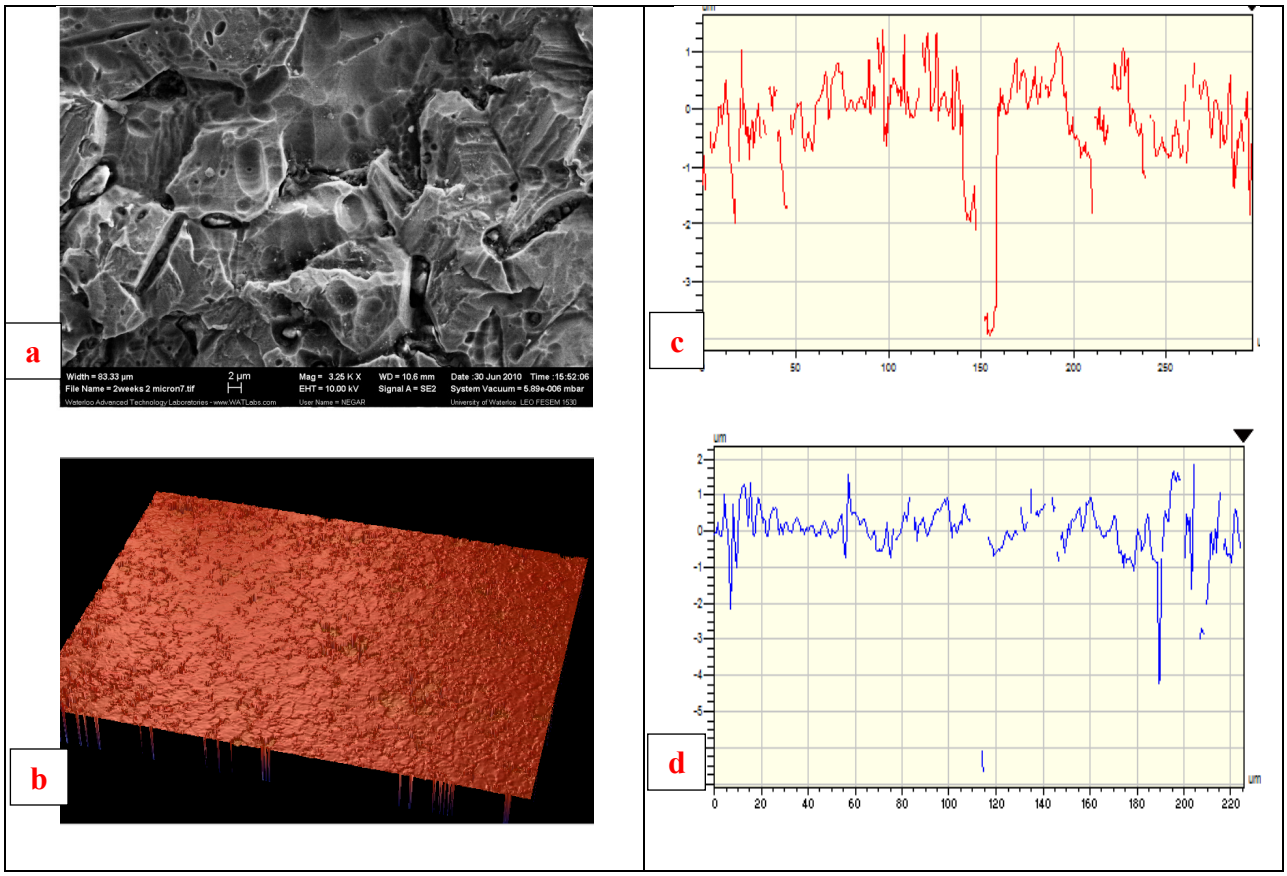

Figure 5-2 HP Soaked sample (a) optical microscopy (b) 3D image of Optical profilometry (c) X profile and (d) Y profile

Ground surfaces (G) are developed by grinding titanium with grinding papers with grit of 200 to 600. The average roughness of the ground substrate is similar to the average roughness of the HP soaked samples; however, the surface presents a different topography. HP soaked substrates have an uneven roughness, while ground substrates have uniform microgrooves in one direction.

Optical microscopy and profilometry characterization of grinded surfaces is presented in Figure 5-3. The parallel grooves are presented in both optical microscopy and the 2D and 3D

optical profilometry images. The R_a and the R_q of the x and y profile are roughly 500 and 600 nm, respectively.

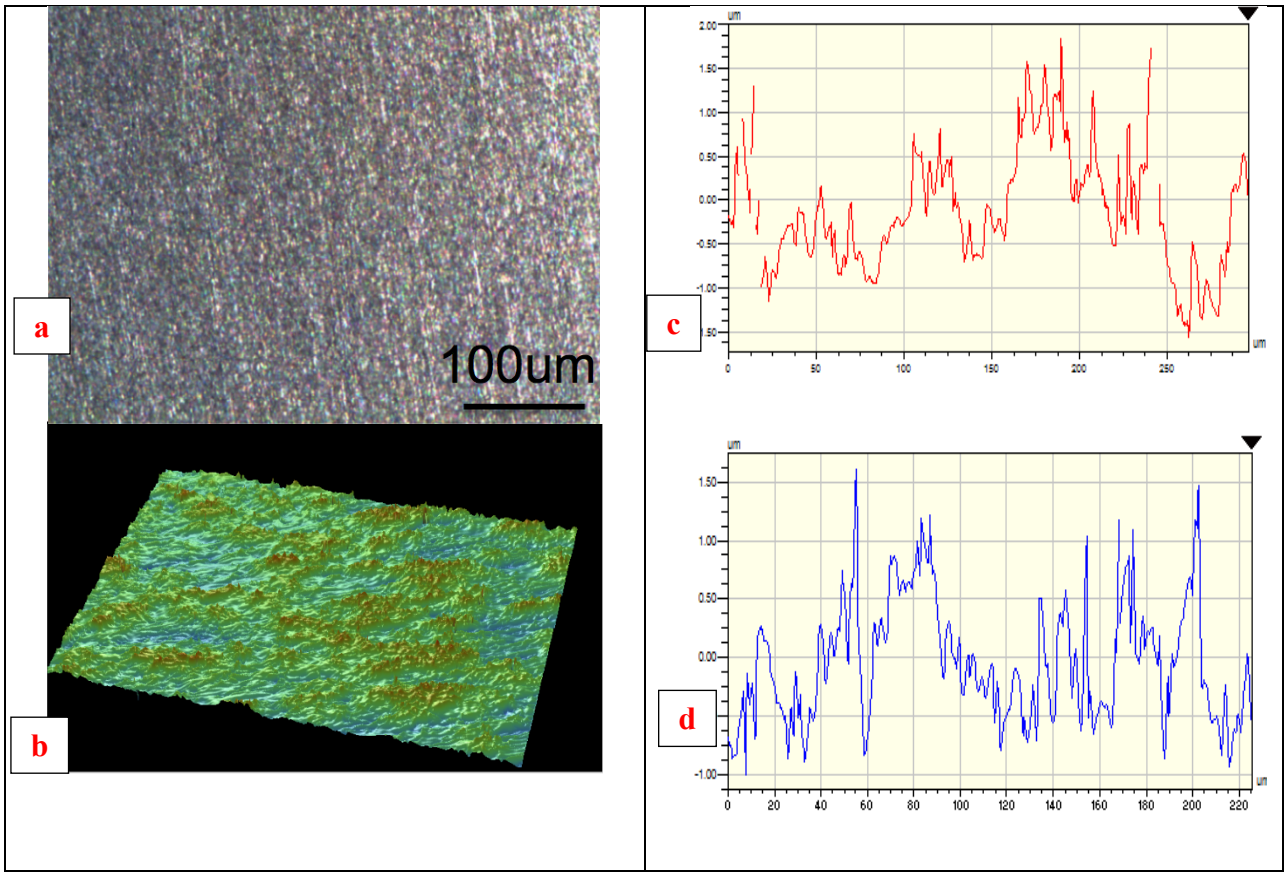

Figure 5-3 Ground sample with paralleled grit lines (a) optical microscopy (b) 3D image of optical profilometry (c) X profile and (d) Y profile

Pseudo-periodic based rough surfaces (R) are surfaces covered with roughness formed by the laser technique introduced in this study. Passing a laser over the surface develops these surfaces and then offsetting subsequent laser passes by a measurement equal to the size of the laser track.

Each laser pass forms a dome shaped path that protrudes from the surface. Even when the laser pass offset is smaller than the width of the laser path footprint, a small distinguishable line

can be observed between each laser path. The formation of this line could not be avoided, even with an offset smaller than the laser footprint.

As discussed in chapter three, changing the laser process parameters can easily control the roughness, size and shape of PP structures. Effective energy (via controlling velocity) was introduced as the main process parameter that could affect the structures. In order to determine the best structure for improving osteoblast integration, three different surfaces with PP structures with the average roughnesses of R_a1, R_a2, R_a3 and root mean square roughnesses of R_q1, R_q2, R_q3 were developed and analyzed. Profilometry images of three single laser paths with three roughness values are depicted in Figure 5-4 to Figure 5-6.

The 2D and 3D images demonstrate that surfaces with R_a1 and R_q1 micro-structures have not sputtered enough above the surface; therefore, the area for cell-material contact is comparable with the initial unprocessed substrate. Surfaces with R_a2 and R_q2 have conical structures on the surface, which increases the effective contact area and provides larger bedding for cells to spread on. Profilometry images of substrates with R_a3 and R_q3 reveal that, at these higher effective energies, micro-structures stop growing and local melting occurs, resulting in the presence of smooth zones on the surface with lower nano-roughness.

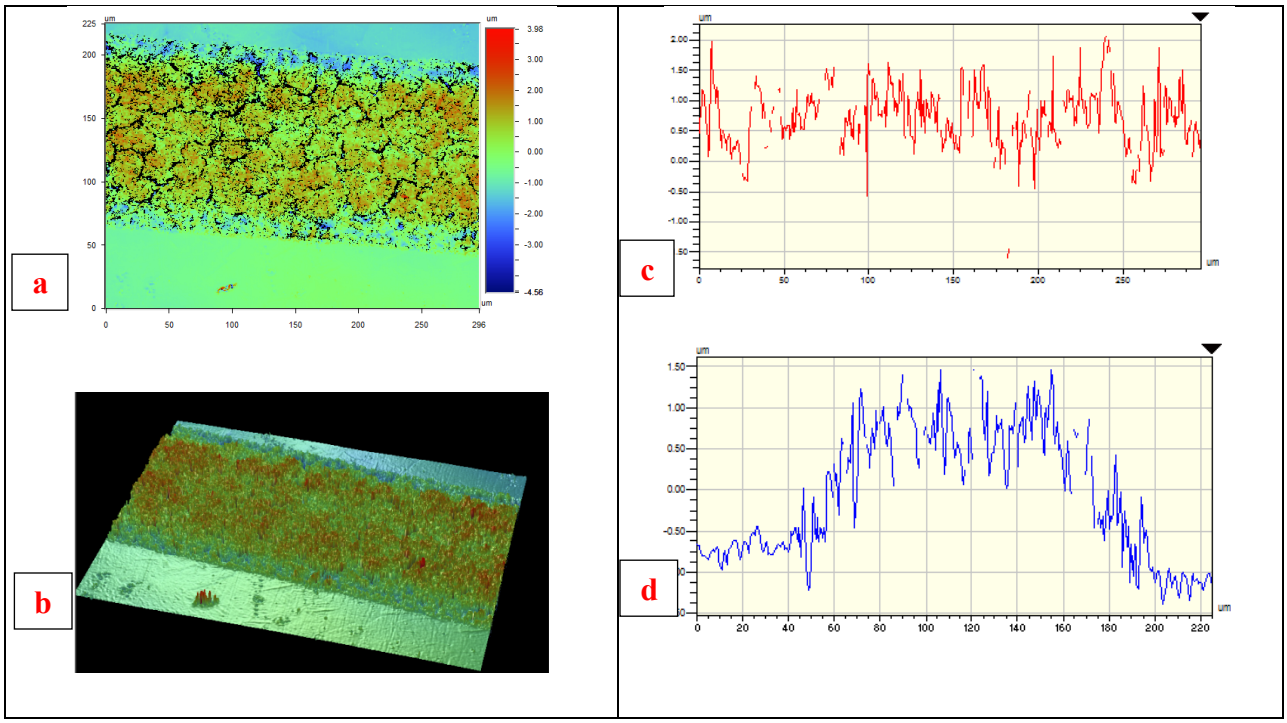

Figure 5-4 Pseudo-Periodic based Rough Surface with R_a1 and R_q1 (a) 2D profilometry image (b) 3D profilometry image (c) X profile and (d) Y profile

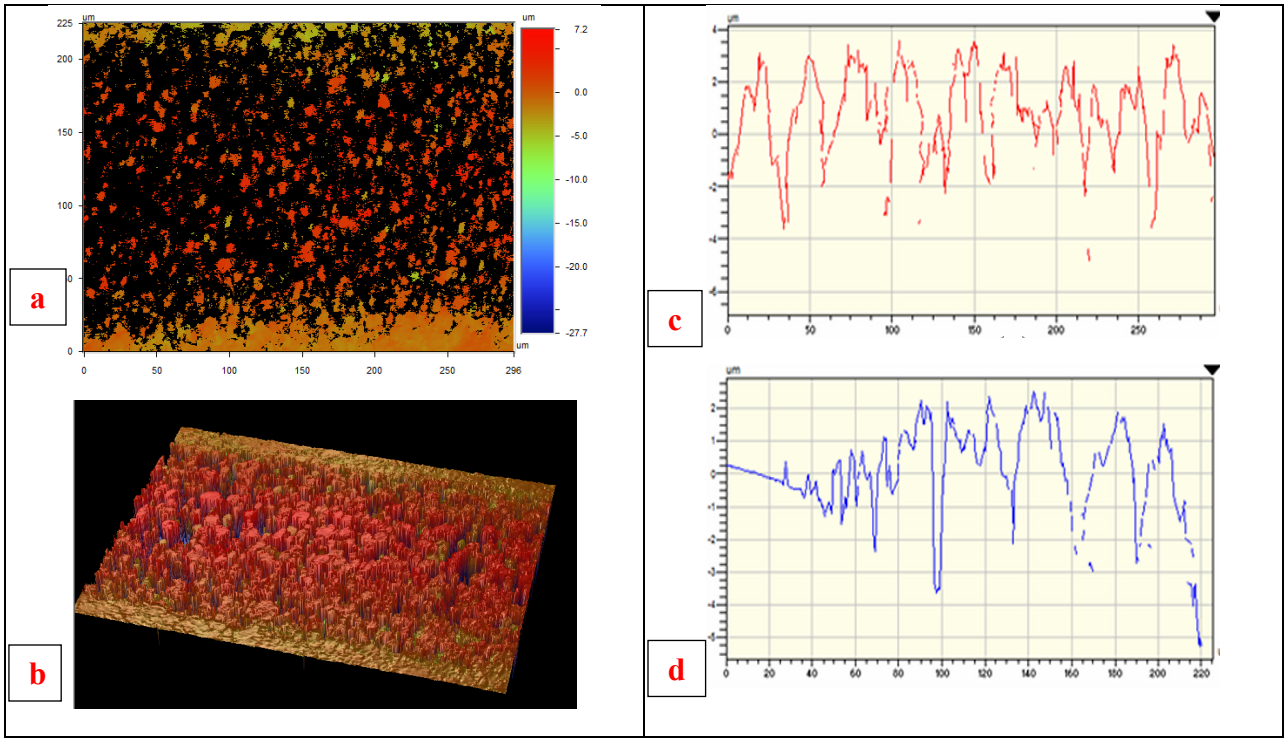

Figure 5-5 Pseudo-Periodic based Rough Surface with R_a2 and R_q2 (a) 2D profilometry image (b) 3D profilometry image (c) X profile and (d) Y profile

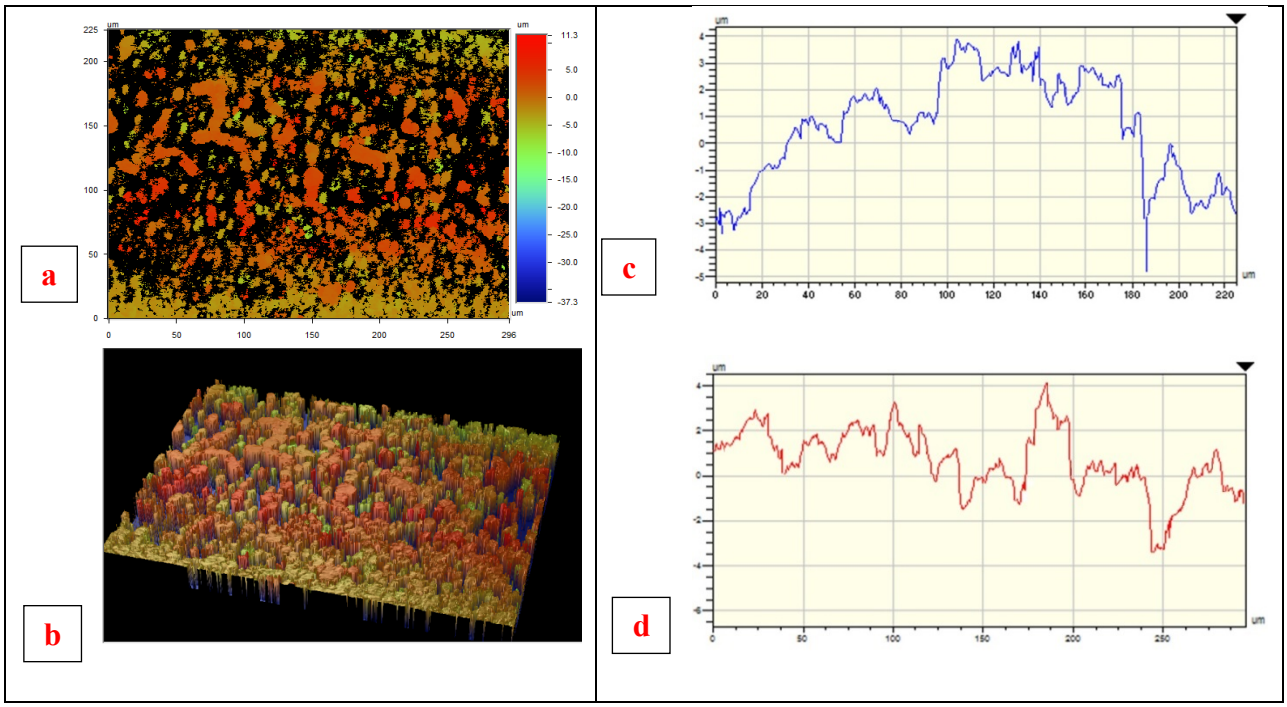

Figure 5-6 Pseudo-Periodic based Rough Surface with R_a3 and R_q3 (a) 2D Profilometry image (b) 3D profilometry image (c) X profile and (d) Y profile

The PP-based micro-grooved substrates (MG) are developed similar to the PP-based rough surfaces. The difference is that the offset is larger than the laser path footprint. This process leaves spacing with initial unprocessed surface quality between laser passes. PP-based microgrooves are characterized by three dimensions: height, spacing and width of grooves, as shown in Figure 5-7. The spacing between the grooves can be changed by varying the offset values. The height difference is dependent on the value of R_q of the PP micro-structures, which is controlled by the laser process parameters. The width of the grooves is essentially constant for the process developed in this experiment.

In order to study the effect of the spacing on the osseointegration process, surfaces with different spacing (i.e., 10 µm, 60 µm and 120 µm) but the same roughness value (i.e., Ra2 and R_q2) were developed.

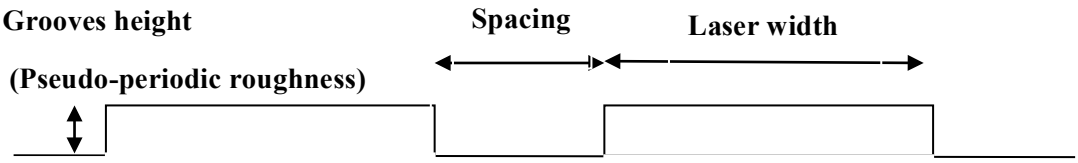

Figure 5-7 Schematic image of Pseudo-periodic based grooved surface

The main expected effect of the presence of microgrooves on the surface is to orient cells in the direction of the microgrooves. As mentioned in the literature, there are different methods for creating microgrooves on the surface of titanium. In this chapter, in order to emphasize the advantages of the microgroove structures formed through the introduced laser processing, three types of surfaces with parallel microgroove are compared:

- Ground surfaces (G): the size of parallel lines is dependent on the grit size of the paper.
- Parallel microgrooves formed by laser PP-based micro-structures sputtered out of the substrate (MG). The effect of microgroove spacing on the cell orientation will be considered.
- Parallel microgrooves formed through ablation of material at higher intensities (A). This type of surface has not yet been discussed in this experiment. The reason for discussing this concept in this section is to emphasize the advantage of the creation of microgrooves through self-assembled PP-based micro-structure formation.

Figure 5-8 represents the cross section of two different types of microgrooves; MG and A. Figure 5-8 (a) shows microgrooves developed by self-assembled PP-based micro-structures protruding from the substrate, as developed in this study. The main theory behind the formation of these structures, as was explained in Chapter three, is the melt displacement of locally melted

substrate created by laser processing at intensity levels close to the material threshold intensity. Figure 5-8(b) represents a different texture that was developed by other groups [93].

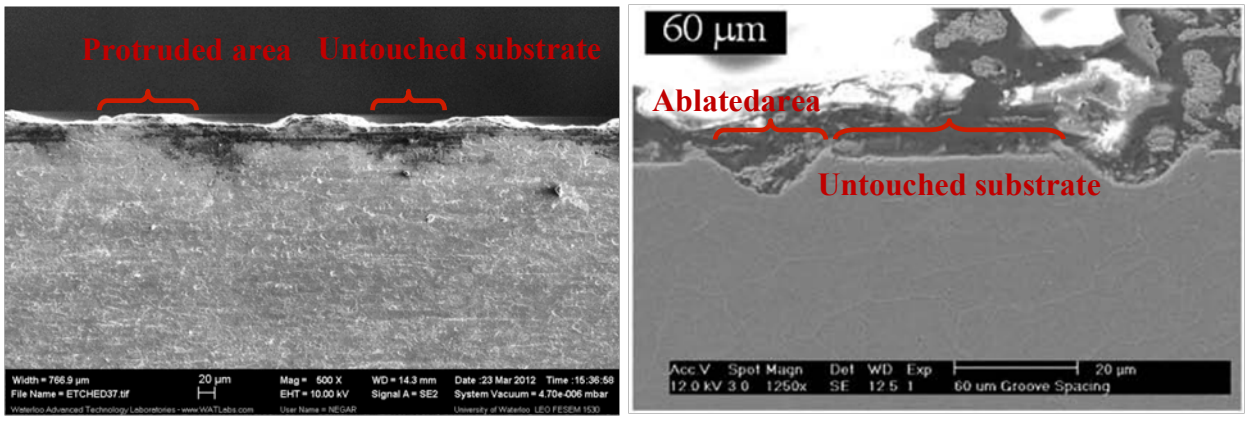

Figure 5-8 Comparison between two laser developed micro-grooved structures; (a) self-assembled PP-based micro-grooves sputtered above substrate (b) Ablated based microgrooves created into the substrate depth [93]

The ablated based microgrooves (A) are developed so that a comparison between cell orientation on the surfaces with microgrooves that are sputtered above the surface of the substrate (i.e., laser sputtered pseudo-periodic based microgrooves) and grooves made onto the substrate (i.e., laser ablated based microgrooves) can be made. This will allow for the comparison of this study's introduced surface with surfaces that are already discussed in the literature. This comparison will prove the advantages of this study's method over the previous methods.

Ablated-based microgrooves are developed for this part of study using the same nanosecond fiber pulsed Ytterbium laser. The process parameters for generating these types of structures are different from the ones used for generation of the PP structures. In order to achieve the laser

intensity that results in surface ablation, the beam splitter was removed from laser path to decrease in laser power loss. Laser power on the processed area measured to be 15 W at laser frequency of 20kHz. Beam spot size was chosen to be 50 μm. Ablated micro-grooves were processed at scanning speed of 0.4 mm/s.

Figure 5-9 shows the difference between the PP-based sputtered and ablated microgrooves. Figure 5-9 (a) shows the sputtered PP micro-structures. The highest levels on these structures are the micro-structures that are above the original surface. Figure 5-9 (b) shows the ablated based microgrooves. The highest level is the bare titanium, while the ablated surfaces are approximately 5 to 10 μm below the surface (depending on the laser intensity).

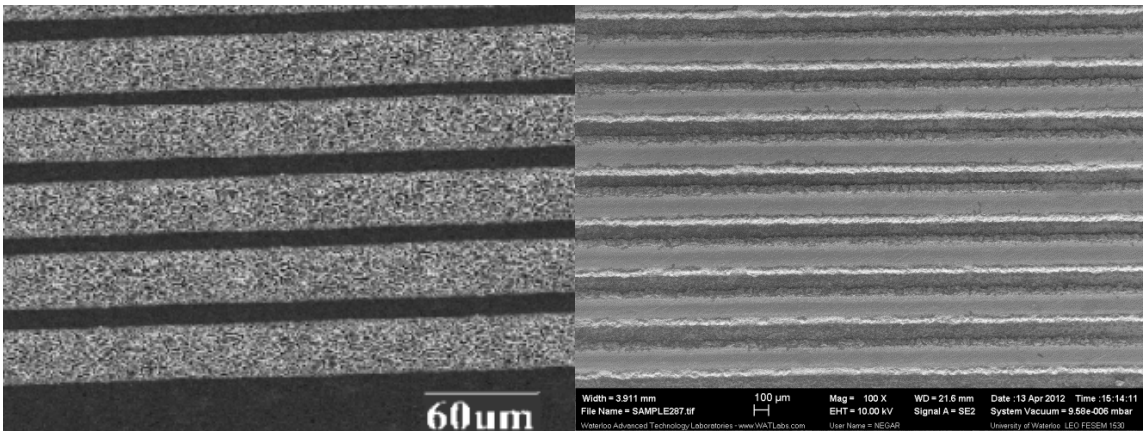

Figure 5-9 Optical microscopy image of (a) Pseudo-periodic based grooved substrate (b) abated based grooved substrate

5.3 Cell Culturing Experimental Procedure

On the selected substrates, $1x10^5$ cells/cm^2 MG-63 bone extracted cells were cultured to determine the effect of surface modification on the cell behaviour. Cell culturing of samples was

done in collaboration with Dr. Maud Gorbet's lab in the System's Design Engineering Department and Optometry Department (University of Waterloo).

In the following sections, the sample and cell preparation for cell culturing in-vitro analysis is introduced. The cell culturing procedure is then presented and the surface analyses that were conducted to investigate the cell biocompatibility on the developed surfaces are explained.

5.3.1 Sample Preparation for Cell Culturing

The six introduced substrate categories are used for cell culturing. Five samples from each condition/category are prepared and sterilized for cell culturing. In order to prepare substrates for cell culturing, all samples were kept in conical tubes and ultrasonically (VWR-B1500A-MT, USA) cleaned in three different steps using different solutions, including distilled water, detergent soap, and acetone, each for half an hour [93]. Samples were then sterilized in ethanol for five minutes. Finally, samples were rinsed three times with PBS, dried with nitrogen gas, and kept under UV light for 20 minutes.

To target the same area on each sample, biocompatible press-to-seal silicone sheets with 0.5 mm thickness adhesive (Life technologies, USA) were used to make a boundary wall to cover a 0.38 mm^2 area on the modified surfaces. Silicone papers were also sterilized and washed using ethanol and exposed to UV light for 20 minutes.

5.3.2 Cell Preparation for Cell Culturing

The MG-63 cell line (ATCC, CLR-1427, USA) was taken from an osteosarcoma of a 14-year old Caucasian male for cell culturing. MG-63 cells are kept in different cryovials and frozen in a

-80 ^{o}C freezer overnight, then transferred into liquid nitrogen for storage. Before cell culturing, cells are thawed and seeded. Cell thawing of each cryovial is done by dipping the bottom ¾ of the cryovial in a 37^{o}C water bath (Isoterm, 205, USA) and swirling gently for 1-2 minutes until the contents are thawed. After melting the last sliver of ice, the cryovial is rinsed with 70% ethanol and wiped dry in a biological hood. Thawed cells are then transferred into a prepared 25 ml flask with added keratinocyte serum-free medium (KSFM) (9 ml), which is equilibrated for 30 minutes. KSFM (Sciencell) is prepared by adding 1% penicillin/streptomycin and bovine pituitary extract. Gentamycin (Gibco #15710-064) with 1:1000 dilution (for 500 ml bottle of medium, add 500 μl) may be needed if contamination is observed.

Cell seeding is done in a 37^{o}C, 5% CO_2 incubator. Cells must be suspended and dispensed into a flask. Growth medium must be warmed up to 37^{o}C and added to the flask the next day after the seeding (10 ml for 25 ml flask). When cells appear healthy, the growth medium should be changed every 2-3 days. During cell seeding, cells are examined daily using a microscope so as not to allow cells to become over confluent and stay at confluence for more than 2 days, which might cause cells to suffer irreversible contact inhibition.

Cell splitting is done once cells are confluent in the dish. Medium is then removed from the culture dish by aspiration, and cells are rinsed with 5 ml of sterile PBS and aspirate. TriplExpress (3 ml) is then added to the flask, followed by rocking the dish gently to ensure cells come in contact with the dissociation solution. Cells are incubated at 37^{o}C for 30 minutes until the cells detach. After the cells are detached, a 10 ml solution of DMEM is added to the dish to neutralize the solution. The medium is pipetted up and down several times to rinse and collect the majority of the cells. The medium is then collected in a 15ml conical tube.

The tube is spun at 1300 rpm (320 g) for 6 minutes in a clinical centrifuge to pellet the cells. The supernatant is carefully removed and the pellet is re-suspended in a small volume of KSFM (3 to 5 ml). The cells can then be divided for seeding into several dishes containing KSFM.

A centrifuge is used to separate cells from media and to generate condensed cells using an Allegra X-22 Series centrifuge (Beckman Coulter Inc, USA). The sample is kept in the machine and mobbing by 800 rpm for 10 minutes. Cells are then mixed well to ensure a uniform suspension and are counted in a small amount of suspension volume using a hemocytometer bright light (Horshan/Hausser Scientific, USA). The volume can be adjusted based on the pellet size to achieve a reasonable density for counting. The number of cells for each sample for this study was $1x10^5$. 700 μl of KSFM is then added to each well and the seeding well is kept overnight. On the next day, aspirate medium is replaced by a 700 μl fresh warmed medium and incubated for another 24 hours until they are ready to be seeded on the substrates.

5.4 Experimental Observations

As discussed in chapter two, the main effect of surface texture is on the short stages of cell integration. Cell attachment takes place in the initial hours of cell culturing, followed by the cell adhesion process, which takes place within the first two days of culturing. Cell proliferation starts after cell adhesion. The very first process of cell culturing (i.e., cell attachment and cell adhesion) has a crucial effect on the later process of cell proliferation and cell differentiation. The number of cells that can successfully be anchored to the surface, their adhesion strength, and also the orientation of cells on the surface are the main factors that will affect the durability of the implanted device in long term. Therefore, in order to investigate the effect of surface modification on the surface biocompatibility, it is of great importance to see the effect of cell

culturing on the cell's short-term responses to the substrate (i.e., cell attachment, adhesion, and initial stages of proliferation). Analyses of cultures' surfaces are all done from 10 hours up to three days (72 hours) following cell culturing. At this stage, osteoblast like cells have been proliferated and they start to post mimic the differentiated phenotype.

5.4.1 SEM Analysis

In order to prepare samples for SEM analysis, the cells that have successfully attached must be fixed on the surface. In order to fix the cells, the cultured samples were washed with a 0.2 M sodium phosphate buffer at pH 7.2. Then 2.5% glutaraldehyde in a 0.2 M sodium phosphate buffer at pH 7.2 was added to the surface and stored in a sealed container at 4°C. Before ethanol-drying, 2.5% glutaraldehyde is aspirated to fix the biomaterial in 0.2 M sodium phosphate buffer at pH 7.2 for 4 minutes. This process is repeated twice. After the buffer is removed, 10% ethanol is added to the well and incubated at RT for 10 minutes. After the removal of 10% ethanol, the same step is repeated with 25% ethanol, 50% ethanol, 70% ethanol (twice), 90% ethanol, and finally 100% ethanol twice. Samples are then dried overnight in a safety cabinet. After fixing the cells, samples are gold coated to become ready for SEM analyses.

Cell area, orientation and circularity are investigated through image processing based on ImageJ software (Public domain). This was done manually by considering 50 cells per sample in a TIFF format of backscattered pictures that offers the highest contrast of color between the titanium substrate and the osteoblast cells.

5.4.2 Alamar Blue Test

Alamar blue (Life technologies Co., Canada) analysis is conducted for quantitative analysis of cell viability and cell proliferation. Alamar Blue is a water soluble dye that works based on metabolic activity detection. Metabolic activity will reduce Alamar Blue and will result in a change in its color from blue to red. This is the simplest nontoxic way to determine whether cells have enough energy and are capable of proliferation.

Each sample was located in a separate cell in a 12-well plate after removing medium and washing with PBS. Alamar blue solution is prepared by shaking and mixing 1 ml 10% Alamar blue and 20 ml of 10% phosphate buffer. 500 µl of mixture of Alamar blue solution was poured on each sample. The 12-well plate was then placed back into the incubator and left for one hour.

The same number of cells per volume was used on all samples, therefore, the same incubation time was also used. Incubation time was 1 hour then solvent was observed under Fluorescence microscope.

After 1 hour incubation time, 150 µl from each sample was taken and was put in a separate well to be used in the Alamar blue analysis. Of two methods available for monitoring cell viability (i.e., fluorescence based and absorbance based) fluorescence-based monitoring is possible at 530-560 nm wavelengths. Alamar blue assay detects the metabolic activity and oxidation-reduction of growth medium by exhibiting the fluorometric change. The prepared solutions were analyzed by SoftMax® Pro Data Acquisition & Analysis Software, by selecting the appropriate plate cells to read the EX, Em, and cut off the conditions of 530 nm, 560 nm, and 590 nm, respectively. Fluorescence is measured by exciting at 530 nm and measuring emission at 590 nm using a fluorometer. Fluorescence is monitored at 530-560 nm excitation wavelengths

and 590 nm emission wavelength. Alamar blue is reduced by the removal of oxygen and its replacement by hydrogen. The Alamar blue technique is demonstrated in Figure 5-10.

Alamar blue is a non-toxic to cells, as it does not interfere with the cell's normal metabolism. Therefore, cells were replaced in the incubator after each series of tests and were investigated at different time intervals of the cell culturing.

$$\textbf{AlamarBlue®}_{OX}\textbf{+2H+2e}^{-}\textbf{……AlamarBlue®}_{Red}$$

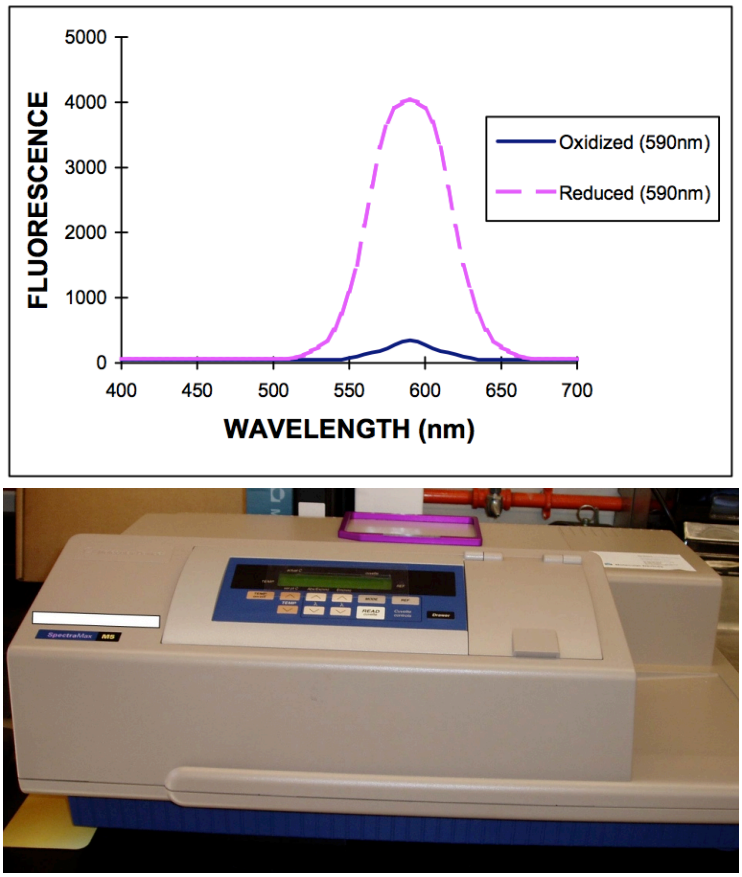

Figure 5-10 Alamar blue measurement

5.4.3 Trypsinization Test

Enzymatic detachment testing is performed to quantitatively study the effect of surface on cell adhesion. To complete this testing, samples are removed from incubator, and rinsed three times with PBS to remove the dead cells on the surface. Then 500 µl trypsin solution (EDTA) is poured on the surface of samples, and removed cells were counted at different time periods of 2.5, 5, 10, 15, 20, and 40 minutes. Finally, at the last increments, samples were immersed in EDTA and were kept in the orbital plate shaker machine (Model type: Standard 3500, VWR) to remove all cells from the surface. After each increment, 20 µl of solution is removed from the surface of the sample and kept in 96-well plates. 20 µl Trypan blue solution 0.4% (Sigma, country) is added to each well. 10 µl of the final solution is taken by pipette to be measured in the hemocytometer, as shown in Figure 5-11. The number of cells after each increment is collected to be compared with the total number of cells detached after the final increment. The comparison of the number of detached cells after each increment in the number of cell-trypzination curve quantitatively represents the effect of different conditions on the cell adhesion. Cell count is performed, and results are normalized with respect to the total number of cells of each sample.

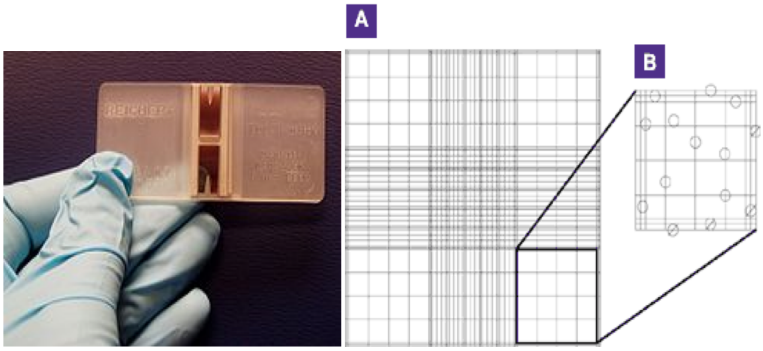

Figure 5-11 A hemocytometer being used for the measurement of number of detached cells

5.5 Results and Discussion

5.5.1 Qualitative Analysis of Cell Behaviour on Different Structures

To exhibit general cell behaviour on different surfaces, a typical SEM image of each condition is shown to give a general insight on the quality of osseointegration process on each surface category. Figure 5-12 to Figure 5-18 show both secondary and backscattered images of SEM analysis to depict both substrate structure and to distinguish between surface micro-structures and bone cells.

Figure 5-12 demonstrates the random spreading of osteoblast-based cells on a polished surface and represents cells without specific orientation. The random spreading at different scales shows that the substrate has little or no control on the cell attachment process. The accumulation of cells shown at the right hand side of picture represents that the effect of cell-to-cell (cadherin) protein bonding is more dominant than the cell-to-surface (integrin) bonding due to the lack of roughness on the surface and the inability of the surface to control the osseointegration process.

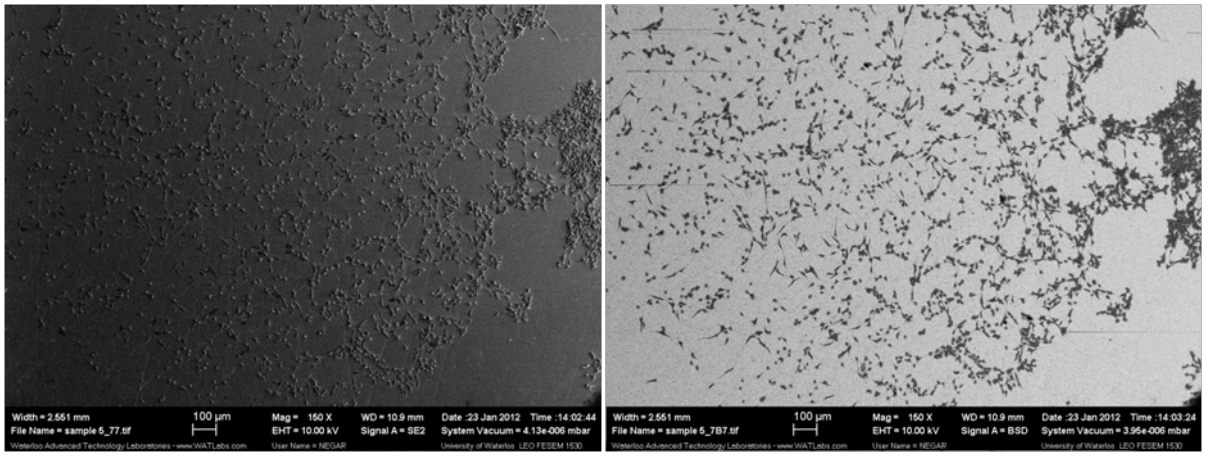

Figure 5-12 SEM image of polished titanium substrates after 10 hours of cell seeding (left) secondary image (right) backscattered image

Figure 5-13 shows the SEM image of HP soaked surface that represents a very disorderly roughness on the surface. Although the average roughness is almost the same as ground surfaces, the roughness is not uniformly distributed on the surface. This variation will lead to the formation of some elongated cells with spread focal adhesion points and some cells with no adhesion points with their initial spherical morphology.

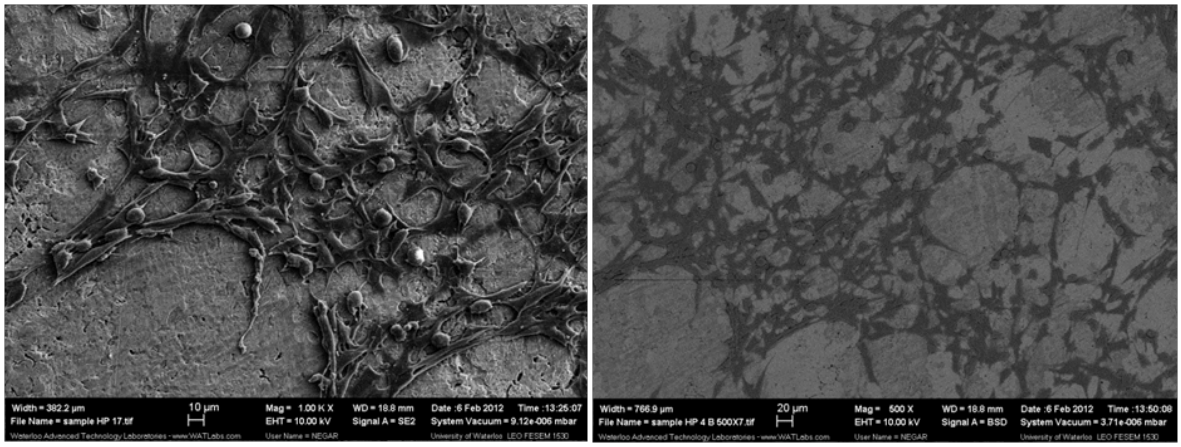

Figure 5-13 SEM image of HP soaked surface after 10 hours of cell seeding (left) secondary image (right) backscattered image

Figure 5-14 represents how cells orient in the direction of the ground surface at different scales. Although the relatively parallel micro-lines developed on the ground surface are not comparable with osteoblast cell size, they still established a well-oriented line of cells in the direction of grinding lines.

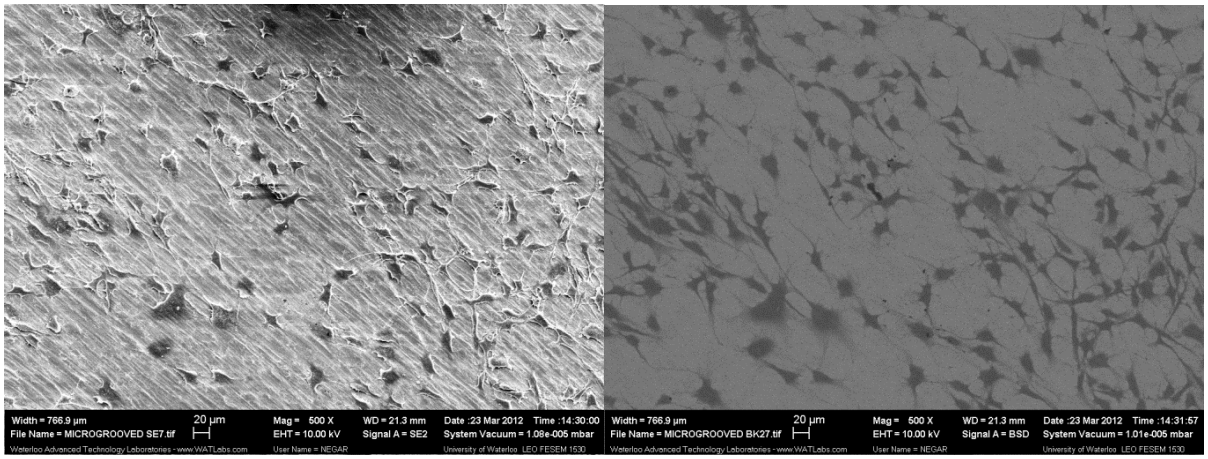

Figure 5-14 SEM image of ground surface after 10 hours of cell seeding (left) secondary image (right) backscattered image

Figure 5-15 shows cells on rough surfaces developed by PP micro-structures after 10 hours of cell culturing. The cells on this sample demonstrate a rounded and star like morphology. Figure 5-16 shows the same surface after three days of cell culturing, resulting in increased confluence of cells with elongate shapes oriented in the direction of the laser path. This demonstrates the ability of the surface to direct cell migration and cytoplasmic activity.

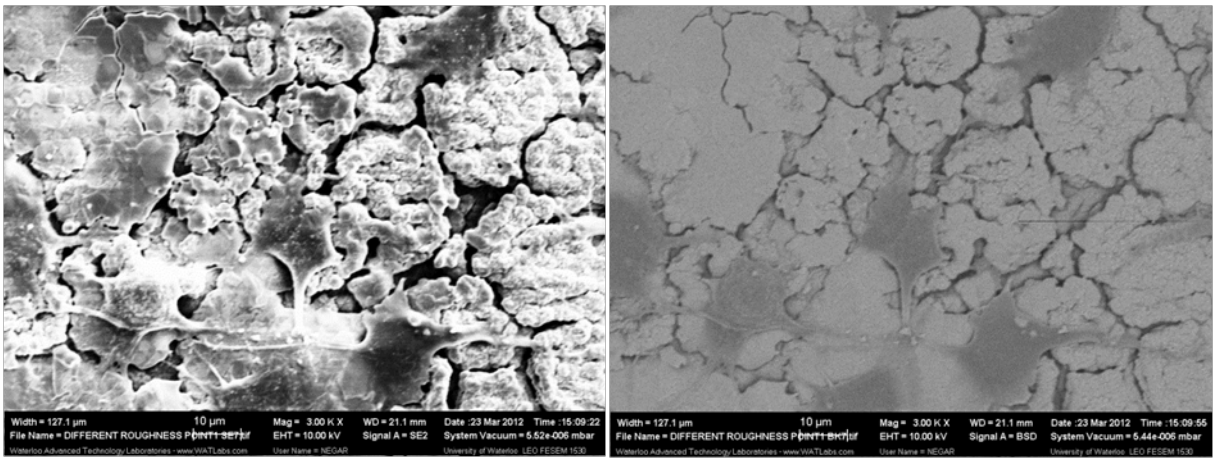

Figure 5-15 SEM image of PP-based rough surface after 10 hours of cell seeding (left) secondary image (right) backscattered image

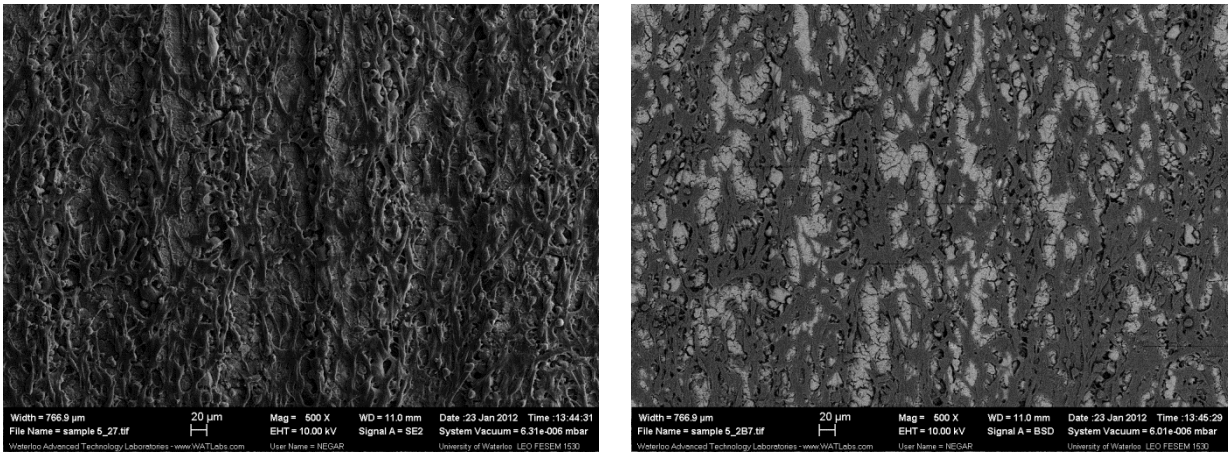

Figure 5-16 SEM image of PP surface after three days of cell culturing, (left) Secondary image (right) backscattered image. Laser path is alighned with the vertical direction.

Figure 5-17 shows how cells line up on the edge of the micro-grooved surface. It shows the random spreading of cells on the rough surface and that they start to orient close to the edge of microgrooves. Therefore, self-assembled PP-based microgrooves will result in well-spread cells that start to line up at the edge of microgrooves. The effect of the lined up cells will then influence the cells that are spread on the micro-structures and will allow them to orient similarly.

If a laser path is developed in the same direction as the base samples were ground, then the orientation of cells on the spacing between microgrooves will enhance the orientation of cells on the micro-structures.

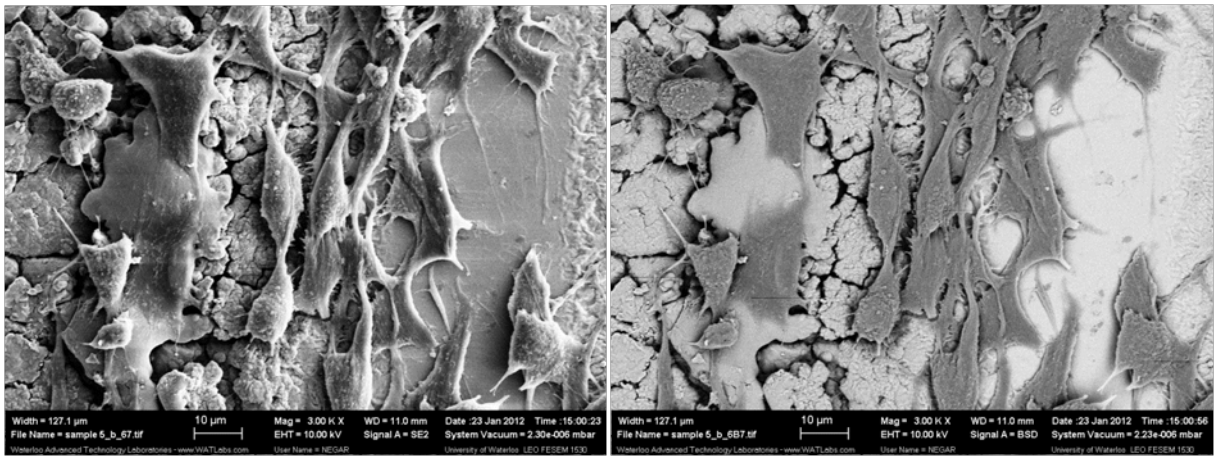

Figure 5-17 SEM image of PP micro-grooved surface after 10 hours of cell seeding, (left) secondary image (right) backscattered image

Figure 5-18 represents the cell attachment to the ablation-based microgrooves. The Ytterbium nanosecond fiber laser used in this experiment is capable of developing the ablation-based microgrooves. The concept of this type of surface has only been included in this chapter for comparison with self-assembled PP-based microgrooves. A more detailed discussion on the effect of ablation-based microgrooves structures on cell-orientations will be given in section 5.5.2.3. Figure 5-18 shows highly orientated cells on the ablated based microgrooves. This is due to the higher height of the microgrooves compared to PP-based microgrooves. Walls of ablated grooves prevent cells from sending signals through actin filaments, which form focal adhesion points; therefore, cells will send signals in the direction of the laser path and will eventually line up in the same direction. Figure 5-18 also demonstrates the melting of titanium during the ablation process, which smoothes the edges of the microgrooves, resulting in decreased roughness for cells to attach to. The lack of roughness on the area prevents cell adhesion

formation and enhances orientation in the ablated area and separates this area from the top surface.

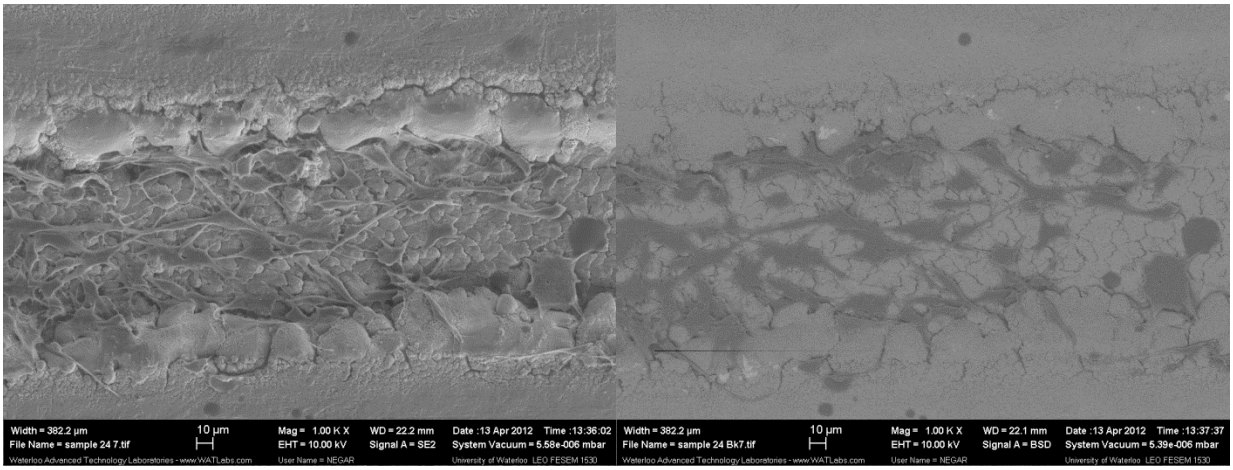

Figure 5-18 SEM images of ablation based grooved substrate after 10 hours of cell seeding, (left) secondary image (right) backscattered image

These observations on the quality of cell behaviours on different substrates will help with the understanding of the cell osseointegration process, which will be explained by quantifying the following parameters:

- Cell morphology (i.e., cell orientation, cell area and cell circularity)
- Cell density
- Cell migration.
- Cell adhesion
- Cell viability, growth and metabolic activity (essential for cell proliferation)

5.5.2 Quantitative Analysis of Cell Behaviour on Different Substrates

5.5.2.1 Effect of Different Structures on Cell Orientation

In order to study the effect of surface structure on cell orientation, three parameters (i.e., two centerlines and the effective angle, which enabled the introduction of cell orientation) are defined, as are shown in Figure 5-19:

- The cell center-line is the line that connects the two points of the cells that have the longest distance from each other.
- The substrate centerline lies in the direction along which it is desirable for cells to orient. A separate surface centerline is defined for each of the under-the-test substrate category. The left edge of SEM image is selected as the centerline for P and HP substrates. The direction of the ground grooves is the centerline for the so-called "G" substrates. Finally, the direction of the laser processing is defined as the centerline for R, and MG substrates.
- The cell effective angle is the smallest angle between the two introduced centerlines.

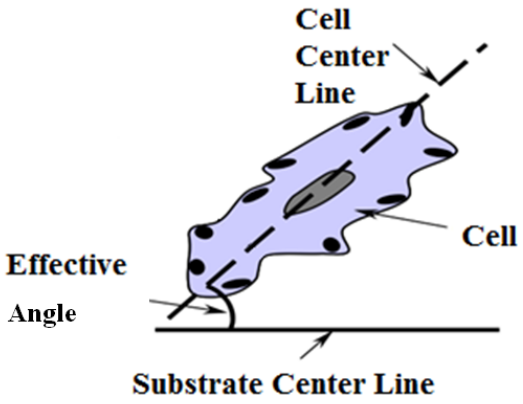

Figure 5-19 The schematic image of the cell with the parameters introducing the cell orientation on the surface

Based on the introduced parameters, the cell effective angle is obtained from the SEM images and is analyzed in the ImageJ software. The results are presented in Figure 5-20, which

shows the presence of very random orientation on P and HP substrates. Culturing cells for even longer period will not improve the orientation of cells and they keep preserve their random orientation through time.

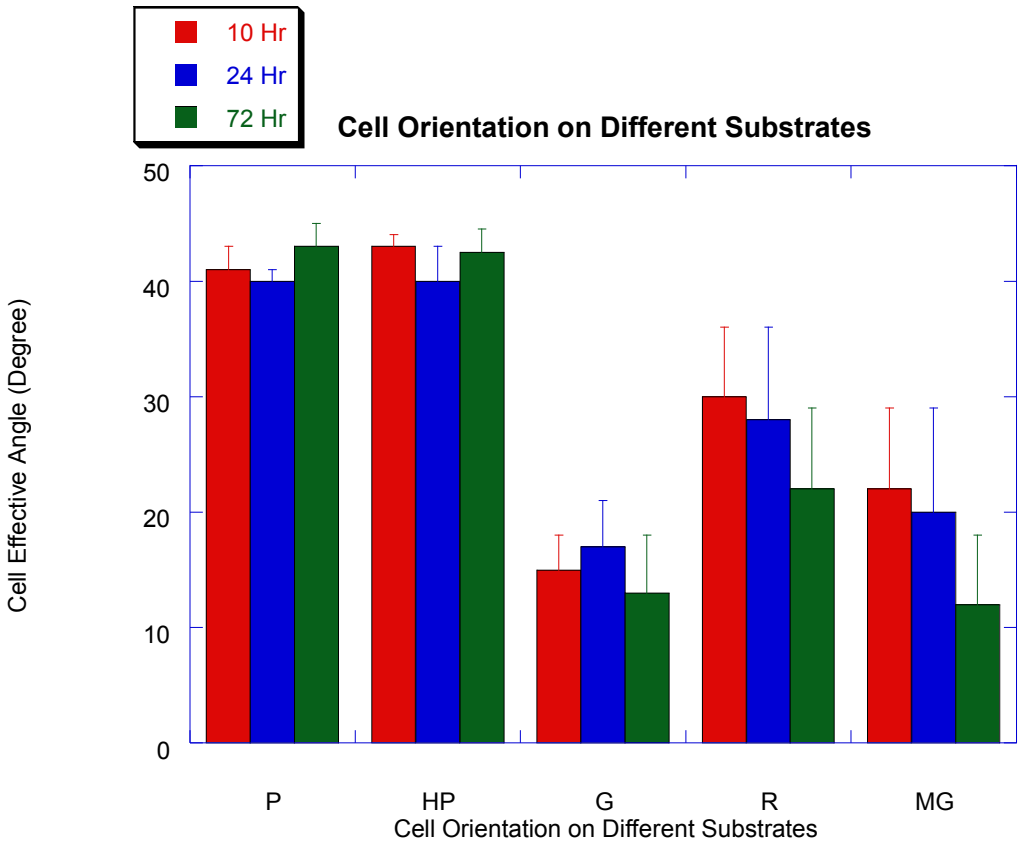

Figure 5-20 Cell orientation on different structures at different incubation time

The cells on the ground substrate start to orient in the direction of ground grooves, even in the initial stages of cell culturing, and they retain their orientation at longer culture durations. The reason for the small jump in the value of the cell effective angle after 24 hours of cell culturing is due to the presence of cells that are still not perfectly adhering to either the substrate or to other cells. By culturing ground substrate for a longer duration, cells continue to follow the substrates and other cells' orientations.

Cell orientation on substrates with self-assembled PP-based roughness is significantly lower than on ground surfaces at the first stages of cell culturing. The lower orientation is due to the fact that cells tend to create focal points at any anchors and the presence of micro-structures all over the surface creates numerous sites for cells to adhere to. The main factor that improves cell orientation on R substrates is the presence of the edge of a laser path kerf. Each laser path is developed with a slight overlap with other paths. However, due to the Gaussian property of the laser beam, the structures that are created on each laser kerf are somehow symmetric over the middle line of each path, which forms dome shaped micro-structures. Therefore, cells fill in the edge between each level and will line up through each separation. The presence of the oriented cells on the edges will affect the orientation of other cells lying on PP-based micro-structures at a longer culture time. Therefore, increasing the culture time decreases the cell effective angle degree.

Figure 5-20 shows a higher orientation on MG surfaces compared to R surfaces. Orientation of MG surfaces is shown to be lower than G surfaces in the first hours of cell culturing; however, the orientation will improve in later stages. Two factors improve the orientation of MG surfaces: 1) the effect of the laser path edge and 2) the effect of parallel zones between laser processed and unprocessed surfaces. The combination of these two factors will eventually affect the orientation of other cells, which are randomly spread over the area. It can be predicted that during the in-vivo experiment, cells may even orient better on R and MG substrates. When there are more cells adhering to the substrate, there will be more interactions between them and, therefore, they transfer the orientation of the cells that are lining up at the edges to the cells in the middle of the path.

The high variance of the results of the surfaces with R and MG qualities is due to the variety of sample selections. The variations between the results of PP-based rough surfaces (R) are due to having different roughness values (R_as and R_qs), which have a direct effect on cell orientation.

The main variation in the cell orientation on microgrooved laser modified surfaces is due to different spacing between each laser path (i.e., grooves). Therefore, a more in depth experiment is performed in the next sections to study the effect of roughness and spacing on the orientation of R and MG surfaces, respectively.

5.5.2.2 Effect of Surface Roughness on Cell Orientation

Figure 5-21 shows the cells effective angle on rough surfaces with different R_as and R_qs. On surfaces with lower roughness (R_a1 and R_q1) and higher roughness (R_a3 and R_q3), cell orientation is higher after 10 hours of culturing and it then drops after 1 day of culturing. However, cells regain their orientation again after a longer culturing time (3 days). In contrast, cell orientation on surfaces with R_a2 and R_q2 improves at all stages of cell culturing. In the following section, it will be shown that the adhesion strength is lower on surfaces with low and high roughness, while the highest adhesion strength is achieved on the surfaces with R_a2 and R_q2 roughness. The lower effective angle on the surfaces with lower adhesion strength (R1 and R3) at earlier stages can be explained by the fact that cells have made less focal bonds to the surface, which could be affected more easily by the edge effect.

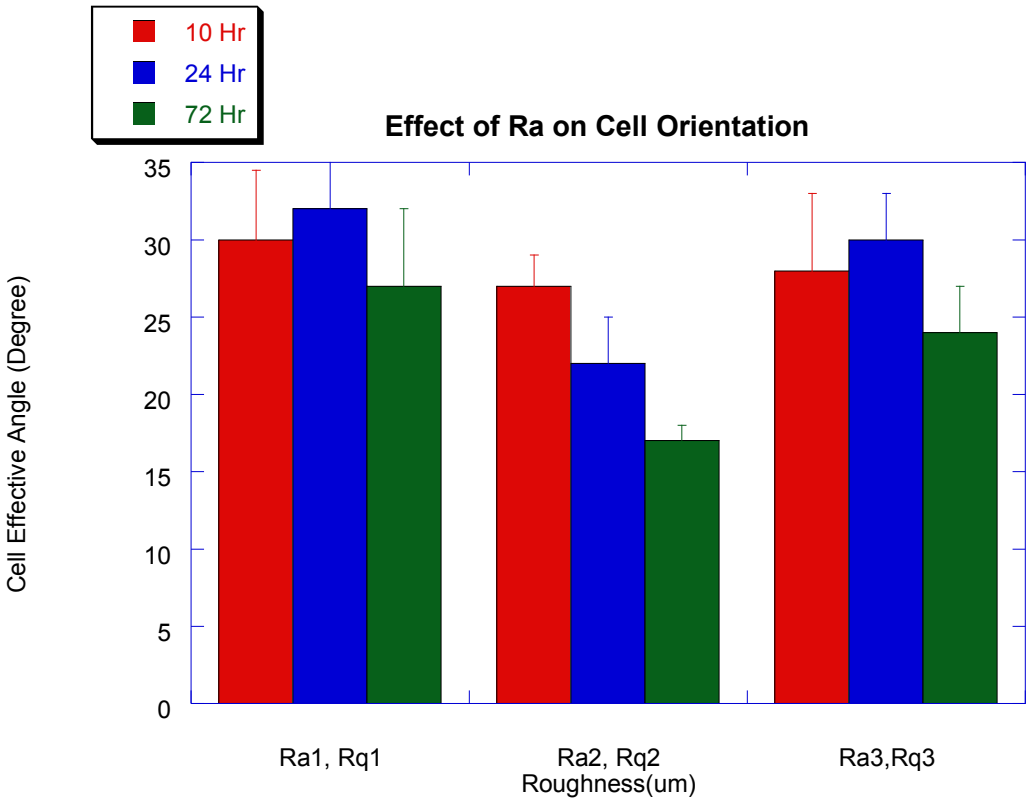

Figure 5-21 Cell orientation on rough surfaces with different roughness

5.5.2.3 Effect of Microgrooves on the Cell Orientation

As shown in the previous section, cells have the highest orientation on MG and G substrates due to the presence of parallel microgrooves. This section presents a more comprehensive analysis on the effect of PP-based microgrooves on cell orientation. The effect of spacing between the grooves on cell orientation will be studied. Cell orientation of MG surfaces at different stages of cell culturing is compared with the laser ablation-based micro-grooved surfaces, in which the microgrooves are created as craters in the surfaces.

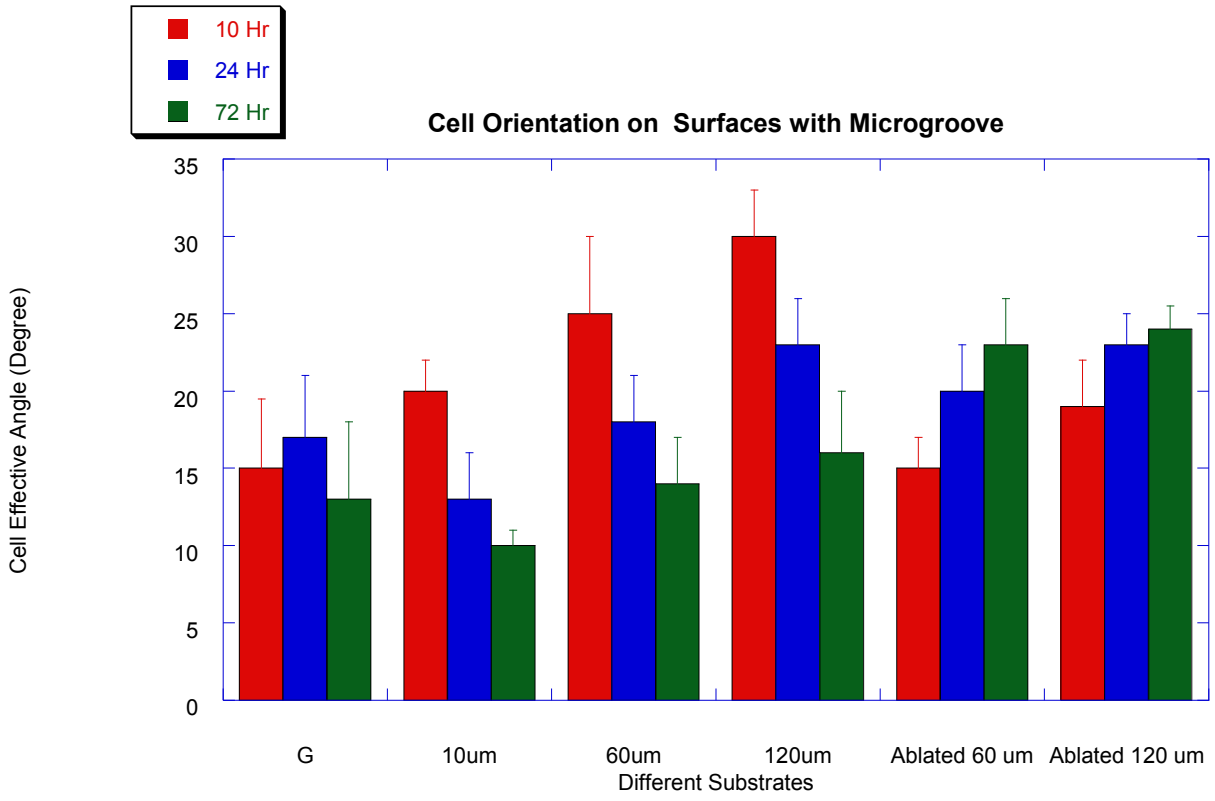

Figure 5-22 Cell orientation on three different micro-grooved surfaces; Ground (G), PP-based Microgrooves (MG) with Ra2 and different spacing and laser ablation-based microgrooves (A) with different spacing

Figure 5-22 shows a comparison between the cell orientations (cell effective angle) on the three types of micro-grooved surfaces: G, MG and A substrates. The orientation of the cells is measured after 10 hours, 24 hours and 72 hours. The effect of microgroove spacing is studied by comparing cell orientation on surfaces with the same roughness but different spacing of 10 µm, 60 µm, and 120 µm. The cell orientation of ablated microgrooves with two spacings of 60 and 120 µm is also compared with other surfaces.

According to the results presented in Figure 5-22, surfaces with G-based microgrooves have the highest cell orientation at the initial hours of culturing. However, the cell orientation decreases with increasing culturing time. The orientation of cells on the PP-based micro-grooved

surfaces is low at the first stages and increases over time due to the introduced edge effect, which has more impact on cell orientation at later stages. The results presented in Figure 5-22 show that surfaces with 10 μm spacing have the highest orientation compared to surfaces with 60 and 120 μm spacing, which have the lowest orientation.

Figure 5-23 shows the SEM images taken from the cells that are cultured on the ablation-based grooved surfaces after 10 hours and 1 day. This shows that cells start to fill the ablated zone without adhering to the unprocessed area due to the presence of roughness on the laser-processed area, which provides more anchors for cells to attach to. This observation from Figure 5-23 explains the cell behaviour on the ablated surfaces in Figure 5-22.

The results demonstrate that cells that are cultured on the ablated surfaces are more oriented at the first stages of attachment. At later stages of cell culturing, they fill the grooves then starting to lose their orientation. The presence of the melted edges results in a decrease in the cells' adherence. Therefore, cell orientation in the craters cannot be transferred to the top surface.

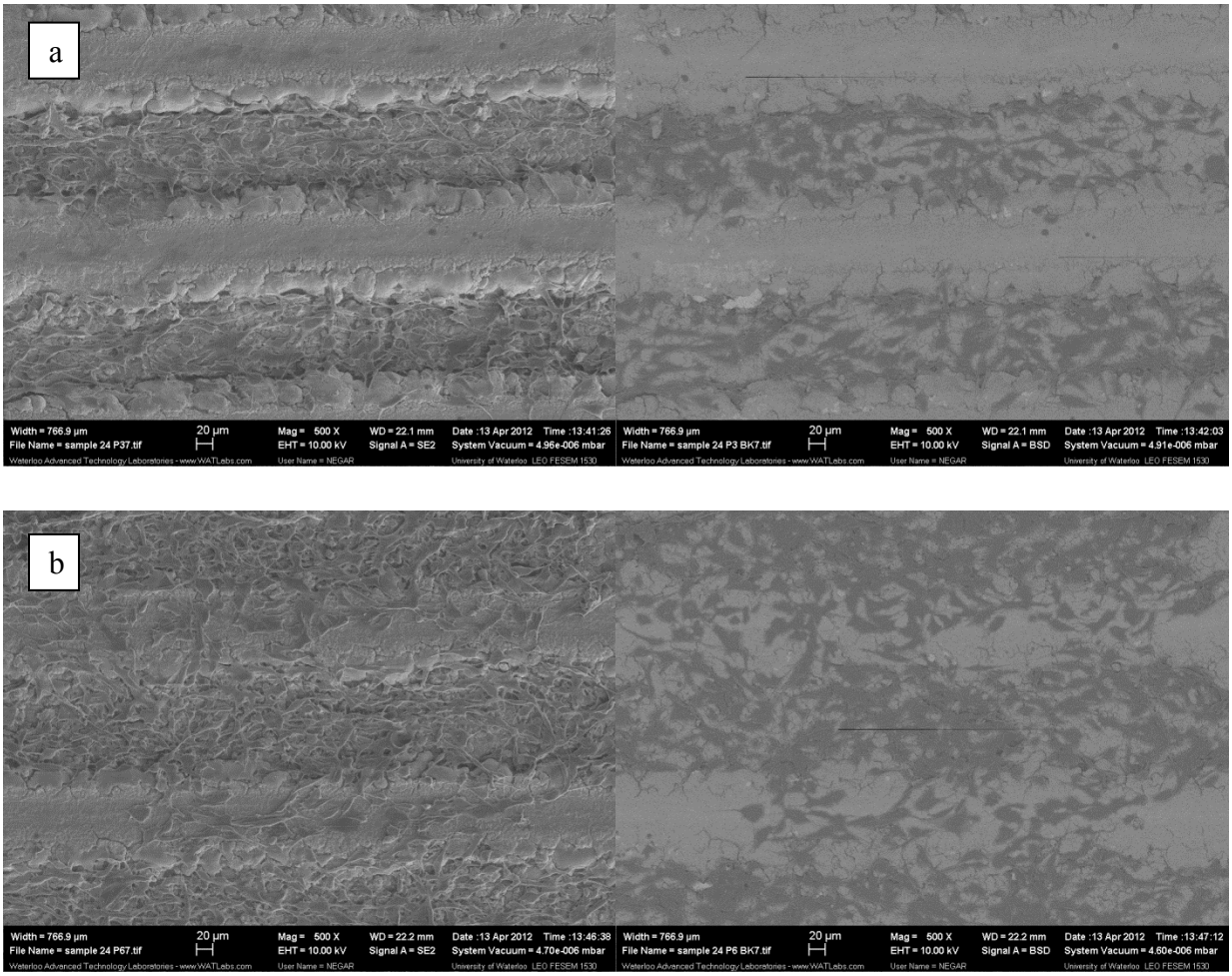

Figure 5-23 SEM image of cell orientation after (a) 10 hours and (b) 1 day of cell culturing (left) secondry image (right) backscattered image

5.5.2.4 Effect of Different Structures on Cell Area

This section demonstrates the effect of surface topography on the formation of focal adhesion points and, eventually, cell area. To conduct this analysis, an area of 20 cells in a 80 µm x 20 µm rectangle frame is detected manually and measured in the ImageJ software and the averaged cell area is reported for comparison.

Figure 5-24 shows that cell areas on the P and HP surfaces are very close to the initial cell size. The initial diameter of the spherical cell that is using for this study is about 7 µm, with an

initial area of almost 38 μm^2. The cell area on G surfaces is larger than P and HP surfaces due to the presence of microgrooves that will allow cells to spread over the surface. The results show that cells have the largest area at on R and MG surfaces. The presence of micro-structures on the substrate in the range of cell's size provide the perfect bedding for cells to spread on and create sites for cells to adhere to and to spread. This allows cells to become progressively larger. Cells start to orient more at longer cell culturing time, being affected by the laser path edge effect. This will result in decreasing their area. The trend of cell spreading on micro-grooved surfaces is very similar to that of the R substrate.

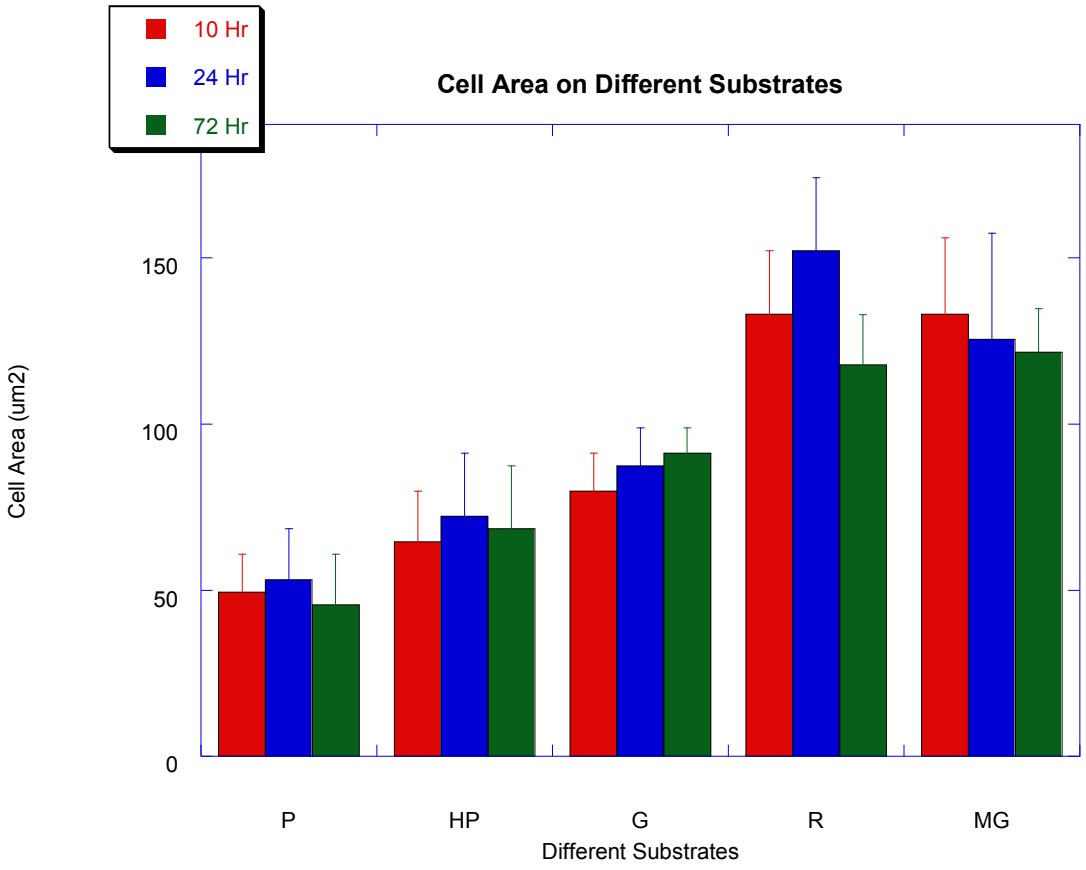

Figure 5-24 Average cell area on different surface structures presented in SEM image

5.5.2.5 Effect of Different Structures on Cell Circularity

Cell circularity is a factor in the cell migration. Circularity of cell is identified through aspect ratios of the lengths between two points of the cell with the longest distance (a), over the length of the cell on the perpendicular axis (b). The circularity of the cells is measured by averaging the aspect ratio between "a" and "b" for 20 cells in the ImageJ software. The average values are demonstrated in Figure 5-25, which shows that there is almost no change in circularity of the cell on P and HP surfaces. Also, the aspect ratio is much higher on G, R and MG substrates compared to P and HP. The presence of the high aspect ratio on surfaces with microgrooves (i.e., G and MG) represents the effect of having microgrooves on cell spreading and eventually cell migration.

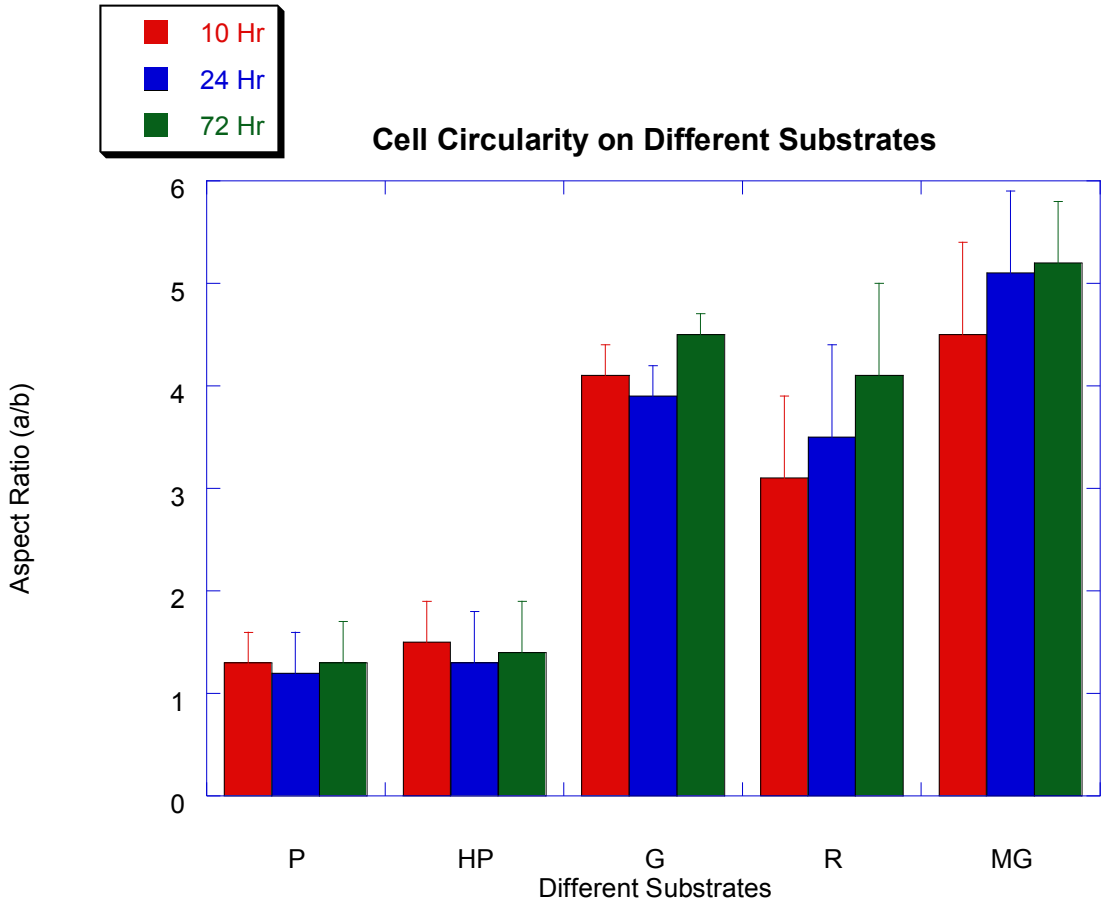

Figure 5-25 Aspect ratio of cells spreading on different substrates

5.5.2.6 Effect of Different Structures on Cell Density

In this section, the effect of different structures on the number of cells that are adhering to surface at different stages of cell culturing is studied. The numbers of cells were counted and reported for a 10 µl fully detached solution using a hemocytometer. The procedure is explained in section 5.4.3.

Figure 5-26 illustrates the cell density on different types of substrates at different culturing times: 10 hours, 1 day, and 3 days. As shown in Figure 5-26, cell population growth shows the same trend of increasing on all types of surfaces. The increase in the number of cells after 10 hours of incubation is more significant on rough (R) and PP-based micro-grooved substrates (MG).

On the polished surfaces, the number of cells does not increase significantly after a longer incubation time. The initial cell population seems to be higher than R and MG based surfaces. The higher cell population indicates that during the initial hours of cell culturing, the rough nature of the surface may push back cells and it is easier for cells to lay on a less rough surface. Over time, the presence of the roughness on the surface will provide better bedding for cells to adhere to. It is also depicted in Figure 5-26 that, despite our expectations, cell density of R and MG surfaces does not increase significantly after one day of cell culturing. The reason for this will be explained and discussed in the following section based on the SEM images shown in Figure 5-27.

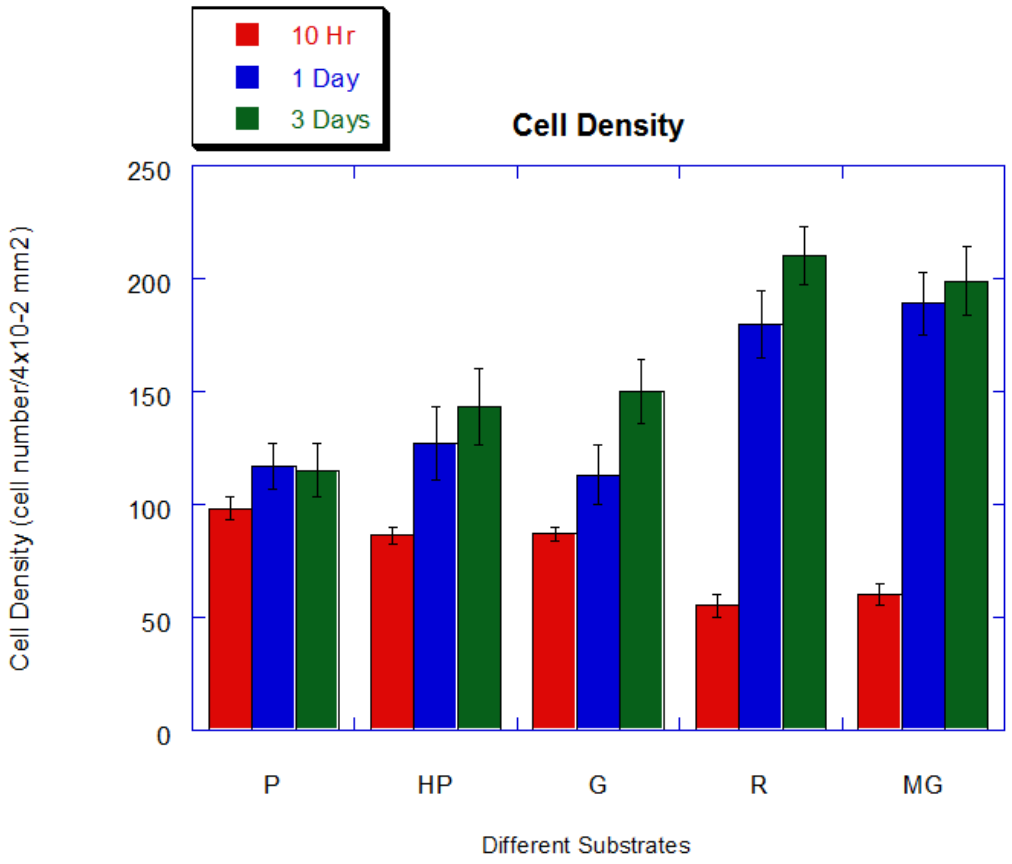

Figure 5-26 Effect of different substrates on cell density at different incubation time; 10 hr, 1 day and 3 days

Figure 5-27 represents the SEM image of cells on a micro-grooved structure after (a) 10 hours (b) 24 hours and (c) 72 hours. The number of cells that adhere to the substrate after 10 hours is considerably lower than at later times. The number of cells after 1 day of cell culturing is almost the same as 3 days of cell culturing. This can be explained by the fact that cell attachment process happens mostly in the initial hours of cell culturing. At later stages, cells start to establish bonds with the substrate through cytoplasmic site (focal adhesion points). Before the completion of all bond formation, the cell attachment is loose and might detach easily.

Despite having almost similar cell density on the surfaces that are cultured for 1 and 3 days, it will be shown in the next sections that the adhesion strengths at these two conditions are significantly different.

This shows that the first layer of cells adheres to the surface and the next layers are kept close to the substrate through the cell-to-cell adhesion and are still prone to establishing new integrin (cell-substrate) bonds to the substrate in the next stages. Based on this discussion, it could be concluded that the cell attachment process occurs mostly in the initial hours of cell culturing (i.e., less than a day) and cell adhesion will continue after that allowing cells to enhance their attachment through spreading on the substrate or other cells and establishing more adherent sites.

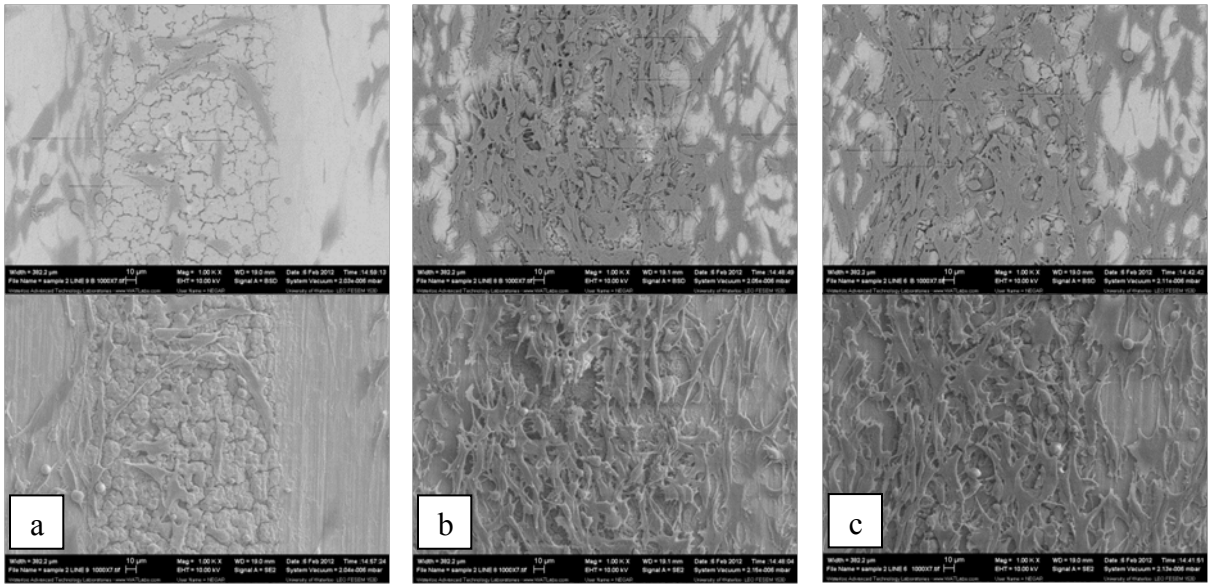

Figure 5-27 Variation in cell density on MG substrate and at different incubation time (a) 10 hours (b) 24 hours (c) 72 hours

5.5.2.7 Effect of Different Structures on Cell Migration

Cell migration is one of the required cell capabilities to form a successful osseointegration process.

Figure 5-28 compares the cell's morphology on the HP, ground and R surfaces, which indicate more oriented elongated cells on the ground and R surface. As a result of cell orientation, cells initiate their migration. Cells on HP soaked surfaces have more symmetric shapes that spread their focal adhesion points in all directions. Unlike cells on HP surfaces, cells on ground surfaces are not symmetric and are laterally elongated in the direction of their orientation. Cell migration is derived through the adhesion points and will carry the nucleus of cells. Figure 5-28 (b) shows the presence of an unsymmetrical cell with more extension of active driven structures (filopodia) at one pole and cell body at the other pole, representing the cell migration and the mobility in one preferential direction. These cytoplasmic projections (filopodia) contain actin filaments, which form the focal adhesions with the substrate and increase the cell adhesion. These filopodia in the cell-to-cell interactions are more visible on rough surfaces. Cells can find a site to anchor to the surface and then vinculin is formed at the filopodia, which leads to focal adhesion. Cell lamellipodia is then guided through the filopodia cites.

Figure 5-28 (c) shows how cells spread on a rough laser PP-basedmicro-structure (R). Roughness allows cells to spread and form more focal adhesion points and adhesion sites. The presence of more adhesion sites helps cells to spread on the surface and to initiate migration.

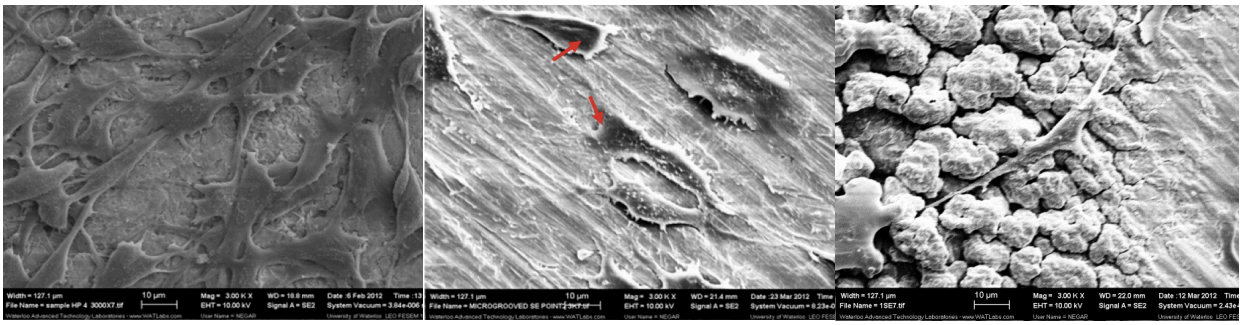

(a) (b) (c)

Figure 5-28 Effect of surface structure on cell morphology and its tendency to migrate on (a) HP soaked surface (b) Ground surface (c) PP-based rough surface

Although cells on the rough surface have random orientations, in a bigger picture; they follow the laser path and will travel through it. The cell migration on the laser pass direction is shown in Figure 5-29.

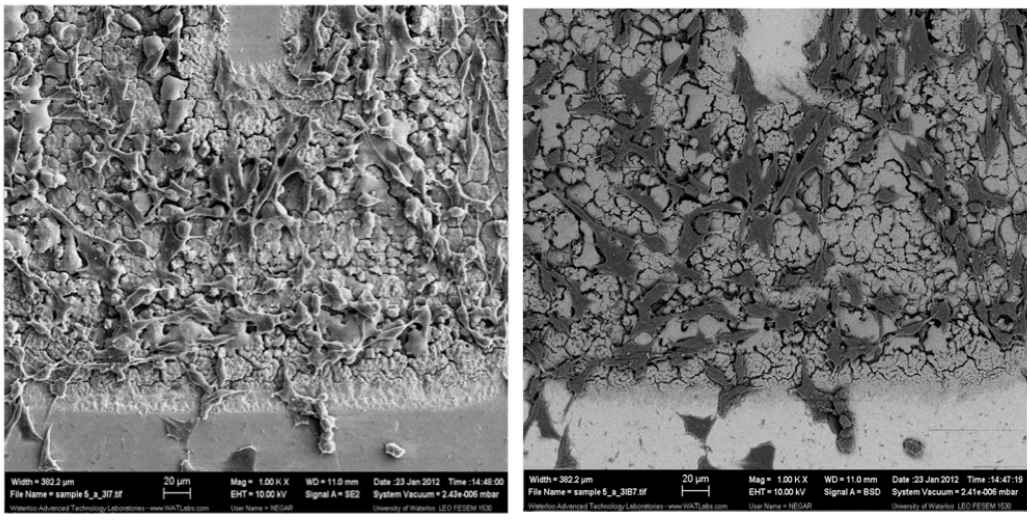

Figure 5-29 Cell migration in the direction of laser path (left) Secondary image (right) Backscattered image

It has been reported that grooves with lengths greater than 20 μm do not affect the orientation [57]. Figure 5-30 shows that cells orient on the surface and start to migrate in one direction even on the grooved surfaces with spacing larger than 150 μm.

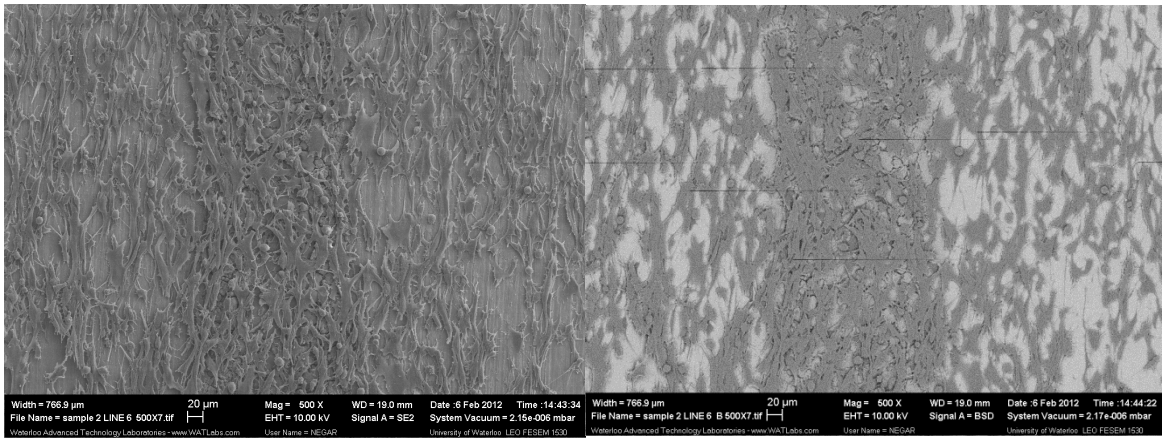

Figure 5-30 Cell orientation in the direction of laser pass for more than 150 μm distance (left) Secondary image (right) Backscattered image

5.5.2.8 Effect of Different Structures on Cell Adhesion Strength

The presence of roughness provides anchors for cells to adhere to through focal adhesion points. The increase in the number of focal adhesion points has a direct effect on the adhesion strength. The capability of different surfaces to establish focal adhesion points with the cultured cells is quantified by the cell adhesion strength of each surface type. In order to study how cell adhesion strength changes quantitatively on different surfaces, an enzymatic detachment analysis is performed on different surface categories after three days of cell culturing. Figure 5-31 shows the comparison study of the trypsinization tests of different surface structures. The X-axis of the presented curve is the duration of total trypsinization time. The Y-axis represents the detachment percentage. The higher the percentage of detachment represents the lower adhesion strength.

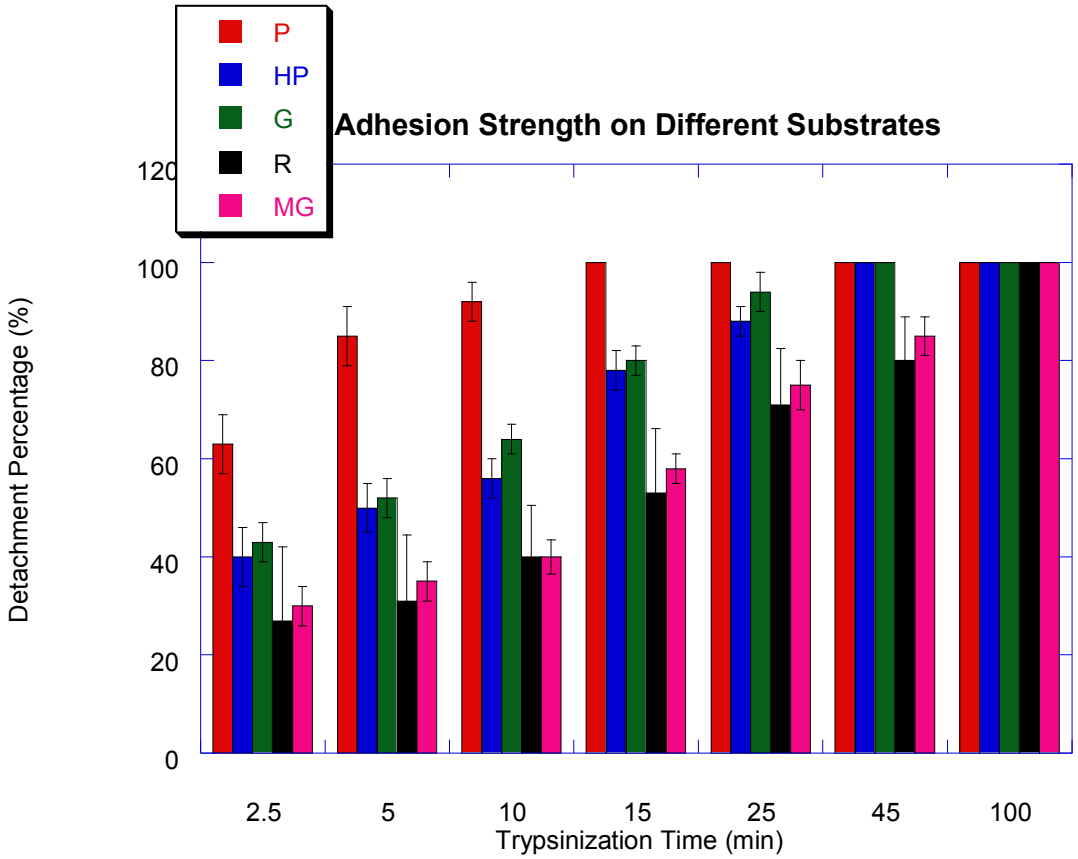

Figure 5-31 Cell detachment percentage on different cell structures after three days of cell culturing

The trypsinization analysis reports low adhesion strength value (i.e., high detachment percentage) on polished surfaces. This can be easily explained by the lack of adhesion sites for cells to adhere to. This is in contrast with the high number of cells that was reported in Figure 5-12. The trypsinization results indicate that the high density of cells shown in Figure 5-12 are either attached to the surface with a weak bonding that could be broken at the very first stage of trypsinization or are due to the cell-to-cell (cadherin) bonding. It is expected to have even weaker bonds in an in-vivo environment with the presence of external forces such as a blood shear force.

The comparison between cell detachment percentage of ground and HP soaked surfaces after three days of cell culturing demonstrates the higher adhesion strength of ground surfaces compared to the adhesion strength of HP soaked surfaces. The roughness values of these two types of surfaces are shown to be almost the same in Figure 5-2 and Figure 5-3. Therefore, it was expected that cells establish bonds with the same adhesion strength on these surfaces. However, Figure 5-31 shows higher adhesion strength for HP surfaces compared to G surfaces. The higher adhesion strength of cells on HP soaked substrate is explained by the presence of titanium dioxide with anatase structure on HP type substrates. The metastable property of the surface and the presence of free ions that could bond to the cultured cells could explain the differences in the adhesion strength between HP and G substrate with almost the same roughness. This important observation underscores the effect of chemical composition of surface on cell adhesion. Despite the fact that the topography of ground surfaces provides better bedding for cells with better orientation, when cells attach to HP soaked surface, they will establish more powerful bonds.

Trypsinization results of R and MG surfaces show a more powerful adhesion compared to the other surfaces. This can be explained by the increase in the roughness of surface. R surfaces are shown to have a higher adhesion strength compared to that of MG surfaces due to the presence of roughness all over their surface.

In the next section a more comprehensive study will be performed on the effect of the fabricated PP structures with different roughness to investigate the effect of roughness values on the cell adhesion strength.

5.5.2.9 Effect of Surface Roughness on Cell Adhesion

As shown in Chapter 3, the size (i.e., area, spacing and height) of PP structures could be controlled by changing laser process parameters. In this section, the adhesion strength of PP based surfaces created, with different roughness, developed using different laser conditions is studied. Studying the effect of roughness values will help in determining the best range of roughness and, consequently, the optimum laser process parameters for generating surfaces with the highest adhesion strength.

Figure 5-32 shows the trypsinization analysis results exclusively for PP-based rough surfaces with different roughness values. The adhesion strength of surfaces with R_a2 and R_q2 remains higher compared to the other two surfaces at all stages of the trypsinization test. Surfaces with R_a3 and R_q3 exhibit the lowest strength due to the presence of local melting sites on the growth micro-structures that eventually result in a reduction of the nano-roughness on the surface. Therefore, despite having larger micro-structures with larger areas of cells to spread on, there are fewer nano-sites to adhere to, which results in a lower adhesion strength.

Low adhesion strength of surfaces with R_a1 and R_q1 can be explained by their small roughness of less than 1μm. The best range for roughness values for improving adhesion strength reported in the literature is also in the range of 1-5 μm. Although the roughness on surfaces with R_a1 and R_q1 is close to the roughness of ground surfaces, adhesion strength is much higher on rough surfaces. This is again due to the presence of more nano-sized roughness and also the proper chemical properties with a thick layer of TiO_2.

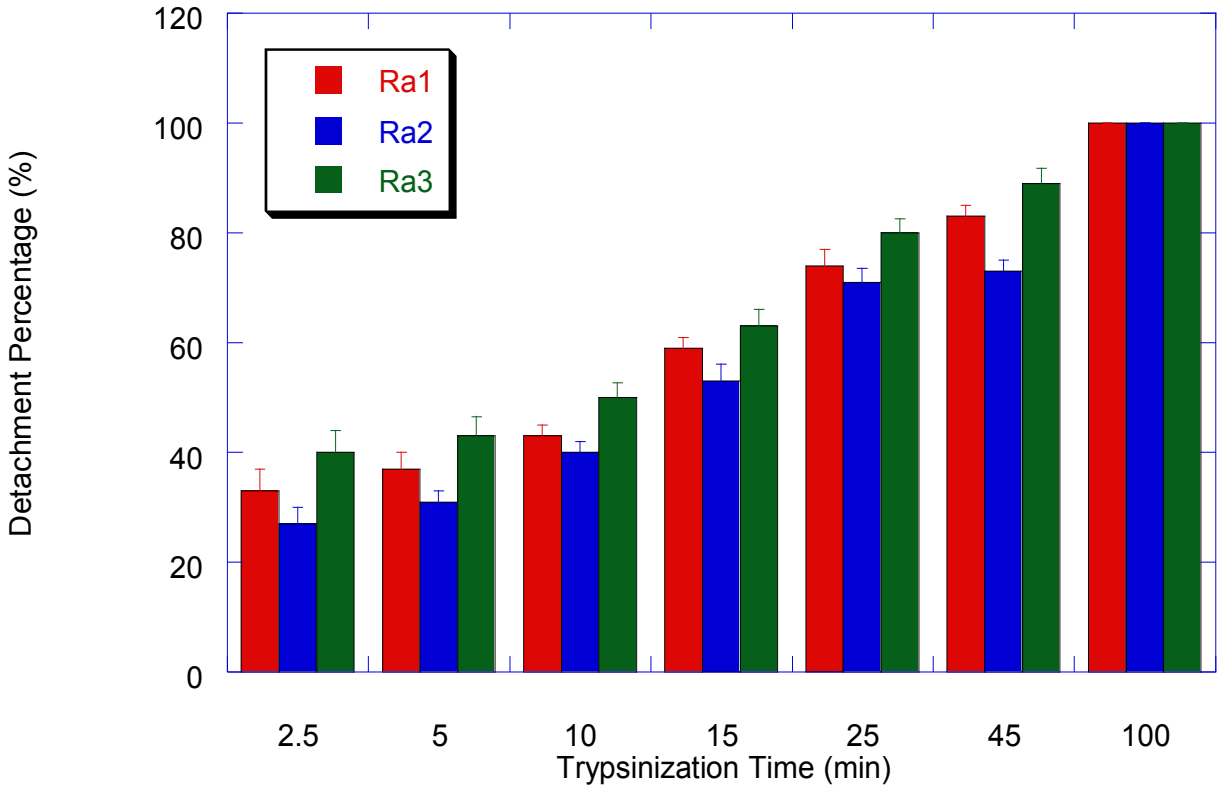

Figure 5-32 Trend of cell detachment on surfaces with different roughness

5.5.2.10 Effect of Different Structures on Cell Viability

Cell viability is an essential property for a successful osseointegration process. In this section, the ability of the tested substrates to support cell growth and cell metabolic activity is evaluated. The results are presented in Figure 5-33, which shows that cell activity increases over time. This indicates that cell growth, as well as oxidation reduction increase over time. As the result of oxidation reduction more non fluorescent Alamar blue transforms to red fluorescence. Alamar blue is taken by cells and reduced from the non-fluorescent to a fluorescent state. The units of fluorescent are called RFU (Relative Fluorescent Units) and are unitless.

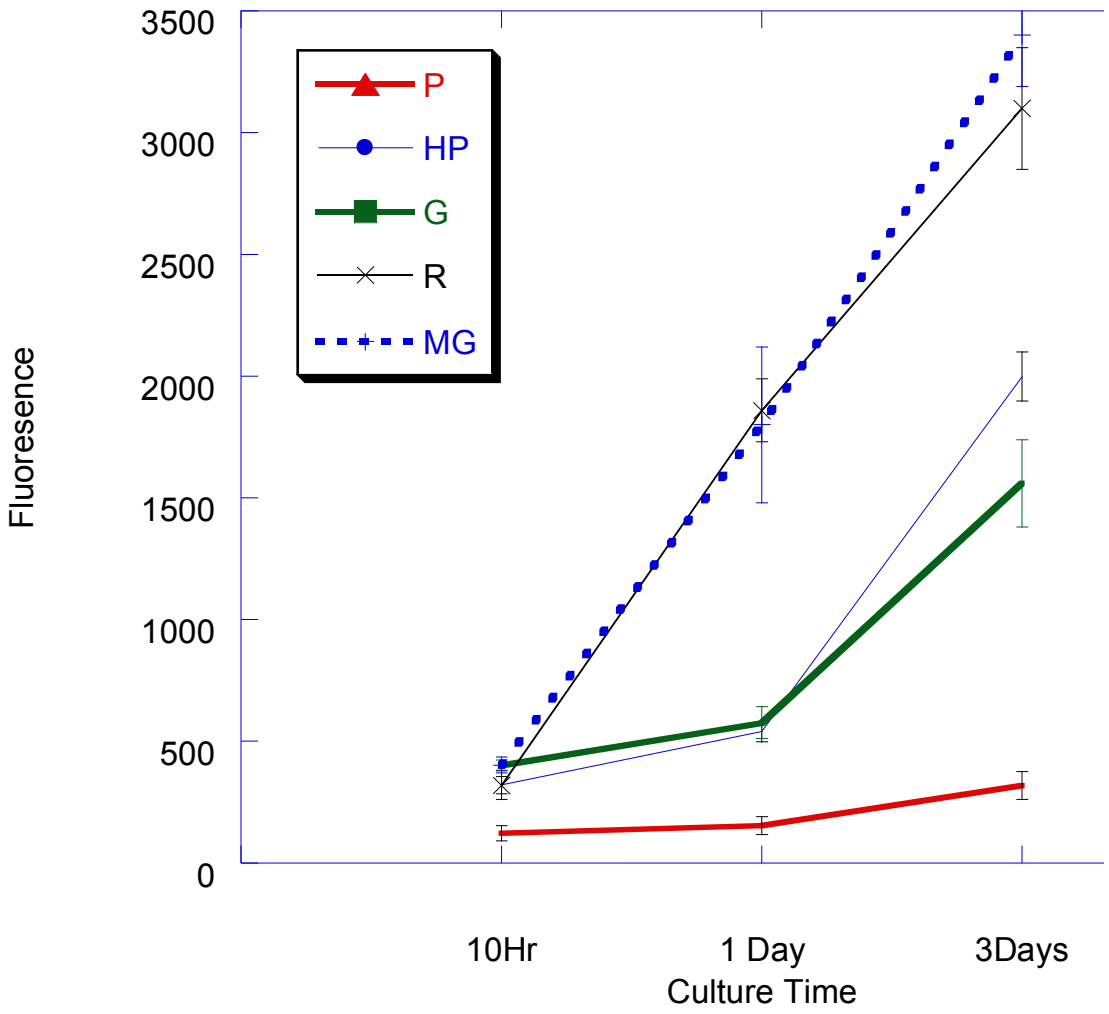

Figure 5-33 Viability analysis of Structures at different stages of cell culturing

The metabolic activity of cells on polished substrate is considerably low compared to other substrates, even for longer culture time periods, due to the low adhesion strength on a polished surface. On polished surfaces, cells are unable to create focal adhesion sites, which are essential for cell growth and viability.

The fluorescence activity on HP and G surfaces is slightly higher than on the ground surfaces; however, it becomes higher on HP soaked surface after three days of cell culturing. This shows that the effect of surface morphology on the cell viability is higher at the first stages

of cell culturing, while the effect of the surface chemistry is more significant at later stages. At the initial stage of cell culturing, cells start to attach more easily to the oriented micro-structures on the ground (G) substrate. The oriented cells have the ability to migrate and grow and eventually have higher viability. At later stages, the already-formed bonds on the HP soaked surfaces become empowered through bonding to the free ions.

Metabolic activity of cells on R and MG substrates is considerably higher than the other three surface types due to the following three characteristics of these surfaces:

- Their generated PP-based micro-structures can absorb more medium to the substrate, which provides a better environment for cells and enhances their activities.
- The oriented cells can migrate and exhibit more growth and viability
- Well-balanced chemical properties and presence of an oxidized layer provide a viable environment for cells.

The difference between the cell metabolic activity of R and MG substrates is less at the first stages of cell culturing (10 hours and 1 day), while it will increase at longer cell culture time periods due to the advantage of having microgrooves on the MG substrate, which is more effective at longer culture time periods. Cells orient on the MG substrate and the orientation of cells allow their activity to increase.

5.6 Summary

In this chapter, the effectiveness of laser-modified surfaces developed using an inexpensive Ytterbium nanosecond pulsed fibre laser in improving the osseointegration properties of implants was studied.

MG-63 cells were cultured on the developed surfaces for different cell culturing periods. Different cell properties (i.e., cell orientation, area, circularity and density) and cell behaviours (i.e., cell migration, adhesion and viability) were investigated after 10, 24, and 72 hours of cell culturing. The following six different surface categories were selected for this study: (i) Polished surface; (ii) Ground surface; (iii) Oxidized surfaces soaked in hydrogen peroxide (HP) media; (iv) Pseudo-Periodic (PP)-based rough surfaces with different R_as and R_qs; (v) PP-based micro-grooved surfaces with different spacing, having the same roughness; and (vi) laser ablated grooves with grooves created as craters into the surface having two spacings of 60 and 120 μm.

The results of the experimental observations that were reported in this chapter are summarized in Table 5-2. All the results are compared/scaled in reference with the cell behaviour on the polished surfaces. The results are reported for the substrates that are incubated for three days.

Table 5-2 Summary of the comparison of different cell behaviours after three days on different surfaces in reference to the polished surfaces

Surface Type		Cell orientation (%)	Cell orientation on grooved substrates (%)	Cell area	Cell density	Cell circularity	Cell Adhesion Strength after 5min trypsinization	Cell viability
P (reference)		1		1	1	1	1	1
HP		2.3		1.5	1.18	1.08	3.75	6.6
G		73.5	73.5	2.1	1.3	3.32	3.36	5.3
R	Ra1, R_q1	55.5		2.62	1.75	2.95	4.42	10.3
	Ra2, R_q2						4.9	
	Ra3, R_q3						4.1	
MG	10	76	80.6	2.66	1.65	3.76	4.75	11
	60		71.3					
	120		65.6					
A	60		49.5					
	120		47					

6 Chapter Six –

Conclusions and Future Work

6.1 Conclusion

The comprehensive study conducted in this thesis describes the development of self-assembled pseudo-periodic (PP) micro-structures on the surface of titanium by laser processing using a single mode Ytterbium nanosecond fiber laser. The effects of the modified surfaces on the biological properties of surfaces are also studied.

Based on the results of this study, laser intensity and laser effective energy are shown to be the two main parameters responsible in the formation of the structures. It is shown that the first stage of initiation of the surfaces is mainly controlled by the laser intensity, which is close to the fluence threshold of the material. The growth of structures and the roughness of the structures mainly controlled by the effective energy parameter through the process speed variation. Therefore, by controlling these two parameters one could control the topography of surfaces. The effect of laser processing on the micro-structures of the heat affected zone (HAZ) is also presented. The optical microscopy study of the analysis demonstrated the HAZ is expanded about three times by the laser path having more elongated βTi micro-structures.

X-ray Diffraction (XRD) analysis results of laser-processed surfaces at different conditions all demonstrate an increase in oxide layer, and also an α to β transformation of the titanium. The presence of βTi will result in an increase in surface hardness of the modified surfaces. The effect of laser process parameters on the surface hardness is quantified through nano-indentation analyses. The XRD results also show the presence of a relatively thick layer of oxidation, including titania, on the surface of titanium. The rapid annealing process of the pulsed

nanosecond laser could also control anatase-rutile transformation, either by changing the lattice of material, or by phase changes. Processing with the pulsed laser will result in the anatase-rutile transformation at much higher temperatures than at a uniform substrate temperature. The laser processing in hydrogen peroxide (HP) medium leads to the formation of titania nanoparticles on the surface. It also results in the formation of new peaks for anatase-titania and a rare structure; Hongquiite, unlike specimens generated in the air. An HP medium may also delay anatase-rutile transformation.

The study of biological properties of the modified surfaces in chapter five demonstrated an improvement in their osseointegration properties due to the presence of the micro-structures in the range of bone cell size with the roughness protruding from the surface of titanium demonstrated to be the proper roughness for osseointegration,. The results from the Trypsinization study report the improvement of the cell adhesion strength due to: (1) the increase in integrin and cadherin bonds on cell adhesion strength to the developed modified surfaces, and (2) a chemically improved surface with free ions for cell and medium to bond to results in an increase in focal adhesion bond strength. Scanning Electron Microscope (SEM) results also demonstrate the improvement in the cell spreading and attachment. The presence of the cone-shaped micro-structures will also increase the cell area and lead cells to make more focal adhesion bonds with the surface and also more integrin and cadherin bonding.

Another factor for the improvement in the biological properties of these surfaces is the presence of the parallel microgrooves, which results in the orientation of cells in one direction. The results from the SEM and trypsinization analysis demonstrate that, although the width of developed grooves is approximately 120 μm, the cell orientation could still be maintained in the direction of the laser path. This is a huge advantage over the results that are reported in the

literature mentioning that having microgrooves with the width larger than 30 μm could not maintain cell orientation [57]. Maintaining the cell orientation on such wide grooves is due to the specific structure of these PP-based sputtered micro-structures. This is due to the effect of having the processes surface sputtered above the surface, as opposed to other methods, in which surface-material interaction starts at the bottom of the processed grooved surfaces. Therefore, after passing a certain cell culture time, the processed surface would not have a considerable effect on the upcoming process and the effect of the initial orientation could not transfer well to the next stages, when the cell-cell interactions would have more effects in driving the orientation. However, PP-based sputtered surfaces show a high orientation at later stages of cell culturing, when cells tend to spread more in the direction of the laser path. This will result in the increase in the cell aspect ratio and a decrease in the cell circularity after passing several hours of cell culturing. The results coming from the Alamar Blue analysis showed the effect of modified surfaces on the improvement of cell viability. This could be explained by the presence of a thick oxide layer developed during the laser processing, which was another main characteristic of the modified surfaces.

Based on the observations from this and previous chapters, one could see the advantage of using the inexpensive nanosecond fiber laser and the thermally induced laser material interactions to improve the biocompatibility of metal surfaces (i.e. titanium) over methods performed with much more expensive pico- and femto-second lasers.

6.2 Future Work

The results of this study demonstrate the improvement of surface biocompatibility of the laser-modified surfaces. In the continuation of this work, the following investigations/contributions could be pursued:

1. **Further increase in the roughness of micro-structures using the same laser-material interaction technique**:

In this study the 100 ns pulse IR laser was used to develop micro and nano micro-structures on the surface of titanium. These micro-structures were developed based on thermal and structural effects during laser material interactions. The surface osseointegration properties could be further improved with the presence of larger protruding micro-structures. To achieve this goal, it is suggested that laser processing be conducted with a laser that has the same pulse width and wavelength but a higher average power. This will result in the formation of micro-structures generated through the same thermal-solidification theory, which allows processing at the higher repetition rate with high effective energy, resulting in the growth of the micro-structures.

2. **Developing a theoretical model for predicting the laser-material interaction**

The concept behind the formation of PP micro-structures was identified through the experimental analysis of this study. It is suggested to develop a theoretical model based on the information that is gained from the experimental analysis to predict the effect of different process parameters. To develop the theoretical model the following steps could be conducted:

- Modeling the initial capillary wave formation under pulsed laser irradiation. This will be achieved through modeling the thermal analysis of laser irradiation. The thermal gradient of surface could be modeled by the calculation of laser intensity.
- Calculating the surface tension of the local melt as a result of the temperature gradient.
- Modeling the melt deformation process as a result of surface tension through the Navier-Stokes equation for the incompressible viscous melt. Material properties of the irradiated surface will be introduced in the Navier-Stokes equation. The following factors could also be introduced in the Navier-Stokes equation:
    - Any external pressure, including atmosphere pressure and photon pressure
    - Pressure caused by evaporation of material due to laser irradiation at each pulse.

This model could be a very good tool in selecting the proper laser and laser properties for developing thermal-solidification based micro-structures.

3. Generating the PP micro-structures in a vacuumed liquid media

In chapter three, laser processing of titanium in liquid oxidized media was studied. The results showed an improvement in the chemical properties of the surface. However, surface topography was influenced by the liquid media, including the effect of liquid bubbles on the laser beam focus and the beam spot size. Therefore, to eliminate the effect of the bubbles on micro-structure formation, it is suggested that laser processing be conducted using the same laser but in a vacuumed oxidized media.

4. **Further analysis on the effect of Hongquiite composition on the tribological properties of the surface**

The XRD results of samples that were processed in HP report the presence of the Hongquiite structure. This is a rare structure, which is reported to have the structure similar to TiC but with superior tribological properties. The nanoindentation analysis of the developed surfaces with a Hongquiite component shows an improvement in the hardness of the surface. Additional study on the Hongquiite composition properties are recommended. Studying the properties of Hongquiite could be a breakthrough in improving surface properties for applications that require high tribological properties.

5. **Conducting more experimental characterization to quantify the cell adhesion strength**

The trypsinization method was used in this study to characterize the effect of surface modification on cell adhesion strength. Trypsinization is a great method that is usually used for the comparison study between adhesion strength on different surfaces. A more conclusive study could be done to quantify the cell adhesion strength by measuring the adhesion force between each cell and the surface. One suggested method is micro-interferometry analysis, which works by visualizing the cell adhesion through the interfering light that is reflected from cell-surface adhesion site. This is done by exposing magnetic tweezers to the adhered cell to apply an enforced lifting force and pulling the receptor-ligand bonds. A study using this method would provide a more quantitative insight on the effect of topographical and chemical modification on cell-surface adhesion.

6. **Developing a theoretical model for quantifying the effect of laser-modified structures on cell adhesion strength**

In order to quantify the effect of the modified surface's properties on cell adhesion strength, the peeling force, which is required to detach the osteoblast cells from the treated titanium surfaces, should be identified. Two parameters are required for calculating peeling force: 1) accumulated stress, and 2) real contact area between the cell and the substrate. The stress at the surface is a function of surface energy and surface energy itself is a function of surface parameters. Real contact area is also dependent on the surface parameters, as well as on the rate of spreading cells on the substrate. Therefore, to be able to calculate the peeling force, a model should be developed to relate different physical and biological processes in one model.

References

1. Brunette D.M., Tengvall P., Textor M., Thomsen P., Titanium in medicine: Material science, surface science, engineering, biological responses and medical applications, New York: Springer; 2001.
2. Davies J.E., Bone bonding at natural and biomaterial surfaces, *Biomaterials*. 2007;28(34):5058-67.
3. Felgueiras H., Migonney V., Biomimetic polygrafted on Ti6Al4V: Effect of pre-adsorbed selected proteins on the MC3T3-E1 osteoblastic development, *IFMBE Proceedings*. 2014; 41:1601-1604.
4. Burridge K., Fath K., Focal contacts: Transmembrane links between the extracellular matrix and the cytoskeleton, *BioEssays*. 1989; 10(4):104-8.
5. Anselme K., Osteoblast adhesion on biomaterials, *Biomaterials*. 2000; 21(7):667-81.
6. Kokubo T., Kim H.M., Kawashita M., Nakamura T., What type of materials exhibits bone bonding, *Bone Engineering*. 2000:190-4.
7. Hu X., Neoh K.G., Zhang J.K., En-Tang.Hu X., Bacterial and osteoblast behaviour on titanium, cobalt-chromium alloy and stainless steel treated with alkali and heat: A comparative study for potential orthopaedic applications, *Journal of Colloid and Interface Science.* 2014;417:410-419.
8. Textor M., Sittig C., Frauchiger V., Tosatti S., Brunette D.M., Properties and biological significance of natural oxide films on titanium and its alloys, *Titanium in Medicine*. Berlin: Sringer; 2001:171-230.

9. Choi M., Hong E., So J., Song S., Kim B.S., Yamamoto A., Kim Y.S., Cho J., Choe H., Tribological properties of biocompatible Ti-10W and Ti-7.5TiC-7.5W, *Journal of the Mechanical Behaviour of Biomedical Materials*. 2014;30:214-222.

10. Park B.S., Heo S.J., Kim C.S., Oh J., Kim J., Lee G., Effects of adhesion molecules on the behaviour of osteoblast-like cells and normal human fibroblasts on different titanium surfaces, *Journal of Biomedical Materials Research - Part A*. 2005;74(4):640-51.

11. Liu X., Chub P.K., Ding C., Surface modification of titanium, titanium alloys, and related materials for biomedical applications, *Materials Science and Engineering: R: Reports*. 2004;47:49-121.

12. Bayram C., Demirbilek M., Yalcin E., Bozkurt M., Dogan M., Denkbas B., Osteoblast response on co-modified titanium surfaces via anodization and electrospinning, *Applied Surface Science*. 2014; 288:143-148.

13. Inzunza D., Covarrubias C., Marttens A.V., Leighton Y., Carvajal J.C., Valenzuela F., Diaz-Dosque M., Mendez N., Martinez C., Pino A., Rodriguez J.P., Caceres M., Smith P., Synthesis of nanostructured porous silica coatings on titanium and their cell adhesive and osteogenic differentiation properties, *Journal of Biomedical Materials Research - Part A*. 2014; 102(1):37-48.

14. Kokubo T., Kim H.M., Kawashita M., Nakamura T., Bioactive metals: Preparation and properties, *Chemistry of Materials*. 2004;15:99-107.

15. Tang G.X., Zhang R.J., Yan Y.N., Zhu Z.X., Preparation of porous anatase titania film, *Materials Letters*. 2004;58:1857-60.

16. Healy K.E., Thomas C.H., Rezania A., Kim J.E., McKeown P.J., Lom B., Kinetics of bone cell organization and mineralization on materials with patterned surface chemistry, *Biomaterials*. 1996;17(2):195-208.

17. Hench L.L., Ethridge E.C., Biomaterials: An introduction approach, *Biomaterial Science*. 1982.

18. Hosseini M.M., On the relationship between osteoconduction and surface texture during peri implant osteogenesis, *Dissertation, University of Toronto*. 2002.

19. Yin B.D., Zhang S.F., Yang J.Y., Deng Z.N., Sun Y., Prepare and properties of Titanium with surface nanostructure by high-energy shot peening, *Advanced Materials Research*. 2013;842:267-270.

20. Boyan B.D., Hummert T.W., Dean D., Schwartz Z., Role of material surfaces in regulating bone and cartilage cell response, *Biomaterials*. 1996;17(2):137-46.

21. Collier T.O., Anderson J.M., Brodbeck W.G., Barber T., Healy K.E., Inhibition of macrophage development and foreign body giant cell formation by hydrophilic interpenetrating polymer network, *Journal of Biomedical Research A*. 2004;69(4):644-50.

22. Kunzler T.P., Huwiler C., Drobek T., Vörös J., Spencer N.D., Systematic study of osteoblast response to nanotopography by means of nanoparticle-density gradients, *Biomaterials*. 2007;28(33):2175-82.

23. Park J.E., Park I.S., Neupane M.P., Bae T.S., Lee M.H., Effects of a carbon nanotube-collagen coating on a titanium surface on osteoblast growth, *Applied Surface Science*. 2014;292:828-36.

24. MacDonald D.E., Rapuanod B.E., Deo N., Stranick M., Somasundarana P., Boskey A.L., Thermal and chemical modification of titanium–aluminum–vanadium implant materials: Effects on surface properties, glycoprotein adsorption, and MG63 cell attachment, *Biomaterials*. 2004;25:3135-46.

25. Vercaigne S., Wolke J.G.C., Naert I., Jansen J.A., Histomorphometrical and mechanical evaluation of titanium plasma-spray-coated implants placed in the cortical bone of goats, *Journal of Biomedical Material Research*.1998;41(1):41-8.

26. Zhou Z., Dai Y., Liu B.B., Xia L.L., Liu H.B., Vadgama P., Liu H.R., Surface modification of titanium plate enhanced fibronectin-mediated adhesion and proliferation of MG-63 cells, *Transactions of Nonferrous Metals Society of China (English Edition)*. 2014; 24(4):1065-1071.

27. Huang X., Zhong X., Zhu B., Sun Q., Jin C., Quan H., Tang Z., Chen W.A., Comparative study of the influence of three pure titanium plates with different micro- and nano-topographic surfaces on preosteoblast behaviours, *Journal of Biomedical Materials Research - Part A*. 2013;101(11):3278-3284.

28. Webster T.J., Ejiofor J.U., Increased osteoblast adhesion on nano-phase metals: Ti, Ti6Al4V, and CoCrMo, *Biomaterials*. 2004;25(19):4731-9.

29. Braceras I., Vera C., Ayerdi-Izquierdo A., Munoz R., Lorenzo J., Alvarez N., De M., Miguel A., Ion implantation induced nano-topography on titanium and bone cell adhesion, *Applied Surface Science*. 2014; 310:24-30.

30. Andersson A.S., Backhed F., Von Euler A., Richter-Dahlfors A., Sutherland D., Kasemo B., Nano-scale features influence epithelial cell morphology and cytokine production, *Biomaterials*. 2003;24(20):3427-36.

31. Jäger M., Zilkens C., Zanger K., Krauspe R., Significance of nano- and microtopography for cell-surface interactions in orthopaedic implants, *Journal of Biomedicine and Biotechnology*. 2007;8: 69036

32. Yang W., Xi X., Shen X., Liu P., Hu Y., Cai K., Titania nanotubes dimensions-dependent protein adsorption and its effect on the growth of osteoblasts, *Journal of Biomedical Materials Research - Part A*. 2013;102(10):3598-3608.

33. Oliveira P.T.D., Nanci A., Nanotexturing of titanium-based surfaces upregulates expression of bone sialoprotein and osteopontin by cultured osteogenic cells, *Biomaterials*. 2004;25(3):403-13.

34. Price R.L., Waid M.C., Haberstroh K.M., Webster T.J., Selective bone cell adhesion on formulations containing carbon nanofibers, *Biomaterials*. 2003;24(11):1877-87.

35. Dalby M.J., McCloy D., Robertson M., Agheli H., Sutherland D., Affrossman S., Osteoprogenitor response to semi-ordered and random nano-topographies, *Biomaterials*. 2006;27(15):2980-7.

36. Hansen J.C., Jung Y.L., Li-Chong X., Siedlecki C.A., Mauger D.T., Donahue H.J., Effect of surface nano-scale topography on elastic modulus of individual osteoblastic cells as determined by atomic force microscopy, *Journal of Biomechanics*. 2007;40(13):2865-71.

37. Mendonca G., Mendonca D.B.S., Aragao F.J.L., Cooper L.F., Advancing dental implant surface technology - from micron- to nano-topography, *Biomaterials*. 2008;29(28):3822-35.

38. Nguyen T.D.T., Park I.S., Lee M.H., Bae T.S., Enhanced biocompatibility of a pre-calcified nano-tubular TiO2 layer on Ti-6Al-7Nb alloy, *Surface and Coatings Technology*. 2013;236:127-134.

39. Cooper L.F., Biologic determinants of bone formation for osseointegration: Clues for future clinical improvements, *Journal of Prosthetic Dentistry*. 1998;80:439-49.

40. Stein G.S., Lian J.B., Stein J.L., Van Wijnen A.J., Frenkel B., Montecino M., Mechanisms regulating oateoblast proliferation and differentiation, In: Bilezikian J.P., Raisz L.G., Rodan G.A., Principles of bone biology. San Diego: *Academic Press*; 1996. p. 69-86.

41. Schwartz Z., Boyan B.D., Underlying mechanism at the bone biomaterial interface, *Journal of Cellular Biochemistry*. 1994;56:340-7.

42. Boyan B.D., Blazer R., Kieswetter K., Liu Y., Cochran D.L., Szmuckler-Moneler S., Titanium surface roughness alters responsiveness of MG63 osteoblast-like cells to la,25-$(OH)_2D_3$. I, *Journal of Biomedical Research*. 1998;39:77-85.

43. Ogawa T., Nishimura I., Genes differentially expressed in titanium implant healing, *Journal of Dental Research*. 2006;85:566-70.

44. Galli C., Piergianni M., Piemontese M., Lumetti S., Ravanetti F., Cacchioli A., Macaluso G.M., Passeri G., Periostin improves cell adhesion to implantable biomaterials and osteoblastic differentiation on implant titanium surfaces in a topography-dependent fashion, *Journal of Biomedical Materials Research - Part A*. 2014; 102(11):3855-61.

45. Abron A., Hopfensperger M., Thompson J., Cooper L.F., Evaluation of a predictive model for implant surface topography effects on early osseointegration in the rat tibia model, *Journal of Prosthetic Dentistry*. 2001;85:40-6.

46. Schwartz Z., Nasazky E., Boyan B., Surface micro-topography regulates osteointegration: The role of implant surface micro-topography in osteointegration*, Alpha Omegan*. 2005;98(2):9-19.

47. Ricci J.L., Grew J.C., Alexander H., Connective-tissue responses to defined biomaterial surfaces. I. Growth of rat fibroblast and bone marrow cell colonies on micro-grooved substrates, *Journal of Biomedical Research A*. 2007; 85(2):313-25.

48. Davies J.E., Understanding peri-implant endosseous healing, *Journal of Dental Education*. 2003;67(8):932-49.

49. Moreo P., Garcı´a-Aznar J.M., Doblare M., Bone ingrowth on the surface of endosseous implants. Part I: mathematical model, *Journal of Theoretical Biology*. 2009;260(1):1-12.

50. Wennerberg A., On surface roughness and implant incorporation, *Dissertation*, Goteborg, Sweden: Goteborg University; 1996.

51. Hansson S., Norton M., Relation between surface roughness and interfacial shear strength for bone-anchored implants. A mathematical model, *Journal of Biomechanics*. 1999;32(8):829-36.

52. Albrektsson T., Wennerberg A., Oral implant surfaces: Part 2: review focusing on clinical knowledge of different surfaces, *The Intentional Journal of Prosthodontics*. 2004;17(5):544-64.

53. Webster T.J., Ergun C., Doremus R.H., Siegel R.W., Bizios R., Enhanced functions of osteoblasts on nano-phase ceramics, *Biomaterials*. 2000;21(17):1803-10.

54. Walboomers X.F., Jansen J.A., Cell and tissue behaviour on micro-grooved surfaces, *Odontology*. 2001;89 (1):2-11.

55. Fu J., Hua Y., Guoa Z., Zhanga Y., Haob Y., Lib S., Effect of surface micro topography of titanium material on the behaviours of rabbit osteoblast in vitro, *Applied Surface Science*. 2008;255(2):286-9.

56. Chesmel K.D., Clark C.C., Brighton C.T., Black J., Cellular responses to chemical and morphologic aspects of biomaterial surfaces. II, *Journal of Biomedical Research*.1995;29(9):1101-10.

57. Chehroudi B., Gould T.R.L., Brunette M., Effects of a grooved titanium-coated implant surface on epithelial cell behaviour in vitro and in vivo, *Journal of Biomedical and Materials Research*. 1988;23(9):1067-85.

58. Clark P., Connolly P., Curtis A.S., Dow J.A., Wilkinson C.D., Topographical control of cell behaviour: II. Multiple grooved substrata, *Development*. 1990;108(4):635-44.

59. Andersson A.S., Olssona P., Lidberga U., Sutherlanda D., The effects of continuous and discontinuous groove edges on cell shape and alignment, *Experimental Cell Research*. 2003;288(1):177-88.

60. Cao Y., Chen J., Adeoye M.O., Soboyejo W.O., Investigation of the spreading and adhesion of human osteosarcoma cells on smooth and micro-grooved polydimethyl siloxane surfaces, *Material Science and Engineering: C*. 2009;29(1):119-25.

61. Ricci J.L., Alexander H., Laser micro-texturing of implant surfaces for enhanced tissue integration, *Key Engineering Materials*. 2001;198-199:179-202.

62. Fernandez-Rodriguez M.A., Sanchez-Trevino A., De L.B.E., Ramos-Torrecillas J., Garcia-Martinez O., Ruiz C., Rodriguez-Velverde M.A., Caberizo-Vilchez M.A., Wettability and osteoblastic cell adhesion on ultra polished commercially pure titanium surfaces: The role of the oxidation and pollution states, *Journal of Adhesion Science and Technology.* 2014; 28(12):1207-1218.

63. Kim M.J., Kim C.W., Lim Y.J., Heo S.J., Micro-rough titanium surface affects biologic response in MG63 osteoblast-like cells, *Journal of Biomedical Material Research A*. 2006;79:1023–1032.

64. Rohanizadeh R., Sadeq M.A., LeGeros R.Z., Methods of preparing different types of titanium oxide on titanium surface: Effects on apatite deposition, *Journal of Biomedical Material Research A*. 2004; 71A(2):343-52.

65. Henrich V.E., Cox P.A., The surface science of metal oxides, *Cambridge University*, *Press*. 1996 . Science - 480 pages

66. Ferraz E.P., Sa J.C., De O.P.T., Alves J.C., Beloti M.M., Rosa A.L., The effect of plasma-nitride titanium surfaces on osteoblastic cell adhesion, proliferation, and differentiation, *Journal of Biomedical Materials Research - Part A*. 2014;102(4):991-98.

67. Cecchinato F., Xue Y., Karlsson J., He W., Wennerberg A., Mustafa K., Andersson M., Jimbo R., In vitro evaluation of human fetal osteoblast response to magnesium loaded mesoporous TiO2 coating, *Journal of Biomedical Materials Research - Part A*. 2014; 102(11):3862-71.

68. Sreemany M., Bose A., Sen S., A study on structural, optical, electrical and microstructural properties of this TiOx films upon thermal oxidation: Effect of substrate temperature and oxidation temperature, *Physics B: Physics of Condensed Material*. 2010; 405(1):85-93.

69. Karthega M., Rajendran N., Hydrogen peroxide treatment on Ti-6Al-4V alloy: A promising surface modification technique for orthopaedic application, *Applied Surface Science*. 2010; 256(7):2176-83.

70. Santiago-Medina P., Sundaram P.A., Diffoot-Carlo N., The effects of micro arc oxidation of gamma titanium aluminide surfaces on osteoblast adhesion and differentiation, *Journal of Materials Science: Materials in Medicine*. 2014;25(6):1577-87.

71. Jonitz-Heincke A., Wieding J., Schulze C., Hansmann D., Bader R., Comparative analysis of the oxygen supply and viability of human osteoblasts in three-dimensional titanium scaffolds produced by laser-beam or electron-beam melting, *Materials*. 2013; 6(11):5398-5409.

72. Jafarkhani P., Dadras S., Torkamany M.J., Sabbaghzadeh J., Synthesis of nano-crystalline titania in pure water by pulsed Nd:YAG laser, *Applied Surface Science*. 2010: 256(12);33817-21.

73. Liu Z., Yuan Y., Khan A., Abdolvand A., Whitehead D., Schmidt M.J., Generation of metal-oxide nanoparticles using continuous-wave fibre laser ablation in liquid, *Journal of Micromechanics and Microengineering*. 2009;19(5):1-7.

74. Zhou Z., Bigerelle M., Anselme K., Roughness statistical influence on cell adhesion using profilometry and multiscale analysis, *Special Issue on Diverse Applications of Surface Metrology III*. 2014; 36(1):2-10.

75. Markwardt J., Friedrichs J., Werner C., Davis A., Weise H., Lesche R., Weber A., Rang U., Meiner H., Lauer G., Reitemeier B., Experimental study on the behaviour of primary human osteoblasts on laser-cused pure titanium surfaces, *Journal of Biomedical Materials Research - Part A*. 2014; 102(5):1422-30.

76. Baltriukiene D., Sabaliauskas V., Balciunas E., Melninkaitis A., Liutkevicius E., Bukelskiene V., Rutkunas V., The effect of laser-treated titanium surface on human

gingival fibroblast behaviour, *Journal of Biomedical Materials Research - Part A*. 2014; 102(3):713-720.

77. Wang R., Xu Y., Yu X.L., Zhou Y.M., Enhanced adhesion of human osteoblast-like cells on femtosecond laser treated Ti-6Al-4V, *Advanced Materials Research*. 2013; 739:101-105.

78. Ohtsuki C., Iida H., Hayakawa S., Osaka A., Bioactivity of Titanium treated with Hydrogen peroxide solutions containing metal chlorides, *Journal of Biomedical Material*. R. 1997; 35:39-47.

79. Mahshid S., Askari M., Ghamsari M.S., Effect of brookite presence on nano-crystalline anatase–rutile phase transformation, *International Journal of Nanotechnology*. 2009; 6 (10):961-72.

80. Oliver, W.C., Pharr G.M., An improved technique for determining hardness and elastic modulus using load and displacement sensing indentation experiments, *Journal of Martials Research*, 1992;7(6):1564-83

81. Dahotre S.N., Vora H.D., Rajamure R.S., Huang L., Banerjee R., He W., Dahotre N. B., Laser induced Nitrogen enhanced Titanium surfaces for improved osseointegration, *Annals of Biomedical Engineering*. 2014; 42(1):50-61

82. Xu Y., Shen M.R., Anatase TiO2 films fabricated by pulsed laser deposition using Ti target, *Applied Physics A*. 2009;94(2):275-80.

83. Okubo N., Nakazawat T., Katano Y., Yoshizawa I., Fabrication of nanoparticle of anatase TiO_2 oxygen supplied pulsed laser deposition, *Applied Surface Science*. 2002;197-198:679-83.

84. Wang M., Ning Y., Zou H., Chen S, Bai Y, Wang A., Xia H., Effect of Nd:YAG laser-nitriding-treated titanium nitride surface over Ti6Al4V substrate on the activity of MC3T3-E1 cells, *Biomedical Materials and Engineering*. 2014; 24 (1):643-9.

85. Mizutani, M., Honda, R., Kurashina, Y., Komotori, J., Ohmori, H., Improved cytocompatibility of nanosecond-pulsed laser-treated commercially pure Ti surfaces, *International Journal of Automation Technology*. 2013; 8(1):102-9.

86. Fusi M., Russo V., Casari C.S., Bassi A.L., Bottani C.E., Titanium oxide nano-structured films by reactive pulsed laser deposition, *Applied Surface Science*. 2009; 255(10):5334-37.

87. Marco de Lucas M.C., Lavisse L., Pillon G., Microstructural and tribological study of Nd:YAG laser treated titanium plates, *Tribology International*. 2008;41(11):985-91.

88. György E., Pérez del Pino A., Serra P., Morenza J.L., Structure formation on titanium during oxidation induced by cumulative pulsed Nd:YAG laser irradiation, *Applied Physics A*. 2004;78(5):765-70.

89. Abdolvand A, Khan S.Z., Yuan Y., Crouse Y., Schidt M.J.J., Sharp M., Generation of titanium-oxide nanoparticles in liquid using a high-power, high-brightness continuous-wave fiber laser, *Applied Physics A*. 2008;91(3):365-8.

90. Han Y., Lin C.H., Xiao H., Tsai H.L., Femtosecond laser induced silicone surface morphology in water confinement, *Microsystems Technology*, 2009; 15(7):1045-49.

91. Shafeev G.A., Freysz E., Bozon-Verduraz F., Self-influence of a femtosecond laser beam upon ablation of Ag in liquids, *Applied Physics A*. 2004;78 (3):307-9.

92. Kruusing A., Underwater and water-assisted laser processing: Part 1-general features, steam cleaning and shock processing, *Optics and Lasers in Engineering*. 2004;41:307-27.

93. Chen J., Ulerich J.P., Abelev E., Fasasi A., Arnold C.B., Soboyejo W.O., An investigation of the initial attachment and orientation of osteoblast-like cells on laser grooved ti-6Al-4V surfaces, *Materials Science and Engineering: C*. 2009 ;29(4,5):1442–52.

94. Darling E.M., Topel M., Zauscher S., Vail T.P., Guilak F., Viscoelastic properties of human mesenchymally-derived stem cells and primary osteoblasts, chondrocytes, and adipocytes, *Journal of Biomechanics*. 2008;41(2):454-64.

95. Mwenifumbo S., Cell/surface interactions and adhesion on biomedical and biomems surfaces: Effects of laser micro texturing and titanium coating. *Dissertation. Princeton University*; 2004.

96. Kietzig A.M., Lehr J., Matus L., Laser-induced patterns on metals and polymers for biomimetic surface engineering, *Proceedings of SPIE - The International Society for Optical Engineering*. 2014;8967.

97. Mwenifumbo S., Morgan N., Perohe A., Chen J., Li M., Soboyejo W.O., In: Nanosecond UV laser processing: Surface micro-groove geometry and micro-structure in ti-6Al-4V alloys *TMS annual meeting*; Feb 13-17 2005; Warrendale, PA 15086, United States: Minerals, *Metals and Materials Society*; 2005. p. 185-203.

98. Mwenifumbo S., Morris N.D., Li M., Keirstead M., Soboyejo W.O., An investigation of nano-second UV laser processing parameters on surface micro-groove geometry and micro-structure in Ti-6Al-4V, *Surface engineering: Materials Science II*; 2003. p. 141-50.

99. Mirhosseini N., Crouse P.L., Schmidth M.J.J., Li L., Garrod D., Laser surface micro-texturing of ti-6Al-4V substrates for improved cell integration, *Applied Surface Science*. 2007;253(19):7738-43.

100. Duncan A.C., Rouais F., Lazare S., Bordenave L., Baquey C., Effect of laser modified surface micro-topochemistry on endothelial cell growth, *Colloids and Surfaces B: Bio-interfaces*. 2007;54(2):150-9.

101. Soboyejo W.O., Mercer C., Allameh S., Nemetski B., Marcantonio N., Ricci J.L., Multi-scale microstructural characterization of micro-textured ti-6Al-4V surfaces, *Key Engineering Materials*. 2001;198-199:203-30.

102. Ulerich J.P., Ionescu L.C., Chen J., Soboyejo W.O., Arnold C.B., Modifications of ti-6Al-4V surfaces by direct-write laser machining of linear grooves, *Proceeding of SPIE*. 2007;6458.

103. Fassi A.Y., Mwenifumbo S., Rahbar N., Chen J., Li M., Beye A.C., Nano-second UV laser processed micro-grooves on Ti6Al4V for biomaterial applications, *Materials Science and Engineering*: C. 2009;29:5-13.

104. Bastow T.J., Ordering of microcraters produced by a laser on a metal surface, *Nature*. 1969; 222(5198):1058-60.

105. Sundaram S.K., Mazur E., Inducing and probing non-thermal transitions in semiconductors using femtosecond laser pulses, *Nature Materials*. 2002; 217-24.

106. Miotello A., Kelly R., Laser induced phase explosion: New physical problems when a condensed phase approaches the thermodynamic critical temperature, *Applied Physics A*. 1999; 69:67.

107. Lewis L.J., Perez D., Theory and Simulation of laser ablation-from basic mechanism to applications, Laser Precision Micro-fabrication, *Springer*. 2010:35-61.

108. Young J.F., Preston J.S., Van Driel H.M., Sipe J.E., Laser-induced periodic surface structure. II. Experiments on Ge, Si, Al, and brass, *Physical Review B*. 1983;27(2):1155-72.

109. Coulson C.A., Jeffery A., A mathematical approach to the common types of wave motion. 2nd ed. London: Longman; 1977.

110. Driel H.M., Sipe J.E., Young F., Laser induced periodic surface on solids: A universal phenomenon, *Physical Review Letters*. 1982;49(26):1955-8.

111. Foltyn S.R., Pulsed laser deposition of thin films. In: Christy DB, Huber GK, editors. Wiley, New York; 1994.

112. Abdolvand A., Lloyd R.W., Schmidt M.J.J., Whitehead D.J., Liu Z., Li L., Formation of highly organized, periodic micro-structures on steel surfaces upon pulsed laser irradiation, *Applied Physic A*. 2009;95(2): 447-52

113. Jackson M.J., Micro and nano-manufacturing, Springer Science, *Business Media*; 2007.702p.

114. Dolgaev S.I., Fernández-Pradas J.M., Morenza J.L., Serra P., Shafeev G.A., Growth of large micro-cones in steel under multi-pulsed Nd:YAG laser irradiation, *Applied Physics A: Materials Science and Processing*. 2006;83(3):417-20.

115. Lloyd R., Abdolvand A., Schmidt M., Crouse P., Whitehead D., Liu Z., Laser-assisted generation of self-assembled micro-structures on stainless steel, *Applied Physics A: Materials Science and Processing*. 2008;93(1):117-22.

116. Schille J., Ebert R., Loeschner U., Regenfuß P., Suess T., Exner H., Micro structuring with highly repetitive ultra short laser pulses, *International Symposium on Laser Precision*, (LMP2008). 2008:08-57.

117. Bensaoula A., Boney C., Pillai R., Shafeev G.A., Simakin A.V., Starikov D., Arrays of 3D micro-columns generated by laser ablation of ta and steel: Modelling of a black body emitter, *Applied Physics A: Materials Science and Processing*. 2004;79(4-6):973-5.

118. György E., Mihailescu I.N., Serra P., Perez Del Pino A., Morenza J.L., Crown-like structure development on titanium exposed to multi-pulse Nd:Yag laser irradiation, *Applied Physics A*. 2002;74:755-9.

119. Dolgaev S.I., Kirichenko N.A., Simakin A.V., Shafeev G.A., Initial stage of the development of three-dimensional periodic structures in laser melting, *Quantum Electronics*. 2004;34:771-3.

120. György E., Pérez D.P., Serra P., Morenza J.L., Laser-induced growth of titanium nitride micro-columns on biased titanium targets, *Journal of Material Research*.2005;20(1):62-7.

121. György E., Pérez D.P., Serra P., Morenza J.L., Depth profiling characterization of the surface layer obtained by pulsed Nd:Yag laser irradiation of titanium in nitrogen, *Surface and Coating Technology*. 2002;173:265-70.

122. Dolgaev S.I., Kirichenko N.A., Simakin A.V., Shafeev G.A., Micro-structures produced on spatially confined substrates exposed to repetitively pulsed laser radiation, *Quantum Electronics*. 2007;37(7):645-50

123. Steen W., Mazumder J., Laser material processing. 4th edition. 2010. Springer